UNIVERSITY OF OKLAHOMA

GRADUATE COLLEGE

INTEGRATED BIOMARKER INVENTORY REVEALS RESPONSE OF MICROBIAL COMMUNITY TO GLOBAL WARMING INDUCED WATER CHEMISTRY CHANGES IN THE BLACK SEA

A DISSERTATION

SUBMITTED TO THE GRADUATE FACULTY

in partial fulfilment of the requirements for the

Degree of

DOCTOR OF PHILOSOPHY

By

OLAWALE OLUWAFEMI ALO

Norman, Oklahoma

2025

Downloaded from SHAREOK. Persistent Handle URL: https://hdl.handle.net/11244/341562

INTEGRATED BIOMARKER INVENTORY REVEALS RESPONSE OF MICROBIAL COMMUNITY TO GLOBAL WARMING INDUCED WATER CHEMISTRY CHANGES IN THE BLACK SEA

A DISSERTATION APPROVED FOR THE

SCHOOL OF GEOSCIENCES

BY THE COMMITTEE CONSISTING OF

Dr. Xiao-Lei Liu, Chair

Dr. Michael H. Engel

Dr. Andrew S. Elwood Madden

Dr. Wei Qin

© Copyright by Olawale Oluwafemi Alo 2025

All Rights Reserved.

For they did not gain possession of the land by their own sword, nor did their own arm save them; But it was your right hand, your arm, and the light of your countenance, because you favored them. Psalms 44:3 (NKJV)

Table of Contents

Acknowledgements vii

Dissertation Abstract ix

Chapter 1: Integrated biomarker inventory reveals the progressive evolution of Black Sea microbial community in the Holocene 1

1.1 Introduction 2

1.2. Study Location and methods 3

1.2.1 Geological setting 3

1.2.2 Sample preparation and lipid analysis 7

1.2.3 Biomarker inventory 8

1.2.3.1 Chlorophyll-*a*-Degradative Derivatives 8

1.2.3.2 Long-chain Alkenones 9

1.2.3.3 Crenarchaeols 9

1.3.4.2 O*v*erly Branched GDGTs 10

1.2.3.5 Dialkyl Glycerol Ethers (DAGEs) 11

1.3 Results 12

1.3.1 Lipid biomarker distributions 12

1.4 Discussion 16

1.4.1 Water column redox and salinity dynamics and effect on photo- and chemoautotrophs 16

1.4.2 Archaeol and Isoprenoid glycerol ether lipids provide insight into the rate of water column anoxia development 21

1.4.3 Effects of water column stratification on deep water microbial community. 23

1.5 Conclusion 27

1.6 References 28

Chapter 2: Simultaneous analysis of long-chain alkenones and chlorophyll derivatives offers new insights into the ecology of *Isochrysis* algae in the Holocene Black Sea 46

2.1 Introduction 47

2.2. Materials and methods 49

2.2.1 Sample preparation and lipid analysis 49

2.2.2 Bulk measurements 50

2.2.3 Targeted lipid biomarkers 51

2.3 Results and discussions 53

2.3.1 Stable *Isochrysis* algae contribution to a low primary productivity before the onset of PZE (11.7 to 7.6 ka, Unit III) 54

2.3.2 Suppressed Isochrysis algae growth due to PZE development (7.6 to 2.6 ka, Unit II) 56

2.3.3 Resurgence of *Isochrysis* algae associated with the late Holocene surface water freshening (2.6 ka to present, Unit I) 59

2.4 Conclusion 60

2.5 References 62

Chapter 3: Long chain alkenone distribution provides insight into haptophytes' ecological dynamics and response to climate variation in the Black Sea during the Holocene 70

3.2. Materials and analytical procedure 73

3.2.1 Samples and sampling resolution 73

3.2.2 Alkenone Analysis with RPLC-ESI-qTOF-MS 73

3.2.3 Alkenone-based proxies discussed in this study 74

3. 3 Results 75

3.3.1 Diversity of LCAs in the Black Sea sediment 75

3.3.2 LCAs distribution in the Black Sea sediments 76

3.3.3 C_{37} and C_{38} based proxies 78

3.4 Discussion 79

3.4.1 Factors controlling the distribution of LCAs in the Black Sea 79

3.4.2 Re-evaluating Black Sea's salinity evolution and limitation of $U37K'$ in paleotemperature reconstruction 83

3.5 Conclusion 84

3.6 References 86

Summary and Implications for future research 98

Acknowledgements

The journey didn't start in the year 2020, but much earlier, and all along it's obvious that there's undeniable help and assistance of one – God, the giver of life and from whom all good things flow. I am thankful to God for the opportunities, strength, good health, for my advisor, committee members, family, friends and all my teachers from elementary school to here at the University of Oklahoma.

I am forever grateful to my advisor, Dr. Liu, for being a great mentor and a kind human. I remember vividly his email with which he communicated the offer of admission to me in late February 2020. Even when it looked like I would have to defer my resumption due to the pandemic, he showed his support. I remember how he helped with getting the keys to my apartment and got groceries for me to sustain me the weekend of my arrival. This means so much to me and my family. Learning from you has been inspiring and has equipped me with the knowledge, tools and mindset to be able to tackle both scientific challenges and life situations. Thank you so much!

I appreciate my committee members – Dr. Michael Engel, Dr. Andrew Elwood Madden, Dr. Wei Qin and my advisor, Dr. Liu for their contribution to the success of my research and completion of my dissertation. During my time at the University of Oklahoma, I benefited from learning from many faculty members at the school of geosciences and the knowledge gained here has made me a better geoscientist and human. I appreciate Dr. Lynn Soreghan, Dr. Megan Elwood Madden, Dr. Shannon Dulin, Dr. Richard Lupia, Dr. Mike Soreghan, Dr. Michael Engel, Dr. Brett Carpenter, Late Dr. John Pigott, Dr. Andrew Elwood Madden and Dr. Heather Bedle. I am also thankful to the director of the school of geosciences, Dr. Matthew Pranter.

The contribution of Dr. Yongsong Huang and Dr. Yi Ge Zhang to my research is very much appreciated and I say, “Thank you”. To fellow graduate students of the Geobiology and organic geochemistry research group - Derek, Fred, Junpeng and Chenxi, thank you for our time together and for the stimulating discussions during our seminars. I appreciate the administrative members of staff of the school of geosciences – Leah Moser, Rebecca Fay, Ginger Leivas and Ashley Tullius for their all-time support and efficiency.

My time in Norman has been remarkable, in no small part due to my family of faith – Redeemed Christian Church of God, Praise Center. The times of fellowship, the care and support are all appreciated. To Pastor Phillip Ayeni, thank you for your leadership and love towards me and my family. To the Redeemed-on Campus (ROC) group, thank you for allowing me to serve and for the friendship. You all remain a huge part of my story and experience in Norman.

To my dearest wife, Itunu, doing life with you has been nothing short of absolute blessing. I am grateful for your support, love, and understanding, always. That we went through the journey of doctorate simultaneously is heartwarming and would be forever cherished. To my daughter, Toluwanimi, you are awesome and a joy to behold. I hope you are inspired by our journey. To my loving parents, supportive siblings and wonderful friends, I am thankful for your support and prayers. You all played no small roles.

This degree is dedicated to the glory of God.

Dissertation Abstract

The Black Sea is a site of intense scientific study because of its rich sediment archive. A semi-enclosed marginal sea, the Black Sea has undergone significant paleoceanographic changes during the late Quaternary, most notably its reconnection with the Mediterranean Sea in the early Holocene (~9,500–7,500 years ago) following the last glacial maximum (LGM). During the LGM (~26,500–19,000 years ago), global sea levels dropped by ~120 m, isolating the Black Sea as a freshwater lake until rising waters allowed Mediterranean inflow, first as a gradual incursion (~9,500 years BP) and then as a fully marine connection (~7,500 years BP), leading to the modern stratified water column with a brackish surface layer and anoxic deep waters. This transition is marked by a shift from freshwater lacustrine sediments to marine sapropelic muds, supported by microfossil evidence. The reconnection induced strong salinity-driven stratification, causing oxygen depletion in deeper waters and establishing the Black Sea's permanently anoxic conditions, with a layered water column consisting of an oxic surface layer (0–100 m), a suboxic zone (100–150 m), and a sulfidic anoxic zone (>150 m) dominated by hydrogen sulfide (H_2S). Sedimentary records reveal redox-sensitive geochemical markers such as molybdenum (Mo) and uranium (U) enrichments, pyrite (FeS_2) formation, and high organic carbon preservation due to limited microbial degradation under anoxia.

Lipid biomarkers can provide additional information about the Black Sea's sedimentation, redox and salinity evolution history. These molecular fossils, combined with isotopic and inorganic geochemical data, reconstruct the lake-to-marine transition, euxinia onset, and anthropogenic impacts, making the Black Sea a critical natural laboratory for studying paleoenvironmental changes, redox evolution, and organic carbon burial in marginal seas. The overarching theme of this work is the application of an integrated biomarker inventory to

understand the co-evolution of the planktonic microbial community and the Holocene Black Sea's salinity and redox changes. A biomarker inventory application rather than the use of single, stand-alone biomarkers is important to capture the existing condition and response of source organisms that dwell at different depths of the water column. This approach potentially helps minimize bias that could arise from the use of single biomarker groups. The work is reported in three chapters.

Chapter 1 concerns lipid inventory of targeted biomarkers to reconstruct unique responses of microorganisms dwelling at different depths of the water column. The targeted biomarkers include Chlorophyll-*a* degradation derivatives, (Chl-*a*-DDs), long-chain alkenones (LCAs), crenarchaeol, overly branched glycerol dialkyl glycerol tetraether (OB-GDGTs) and dialkyl glycerol ethers (DAGEs) which are markers of organisms that dwell at different depths from surface waters to the sea-sediment interface. The inventory reveals differences in microbial dynamics prior to marine incursion, progressive changes during the incursion and dynamics in the Late Holocene. Mediterranean incursion and the resulting stratification impacted chemocline lead to increasing dominance of photosynthesis over chemosynthesis. Euxinia developed gradually in the basin, and it has remained euxinic with the impact of Late Holocene surface freshening stimulating primary productivity but not having much effect on water column stratification.

Chapter 2 focuses on characterizing the unique response of algae versus other photosynthetic organisms to salinity and redox changes. A potential proxy that can help with discriminating Isochrysidales algae from other photosynthetic sources is also discussed. Prior to the incursion, primary productivity was low and relative abundance of other phytoplanktons (proxied by chlorophyll-*a*-degradation derivations) to haptophytes were stable, with Chl-a-

DDs/LCAs values ranging between 0.7 and 1.6. The $\delta^{13}C_{org}$ and $\delta^{15}N_{org}$ data show large variability, likely reflecting mixtures of terrestrial and aquatic organic matter. Isochrysis algae were not well adapted to increasing salinity that accompanied the Mediterranean incursion with estimated concentration dropping to lowest values as marine incursion continued. Progressive increase in TOC, positive carbon isotopic excursion and progressive increase of $\delta^{15}N_{org}$ support the idea of increased primary productivity and enhanced preservation, although the increased productivity was mainly by other phytoplankton groups. There is resurgence in Isochrysis algae with Late Holocene surface water freshening.

Chapter 3 details the detection and distribution of long-chain alkenones and haptophytes' ecological dynamics and response to climate variation in Holocene. Using reversed-phase liquid chromatography electrospray ionization quadrupole time-of-flight (RPLC-ESI-qTOF-MS) LCAs with 37 to 40 carbons, with unsaturation degrees ranging from di- to tetra unsaturated as well as methyl- and ethyl-compounds were detected and quantified. Baseline resolution was achieved for C_{37} alkenone double bond isomers as well as distinct separation of C_{38Me} and C_{38Et} alkenone peaks. A novel discovery is the decrease in the abundance of tetra-unsaturated alkenones with increasing carbon chain length and the intolerance of tetra-unsaturated alkenone-producing haptophytes to elevated salinity.

Chapter 1: Integrated biomarker inventory reveals the progressive evolution of Black Sea microbial community in the Holocene

Authors: Olawale O. Alo[1*], Junpeng Fu[1], Wenshuo Zhao[1], Yi Ge Zhang[2], Xiao-Lei Liu[1]

Affiliations: [1]School of Geosciences, University of Oklahoma, Norman, OK 73019, USA.

[2]State Key Laboratory of Isotope Geochemistry, Guangzhou Institute of Geochemistry, Chinese Academy of Sciences, Guangzhou, China

Abstract

A lipid biomarker inventory integrating compounds produced by organisms dwelling at different depths of a water column provide great proxies for reconstructing source organisms' response to variable climate and evolving water chemistry conditions. This approach can potentially minimize bias that could arise from the use of a single or stand-alone proxy. A sediment core from western Black Sea, covering Holocene deposition, is analyzed for various classes of biomarkers and integrated into an inventory to study the response of a planktonic microbial community to water chemistry shifts that characterized the Black Sea post glacial maximum. The distributions of chlorophyll-*a* degradation derivatives (Chl-*a*-DDs) and long-chain alkenones (LCAs) record changes of primary productivity in the oxic photic zone of the Black Sea water column. The profile of crenarchaeol (and its isomer), produced by ammonia-oxidizing archaea – *Thaumarchaeota,* reflects the dynamics of the chemoautotrophic microbial community dwelling at the base of the photic zone (top chemocline). Overly branched glycerol dialkyl glycerol tetraethers (OB-GDGTs), produced by yet unknown anaerobic bacteria, serve as excellent markers for the abundance of anaerobes in the deeper, more anoxic water, while dialkyl glycerol ethers (DAGEs) are used to reconstruct the activity of benthic sulfate-reducing bacteria. Photo- and chemoautotrophs thrived in the surface to intermediate waters prior to the development of euxinia. Low records of estimated concentrations of phototrophs at this interval can be attributed to an oxygenated water column that does not support preservation. In the deep(er) waters, estimated abundances of anaerobic and sulfate-reducing bacteria increases due to a thriving primary producer community in the surface waters that provide organic carbon to the deep-dwelling heterotrophic community, aided by vertical water column mixing. There is a shift in the microbial community dynamics with the onset of euxinia, corresponding to the sapropel Unit III – Unit II boundary. Increasing salinity levels and changing redox conditions at this stage result in decreasing abundance of LCA-producing algae with Chl-*a*-DDs-source organisms becoming the dominant photoautotroph. A shoaling chemocline with developing anoxia resulted in an initial decline in chemoautotrophy likely due to restriction in nutrient circulation. A persistent decrease in OB-GDGTs and DAGEs profile up to the sapropel Unit I support the hypothesis that the water column remained stratified until the present day, even though there is evidence of Late Holocene freshening in the surface water.

1.1 Introduction

Lipid biomarkers have been successfully applied in reconstructing past environmental conditions (e.g. Bendle et al., 2009; Berke, 2018; Eglinton and Eglinton, 2008; Naeher et al., 2022; Natalicchio et al., 2017;Turich and Freeman, 2011), understanding biogeochemical processes (Connock and Liu, 2023; Kim and Zhang, 2023; Lattaud et al., 2021; Lipsewers et al., 2018) and identifying organic matter source (Bianchi et al., 2002, 2007; Mitra and Bianchi, 2003), among other applications. However, reliance on single lipid biomarkers can present interpretative challenges due to susceptibility to diagenetic overprinting, and the production of similar molecules by diverse organisms. These constraints have prompted the need for an integrated lipid biomarker approach—one that combines multiple biomarker classes and contextualizes their relative abundances and distributions within broader geochemical and ecological conditions.

The water column is often characterized by variable light penetration and chemical species distribution with different microbial communities inhabiting depths having their physiology adapted to the variable light and redox conditions. Biomarker inventory that targets molecular fossils of source organisms dwelling at different depths can therefore minimize bias and aid a more holistic view of a microbial community's response to climate- or anthropogenic-induced water chemistry changes.

The Black Sea water level rise following the last deglaciation that led to the re-connection of the Black Sea with the Mediterranean Sea (Aksu et al., 2002; Bahr et al., 2008; Hiscott et al., 2007; Lister et al., 2015; Major et al., 2002; Ryan et al., 1997) must have resulted in abrupt water chemistry shifts. The Black Sea is separated from the Marmara Sea and Mediterranean Sea by shallow sills and forms the world's most anoxic (Abrajano et al., 2002;

Coolen et al., 2013; Hay et al., 1991; Huang et al., 2000) and the largest land-locked marine basin, approximately 2200 m deep (Bahr et al., 2008; Giosan et al., 2012; Rank et al., 1999; Repeta, 1993). The present-day hydrology of the Black Sea water column is characteristic of an estuary, with a stable pycnocline between 100 to 200 meters that separates a brackish surface water from a saline deep water (Özsoy et al., 2002). Water column stratification with reduced ventilation in deep water is the leading cause of anoxic conditions below approximately 150 m depth. This is corroborated by the $\delta^{18}O$ values of Black Sea waters which vary from - 2.8‰ in the upper 50 m to ~ - 1.8‰ in the more saline water below 200 m (Rank et al., 1999).

The Black Sea water column is highly stratified with an uppermost 200 m oxic to sub-oxic layer, separated from a lower anoxic and sulfidic water column that extends down to 2130 m (Schubert et al., 2006; Sorokin, 2002. The Black Sea, having undergone salinity transition in addition to a redox-stratified water column, provides a suitable sediment record for the deployment of an analytical protocol that integrates biomarkers from different classes from a single run to investigate the correlated co-evolution of a planktonic microbial community with evolving water chemistry and redox conditions.

In this study, we present a comprehensive investigation on the evolution of multiple interlinked microbial groups that accompany the flooding of the Black Sea during the last deglaciation.

1.2. Study Location and methods

1.2.1 Geological setting

The Black Sea (Fig 1.1) is a Cretaceous – Paleogene back arc basin covering a surface area in excess of 420,000 km^2 (Nikishin et al., 2015; Starostenko et al., 2004; Zonenshain and Pichon, 1986). The margins of the Black Sea are characterized by passive continental shelves,

particularly the wide northwestern shelf, which receives significant sediment input from major rivers such as the Danube, Dnieper, and Don (Panin and Jipa, 2002). The Black Sea's geological evolution is closely tied to the tectonic history of the surrounding Alpine-Himalayan orogenic belt, particularly the closure of the Tethys Ocean and the ongoing collision between the Eurasian and African-Arabian plates (Nikishin et al., 2015). It is a composite of the western Black Sea basin and the eastern Black Sea basin, separated by the Andrusov Ridge formed from continental crust submerged below 5 – 6 km thick sediment (Finetti et al., 1988; Nikishin et al., 2003; Starostenko et al., 2004; Tugolesov et al., 1985). These two deep sub-basins have different underlying geology and sediment thicknesses. While the western Black Sea is underlain by oceanic to suboceanic crust with a sedimentary cover up to 19 km thick, the eastern Black Sea basin is underlain by about 10 km thinned continental crust and has up to a 12 km thick sediment pile (Nikishin et al., 2003). Being a part of the ancient Tethys and a site of ancient marine sedimentation until its connection to the Mediterranean was severed, the Black Sea was a site of marine sedimentation that has been greatly influenced by climate (Hsü and Kelts, 1978). The sedimentary deposits in the Black Sea basin have been divided into at least five units based on seismic data: the Upper Cretaceous, Paleocene – Eocene, Oligocene – Lower Miocene, Upper Miocene, and Pliocene – Quaternary (Beloussov and Volvovsky, 1989; Tugolesov et al., 1985). The Upper Cretaceous unit (5–6 km west, 3–4 km east) is carbonate-rich (Tugolesov et al., 1985). The Palaeocene–Eocene unit (5 km west, 3 km east) comprises terrigenous and carbonate rocks (Tugolesov et al., 1985). The Oligocene–Lower Miocene (Maikopian) complex (up to 5 km west, 4 km east) consists of clays (Beloussov and Volvovsky, 1989; Tugolesov et al., 1985). The Middle–Upper Miocene unit is terrigenous, ranging from hundreds of meters to 3 km thick, while the Pliocene–Quaternary unit (2–3.5 km) is predominantly clay (Beloussov and

Volvovsky, 1989; Tugolesov et al., 1985). All sequences are nearly horizontal, with no significant deformation (Tugolesov et al., 1985). The lower sedimentary cover's stratigraphy remains poorly constrained (Beloussov and Volvovsky, 1989; Finetti et al., 1988; Robinson, 1997; Tugolesov et al., 1985). Aptian–Albian rift units may underlie the Upper Cretaceous. Normal faults in the basement suggest an extensional origin (Finetti et al., 1988; Robinson et al., 1996; Tugolesov et al., 1985), supported by the adjacent Cretaceous calc-alkaline volcanic belt along the Pontides. This evidence supports a back-arc basin model (Görür, 1988; Nikishin et al., 1998; Okay et al., 1994; Robinson, 1997; Zonenshain and Pichon, 1986;). During the last glacial period and the 'lake stage' of the Black Sea, the Black Sea was isolated from the Marmara and Mediterranean Seas.The surface water during this time was brackish (Aksu et al., 2002) and sources of sediment input and runoff were the rivers (Fig. 1.2). However, the onset of the last interglacial period resulted in a rise of global sea level that led to a marine incursion. This marine incursion is evinced by a progressive appearance of some salt-tolerant foraminifera species in the Black Sea whose $CaCO_3$ shells show marked changes in the $\delta^{18}O$ (Aksu et al., 2002; Ryan et al., 1997). This latest reconnection of the Black Sea to the Mediterranean has been dated to have occurred at 7.5 ka BP (Ryan et al., 1997).

The samples used for this study are from the Giant Gravity Core (GGC18) collected from the western portion of the Black Sea (Fig. 1.1) in 2006 during cruise AK06 on the R/V Akademik (Coolen et al., 2009; Filipova-Marinova et al., 2013; Huang et al., 2021). Thirteen subsamples covering 11.7 ka, spread into three units, I, II and III, following Unit division points defined by Hay et al., (1991) were analyzed for lipid biomarkers.

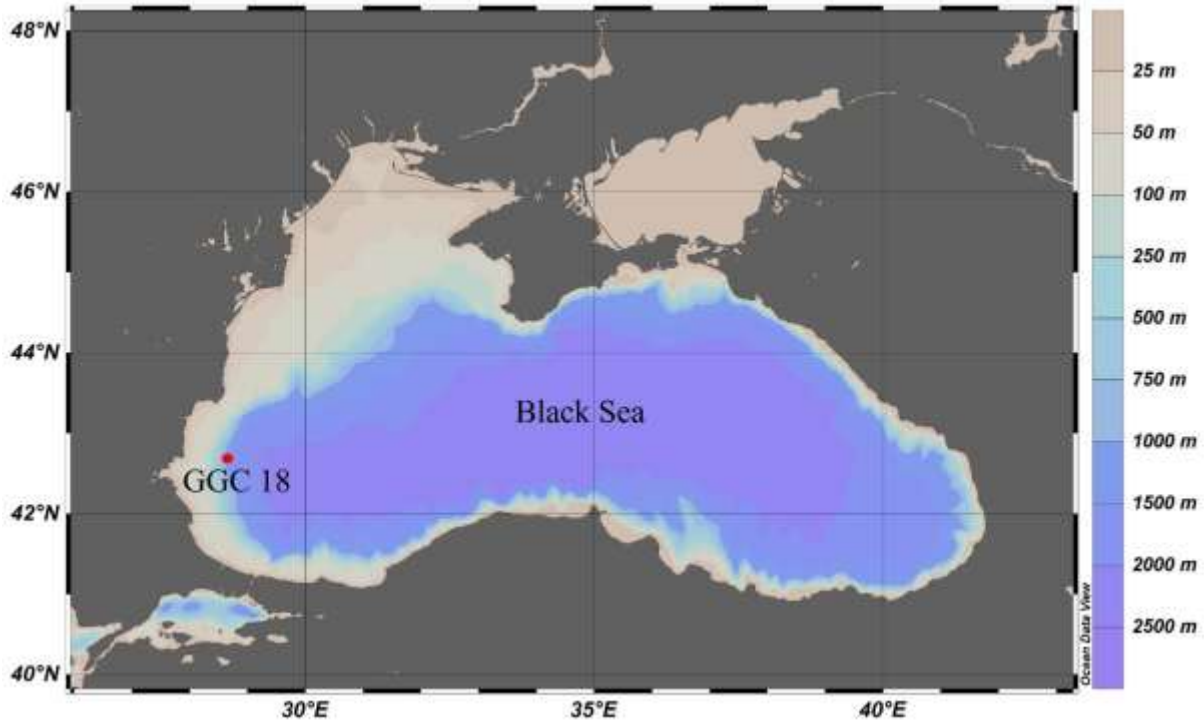


Figure 1.1: Ocean data view image showing the geographic locations of the Black Sea and the Marmara Sea. The Mediterranean Sea is located west of the Marmara Sea (Generated using Ocean data viewer, https://odv.awi.de).

The combination of ^{14}C AMS dating of bulk organic carbon that covered samples from Units I and II (Coolen et al., 2009) and the result of dating of samples from 131 cm, 153 cm, 162 cm, 206 cm, 262 cm, and 334 cm covering Unit III (Huang et al., 2021) provided an age model for the study interval. Huang et al (2021) calibrated the ages using the IntCal13 curve (Reimer et al., 2013) while ages from Coolen et al., (2009) were calibrated using the Marine13 curve from the Bacon 2.2 package and corrected for reservoir age offsets based on data from Yanchilina et al. (2017).

1.2.2 Sample preparation and lipid analysis

Sample preparation and analytical procedure is modified after Connock et al., (2022). Approximately 0.5 g from each of the freeze-dried samples was transferred to 4ml vials, and 500 ng of internal standards – C_{46} glycerol trialkyl glycerol tetraether (C_{46}-GTGT) and Ni tetraphenylporphyrin (Ni-TPP), were added for quantitative analysis of targeted compounds. To recover the total lipid extract (TLE) of each sample, 1.5 ml of Dichloromethane (DCM): Methanol (MeOH) (1:1) solution was added, vortexed to achieve homogenization, followed by ultrasonication in water bath for twenty minutes. The extraction of TLE through sonication was followed by centrifugation for five minutes at 3000 rpm after which the supernatant was carefully transferred to a 2 ml vial and gently blown down under N_2 stream. This procedure (adding 1.5 ml 1:1 DCM:MeOH, ultrasonication, centrifugation, transferring and drying under N_2 stream) was repeated two more times and then 1.5 ml of pure DCM was used for the fourth extraction. The combined TLE of each sample was redissolved in 1 ml pure MeOH, ultrasonicated for 10 minutes, centrifuged at 3000 rpm for five minutes and 500 µl (of the TLE redissolved in MeOH) was transferred into a 2 ml injection vial for lipid analysis. LC-qToF-MS was performed with an Agilent 1290 series UPLC system coupled to Agilent 6530 qTOF mass spectrometer through an Agilent jet stream dual electrospray ionization (AJS-ESI) interface. The ESI drying gas (N_2) temperature was set at 300°C, the N_2 flow rate was 8 L min^{-1} and the nebulizer gas (N_2) pressure was 35 psi. The qTOF parameters were set to: capillary voltage 3.5 kV, fragmentor voltage 175 V; skimmer voltage 65 V and octupole voltage 750 V in auto MS/MS scanning mode with MS range of m/z 50-2000 and MS/MS range of m/z 20-2000. Separation of compounds was achieved by injecting 10 µl sample onto an ACE UltraCore Super C_{18} column (5 µm, 2.1 × 250 mm, ACE, Aberdeen, UK) maintained at 45°C. LC program was

set at a flow rate of 0.2 mL min^{-1}, first hold 100% A for 5 min, and to 70% A and 30% B in 25 min, followed by a gradient to 50% B at 50 min and hold for 5 min, and finally re-equilibrated with 100% A at a flow rate of 0.4 mL min^{-1} for 5 min, where eluent A was 95: 5: 0.04 :0.10 of methanol/H_2O/formic acid/14.8 M NH_3(aq.) and B was 50: 50: 0.04: 0.10 of hexane/2-propanol/formic acid/14.8 M NH_3(aq.).

1.2.3 Biomarker inventory

Depth zones of the water column with unique physical and chemical properties are inhabited by microorganisms with distinct physiologies and metabolisms. In this study, a lipid biomarker inventory was analyzed to study the progressive evolution of microbial communities dwelling at different depths as water chemistry changed in the Black Sea during its last transition. This lipid biomarker inventory is composed of five groups of compounds, Chl-a-DDs, LCAs, crenarchaeols, OB-GDGTs, and DAGEs (Fig. 1.2).

1.2.3.1 Chlorophyll-*a*-Degradative Derivatives

Tetrapyrroles refer to a class of compounds whose molecules have four rings of the pyrrole type, generally linked together by single-atom bridges between the alpha positions of the five-membered pyrrole rings (Moss, 1986). They are either linked in a linear or cyclic manner via methine bridges (Layer et al., 2010). Linear tetrapyrroles include heme breakdown products, phycobilins and luciferins while cyclic tetrapyrroles include porphyrins, chlorins, corrins and tetrahydrocorphin. Chlorophylls are a structurally and functionally distinct group of macrocyclic tetrapyrrole pigments that may occur at the porphyrin, chlorin or bacteriochlorin oxidation levels (Grimm, 2006). The macrocyclic structure of chlorophyll may present modifications on the oxidation state of the aromatic system or may be associated with different transition metals, while side-chain substituent undergoes other transformations (Roca et al., 2016). Chlorophylls

are found in diverse plants, algae and cyanobacteria (Pareek et al., 2017). Bacteriochlorophylls occur in various phototrophic bacteria and the source organisms include purple bacteria, heliobacteria, green sulfur bacteria, chloroflexi, *Chloracidobacterium thermophilum*. An important application of the tetrapyrroles is their role as a proxy for primary productivity. In this study, transformative derivative of chlorophyll-*a* which are classified under several sub-categories (Tables S1.2- S1.4) are used in combination with long chain alkenones as biomarkers for phytoplankton in studying the response of microbial community to the reconnection of the Black Sea to the Mediterranean.

1.2.3.2 Long-chain Alkenones

The LCAs, a series of C_{37}-C_{40} containing two to four unsaturated methyl and ethyl ketones (Liu et al., 2009; Pearson et al., 2008; Prahl et al., 1988), are an important class of biomarkers for haptophytes in marine environments. They are ubiquitous and often well preserved in marine sediments (Pearson et al., 2008). Haptophytes are unicellular phytoplankton and together with cyanobacteria, diatoms, dinoflagellates and prasinophytes make up the bulk of primary producers in the ocean (Kaiser et al., 2019). This therefore makes them an important biomarker for primary productivity. The Black Sea, having undergone salinity changes since the last deglaciation, the alkenone records can help to better understand and to characterize these changes and by implication can be applied to study the effect of salinity changes on the primary producers.

1.2.3.3 Crenarchaeols

Isoprenoidal glycerol dialkyl glycerol tetraethers (iso-GDGTs) are key membrane lipids of archaeal origin (Koga and Morii, 2005, 2007; Sinninghe Damsté et al., 2018). They have core structures that have been identified using a variety of techniques often designated as GDGTs-0 to

-8 where the numbers denote internal cyclopentane rings (Pearson and Ingalls, 2013; Schouten et al., 2013). Contrary to earlier views, archaea have been shown not to be limited to organisms that inhabit extreme conditions (Eglinton and Eglinton, 2008; Pearson and Ingalls, 2013; Sinninghe Damsté et al., 2002). *Thaumarchaeota*, a ubiquitous, ammonium-oxidizing group of archaea in marine environments, have membrane lipids that contain a specific GDGT called crenarchaeol. Crenarchaeol, which in addition to four cyclopentane rings contains a cyclohexane moiety (Sinninghe Damsté et al., 2002), with its isomer, are almost exclusively found in *Thaumarchaeota* cultures but not in other archaeal cultures, qualifying it as an exclusive marker for *Thaumarchaeota* (Schouten et al., 2013; de la Torre et al., 2008; Pitcher et al., 2010). They are also important for the nitrogen cycle as they often represent the predominant nitrifiers (e.g. Leininger et al., 2006) Although the most common application of crenarchaeol have been in paleoclimatology, as paleothermometers, (Eglinton and Eglinton, 2008; Pearson and Ingalls, 2013; Schouten et al., 2002), they can be successfully used as biomarkers for ammonia-oxidizing archaea and the chemocline. The oxic, epipelagic zone of the water column inhabited by phytoplanktons is often succeeded by the chemocline in the suboxic, mesopelagic zone.

1.3.4.2 Overly Branched GDGTs

Branched GDGTs (Br-GDGTs) are non-isoprenoidal GDGTs with more diverse molecular structures than iso-GDGTs and generally of bacterial origin found in diverse environments (Sinninghe Damsté et al., 2000; Weijers et al., 2007; De Jonge et al., 2014; Tierney and Russel, 2009; Li et al., 2018; Liu et al., 2012a). Overly branched GDGTs (OB-GDGTs) are a sub-class of Br-GDGTs with higher degree of methylation than Br-GDGTs. Their in-situ production in anoxic marine water has been demonstrated (Liu et al., 2014) and in this study, OB-GDGTs are applied as biomarkers to monitor the development of a deep anoxic water

column during the last transition of the Black Sea. Non-isoprenoidal, branched GDGTs do not have as many abundant reported lipids as isoprenoid GDGTs except for sparse amounts of GDGT-I identified from cultures of two members of the *Acidobacteria* (Weijers et al., 2006). Through derivatization and NMR spectroscopy, the stereochemistry of the glycerol moiety of branched GDGTs has been shown to be the inverse of archaeal isoprenoid GDGTs (Weijers et al., 2006) which shows a distinct evolutionary difference between membrane lipids of bacteria and archaea, affirming bacteria as the source. The concentration of OB-GDGTs has been reported to initially peak in the upper anoxic zone of the Black Sea and then increase towards the deeper anoxic waters (Liu et al., 2014) further corroborating their enhanced in-situ production in the deeper anoxic water column. With this reported trend, OB-GDGTs can serve as important biomarkers for the changes that characterized the deeper, more anoxic water column during the last transition of the Black Sea.

1.2.3.5 Dialkyl Glycerol Ethers (DAGEs)

The prevalence of DAGEs has been reported among lipids of marine mesophilic sulfate-reducing proteobacterium *Desulatibacillum alkenivorans* (Grossi et al., 2015) which supports the biosynthetic pathways to monoalkyl/monoacyl- and dialkylglycerols in anaerobic bacteria. Chemical composition of the cell wall forms a major basis for differentiating between the prokaryotic domains- Archaea and Bacteria (Woese et al., 1990). While bacterial phospholipids have ester bonds linking glycerol moiety with fatty acids, archaeal membrane lipids consist of isoprenoid chains that are covalently bonded to glycerol via ether bonds and these structural differences can be linked to the respective unique ecology and evolution of prokaryotes' domains (Grossi et al., 2015). The prevalence of dialkyl glycerol ether lipids (DAGEs) has been reported among hydrolyzed lipids of marine mesophilic sulfate-reducing proteobacterium

Desulatibacillum alkenivorans (Grossi et al., 2015) which supports the biosynthetic pathways to monoalkyl/monoacyl- and dialkylglycerols in anaerobic bacteria. The DAGEs, therefore, are great markers for tracking the activities of sulfate-reducing bacteria at the sediment-water interface and I use this group of biomarkers that our analytical method can detect to reconstruct how the sulfate-reducing bacterial community responded to the change in water chemistry in the Black Sea during the last transition.

1.3 Results

1.3.1 Lipid biomarker distributions

Based on estimated concentrations and relative abundances of targeted lipid biomarkers (Figs. 1.3 and 1.4), the distribution of biomarkers is described following Units I - III classification. There is pronounced proliferation across source organisms in Unit III, followed by Chl-a-DDs' dominance of phytoplankton community as anoxia developed (Unit II). Unit III shows some dynamic readjusting in the surface water with haptophytes showing a resurgence.

Late Lake Stage to Start of Anoxia Development (Unit III; ~11.7 to 7.6 ka): The present interglacial, the Holocene, was initiated by postglacial warming over the northern hemisphere (Walker et al., 2009) with the accompanying sea-level rise resulting in the reconnection of the Black Sea to the Mediterranean. This unit is made up of over 2 kyr of sediment pile before the reported initial marine incursion at ~9.4 ka (Coolen et al., 2013; Giosan et al., 2009; Huang et al., 2021; Major et al., 2006;). There are observable differences in the composition of water column microbial communities' pre- and post- initial marine incursion in Unit III. Phytoplankton contribution in this stage ranges from 60 – 75% (Fig. 1.4) with the increasing trend in relative abundance of LCAs before the initial marine incursion reversing after the start of the incursion.

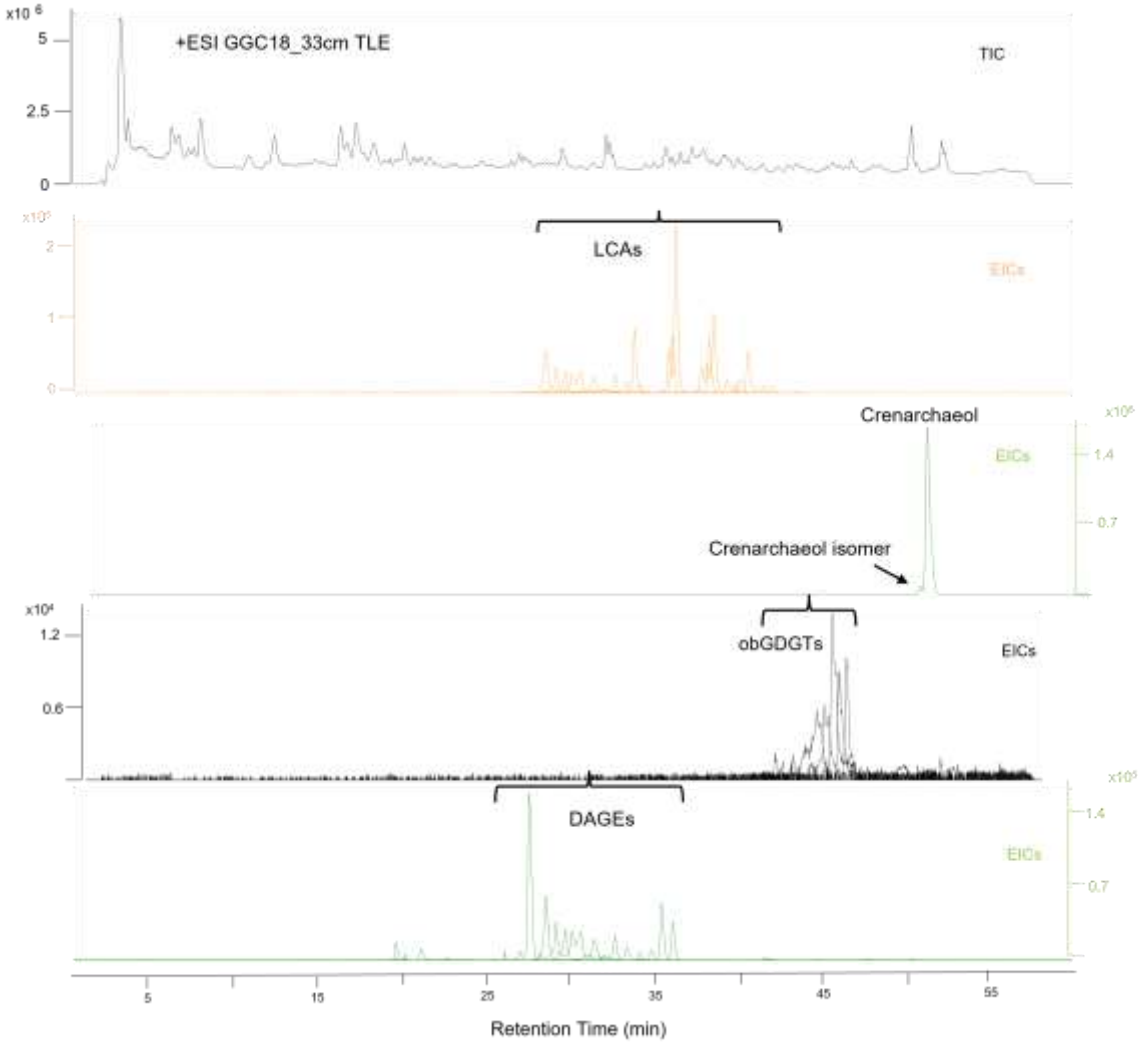


Figure 1.2: Total ion chromatogram (TIC) and combined extracted ion chromatograms (EICs) of some targeted biomarker groups used in this study from LC-qTOF-MS analysis for sample GGC18_33cm. EIC of Chl-*a*-DDs and some representative molecular structure is shown in Fig. 2.1 alongside that of LCAs.

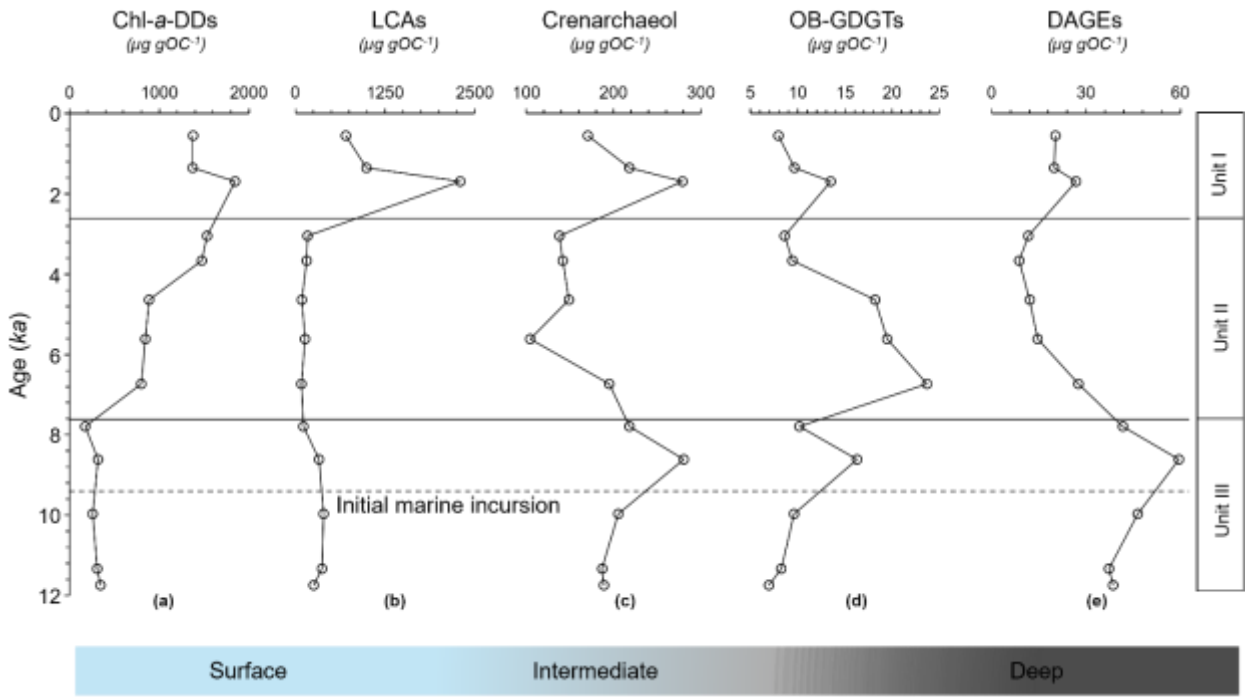


Figure 1.3 Depth profiles of lipid biomarkers through the studied section. From left to right, biomarkers are arranged progressively by the residing depths of source organisms in the water column. Chl-*a*-DDs, LCAs, OB-GDGTs and DAGEs are comprised of multiple compounds (see Fig. 1.2) while Crenarchaeol includes its regio isomer.

Response of anaerobic and sulfate-reducing bacteria community to the change in water chemistry is immediately noticeable, with expanding OB-GDGTs and DAGEs' relative abundance field after the initial incursion in comparison to prior. Based on estimated concentrations, Chl-a-DDs and LCAs have concentrations ranging from 176.3 – 344 µg/ gOC and 112.7 – 391 µg/ gOC, respectively. Crenarchaeols' estimated contribution shows higher concentration in the Lake phase prior to the initial marine incursion with concentration reaching 280.3 µg/ g OC before dropping to 218.1 µg/ g OC at the start of the incursion (Fig. 1.3c). The

concentration of OB-GDGTs and DAGEs showing increasing trend (Fig. 1.3d and e) with ranges 6.9 – 16.3 µg/ gOC and 37.3 – 59.6 µg/ gOC respectively.

Anoxia Development (Unit II; ~ 7.6 – 2.6 ka;): Rising sea levels from the glacial melt that breached the Bosphorus sea and transformed the lake into a marine basin (Ryan et al., 2003; Yanchilina et al., 2017) created a permanent stratification in the water column (Murray et al., 1991). Decomposing organic matter from the surface productivity consumes oxygen faster than it can be replenished (Jørgensen et al., 1991), paving the way for sulfate-reducing bacteria to metabolize organic matter producing hydrogen sulfide effectively turning the basin euxinic (Sorokin, 2002). A change across all reference biomarker groups defines the Unit III – Unit II boundary (Figs. 1.3 and 1.4) with changes in phytoplankton community the most pronounced. Although the relative abundance of phytoplankton in the targeted lipid biomarker pool increased to an average of 84.5 % from 69.3% in Unit III, a new pattern is observed between Chl-*a*-DDs and LCAs with LCAs contributing less than 9% on average in this interval relative to more than 34% it contributes to Unit III. The impact of salinity and redox changes on chemoautotrophs as proxied by crenarchaeol shows it took some time for infiltrating Mediterranean waters to impact the chemocline supported by the initial drop in concentration at the start of Unit II which further declined as anoxia developed (Fig. 1.3c). After ~ 5.6ka there is an increase in crenarchaeol concentration with value maintaining a near stable value until the start of Unit I deposition. Growing anoxia and developing euxinic conditions provide a suitable environment for anaerobic bacteria evinced by an increase in the concentration of OB-GDGTs (Fig. 1.3d). Average concentration of OB-GDGTs at this interval is 15.9 µg/ gOC compared to 10.3 µg/ gOC in Unit III. Further down the water column at the sediment-water interface, the sulfate-reducing bacteria community was adversely impacted by the stratified and euxinic water column. The DAGEs

concentration declined with the development of progressive euxinic conditions with concentrations dropping to as low as 8.8 µg/ gOC (Fig. 1.3e).

Late Holocene (Unit I; ~2.6 – 0.5 ka): The transition from Unit II to Unit I is defined by the invasion of the coccolithophorid *Emiliana huxleyi* (Lamy et al., 2006). This period is characterized by increasing land use in both upper and lower Danube basin (Giosan et al., 2012) and sediments consist of coccolith-bearing layers (Coolen et al., 2009). There is increased productivity in the surface water, the resurgence of LCAs being the most prominent (Fig. 1.3b). Chemoautotrophy also peaked at this stage corresponding with a photosynthetic community. It is assumed that the water column remains stratified and blooming productivity in the surface and intermediate waters seem to provide substrate to the deeper water-dwelling microbes as both OB-GDGTs and DAGEs profiles show increasing trends, though not sustained in both biomarker groups.

In general, the concentrations in this section varies from 1375.4 – 1844.9 µg/g OC for Chl-*a*-DDs, 702.3 – 2294.5 µg/g OC for LCAs, and 170.8 – 279.4 µg/g OC for crenarchaeols. OB-GDGTs concentration ranges between 8 and 13.5 µg/ gOC while for DAGEs, concentration range from 19.9 to 26.9 µg/ gOC. (Fig. 1.3, Table S1.1).

1.4 Discussion

1.4.1 Water column redox and salinity dynamics and effect on photo- and chemoautotrophs

Photo- and chemoautotrophs occupy the base of the food chain, utilizing sunlight and oxidation of inorganic substances respectively as energy sources to synthesize organic compounds from CO_2. The demand for sunlight by photoautotrophs and chemical species, such as ammonia and hydrogen sulfide, by chemoautotrophs implies that the condition of water

column photic zone and chemocline position are major controls on primary productivity. Photic zone anoxia has been reported in the Black Sea (Huang et al., 2000; Repeta et al., 1989; Repeta, 1993; Sinninghe Damsté et al., 1993) with decrease in fluvial input (Buesseler et al., 1991; Codispoti et al., 1991) or increased nutrient loading (Mee, 1992) postulated as possible mechanism for shoaling of the Black Sea redox interface. Figure 1.5 shows the relative abundance of photoautotrophs and chemoautotrophs. The plot reveals a continuous variation across the two classes of primary producers across salinity and redox boundaries. Even without reference to the amount of relative abundance of each class, the pattern of the variation offers insight into the continuous oscillation of productivity zones separated by the chemocline. The relative abundance of each class across the ~ 11.7 ka interval offers insight into the dynamic response of each class to varying salinity, redox and climate condition with an overall dominance of photoautotrophs.

During the limnic stage of the Black Sea prior to Mediterranean incursion, there is no report of photic zone anoxia and our data (Figs. 1.3c and 1.5) show that ammonia oxidation thrived. Possible factors that could have contributed to the observed Crenarchaeols concentration increase include prevailing aerobic conditions that support ammonia oxidation (Hooper et al., 1997). Decomposing organic matter from photoautotrophs could result in elevated ammonia concentration leading to higher substrate availability for ammonia oxidation (Könneke et al., 2005; Zehr and Ward. 2002). Additionally, rising temperature that characterizes the interglacial can increase activity of the *Thaumarchaeota,* although ammonia oxidizing archaea can also adapt to cold waters (Tourna et al., 2011). Decreased light penetration resulting from high turbidity and enhanced productivity in shelf waters (Huang et al., 2000) could also be a possible explanation for the thriving ammonia oxidizing archaea community at this stage as more turbid waters can

increase ammonia oxidation rates. With marine incursion starting at ~ 9.4 ka, there was further change in the primary production dynamics with profound impact on the chemocline. The Mediterranean inflow introduced salty, dense water which sank and created a stable salinity gradient reinforced stratification (Major et al., 2006; Ryan et al., 1997;) which caused permanent separation of upper oxic and bottom sulfidic layers. By estimated concentration (Fig. 1.3), cyanobacteria probably dominated the photoautotrophs as LCAs does not show a good adaptation to increasing salinity. Crenarchaeols profile, after a slight decrease in estimated concentration, maintained an increasing trend. The rate of proliferation by photosynthetic species seem to outpace chemoautotrophs as the relative abundance plot shows an increasing photoautotroph field. The increasing dominance of photosynthetic organisms over chemoautotrophs could be due to significant rise (shoaling) of the chemocline post-Mediterranean inflow. The shoaling chemocline is aided by increased organic matter flux from a more productive surface water (Arthur and Dean, 1998) and enhanced sulfate reduction that produces hydrogen sulfide (Jørgensen et al., 1991). The Late Holocene algal community shift which is attributed to decrease in sea surface salinity because of local hydrological balance (Huang et al., 2021) must have impacted the chemocline. Productivity is stimulated not just within the photosynthetic group but also observed in the higher intermediate water dwelling chemoautotrophs supported by an increase in estimated concentration of crenarchaeols (Fig 1.3c).

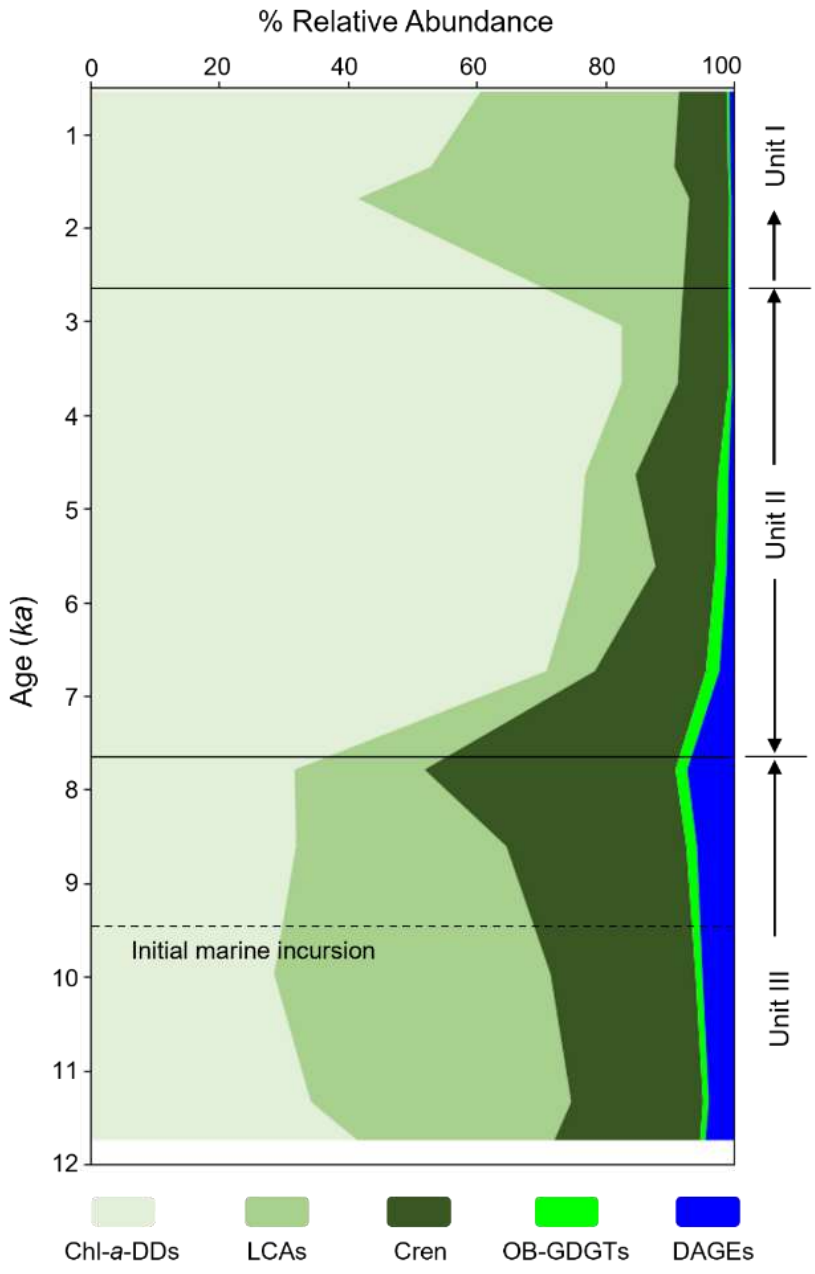


Figure 1.4: Relative abundance plot of targeted biomarkers in the Holocene. Phytoplankton dominates the overall abundance, with shifting proportions between pre-anoxic and anoxic conditions development boundary (~ 7.6 ka). Relative abundance of Crenarchaeol decreases progressively in Unit II and Unit I while OB-GDGTs thrived between the time of initial marine incursion and full anoxia development. There is an expansion of DAGEs relative abundance field with saline incursion but gradually declined water column anoxia.

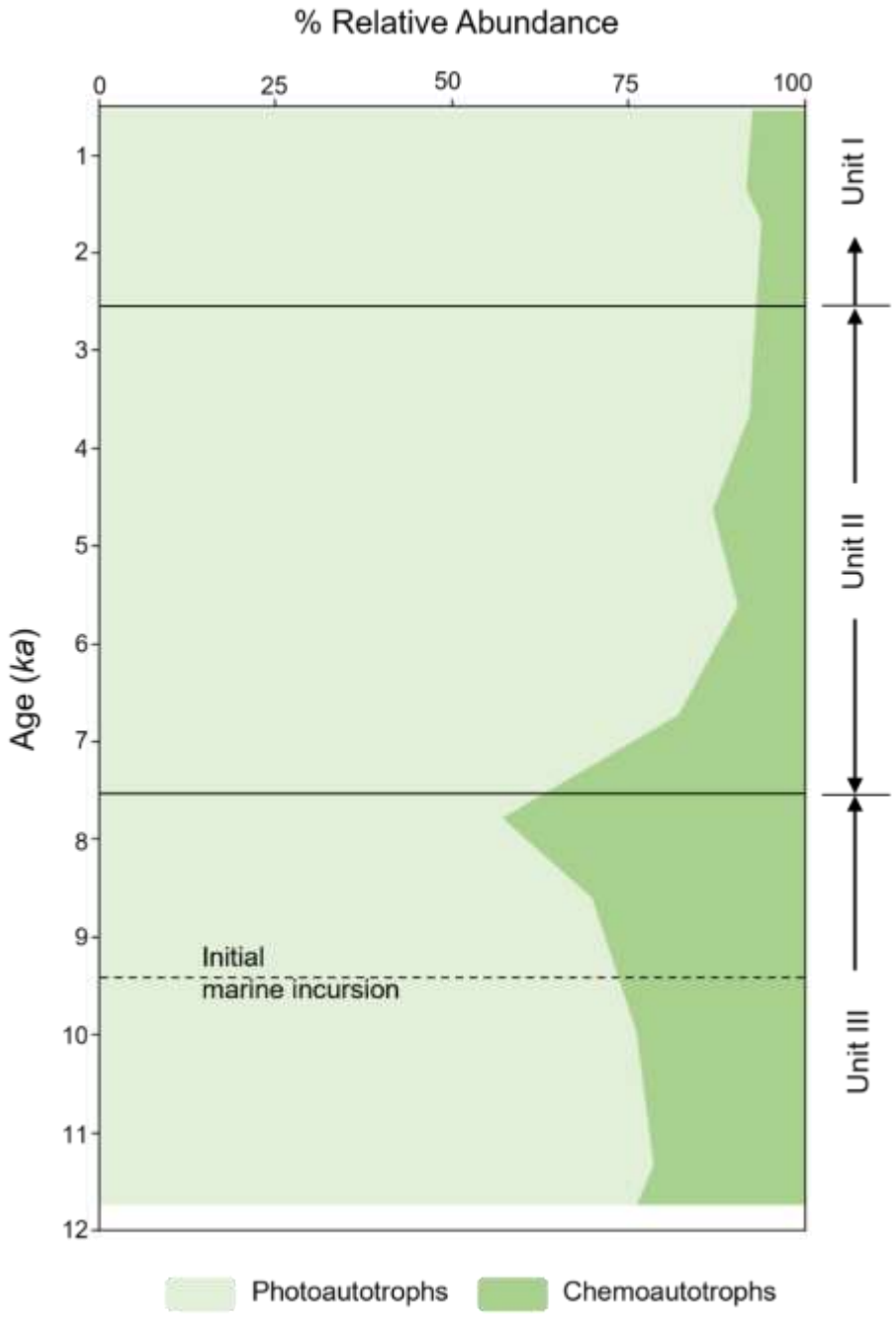


Figure 1.5: Relative abundance plot of photoautotrophs and chemoautotrophs in the Holocene. Photoautotrophs represent the combined abundance of Chl-a-DDs and LCAs while chemoautotroph is taken as the concentration of crenarchaeol and its regio isomer.

1.4.2 Archaeol and Isoprenoid glycerol ether lipids provide insight into the rate of water column anoxia development

The GDGT-0 and crenarchaeol are the dominant iso-GDGTs in archaeal membranes (Pitcher et al., 2010; Schouten et al., 2013; Sinninghe Damsté et al., 2002). While crenarchaeol has a known source - *Thaumarchaeota*, GDGT-0 is less diagnostic of a biological source as it has been reported to be produced by all major groups of archaea (Schouten et al., 2013; Turich and Freeman, 2011). Iso-GDGTs' distribution provides insight into redox evolution in the water column (Fig. 1.6). The GDGT-0 is more abundant in anoxic/euxinic conditions compared to crenarchaeol which is more abundant in oxic conditions. Prior to the onset of basin-wide anoxia (Unit III), crenarchaeol was dominant, which supports an oxic water column condition (Schouten et al., 2002, 2012, 2013). With the onset of anoxia at ~7.6 ka, increasing stratification and rising temperature supported sapropel formation consequently resulting in oxygen depletion and onset of bottom water euxinia (Brumsack, 2006; Eckert et al., 2013; Wegwerth et al., 2018). Rapid anoxia development continued for at least 2 kyr with GDGT-0's increasing trend continuing until at least the start of the dry subboreal climate at ~ 5.2 ka (Coolen et al., 2013). Beyond this period, the water column becomes fully stratified with crenarchaeol and GDGT-0's relative amounts becoming stable.

The ratio of GDGT-0 to crenarchaeol, GDGT-0/Cren (Fig. 1.7b) is a proxy for iso-GDGT source with values < 2.0 suggestive of *Thaumarchaeota* and values > 2.0 suggestive of methanogenic archaea source (Blaga et al., 2009). Computed GDGT-0/Cren in this study show values ranging between 0.28 and 0.97 indicative of a possible *Thaumarchaeota* dominance. However, the plot profile distinctively shows a different pattern between the lake and marine phases. Prior to the start of anoxia development in the basin, values range between 0.28 and 0.35

imply a stronger *Thaumarchaeota* influence. A sharp rise at the transition to Unit II, progressively reaching values up to 0.97, suggests that while *Thaumarchaeota* contribution continues, methanogenic archaea input is likely. This also supports the fact that the Black Sea water column remains anoxic and stratified. Methanogenic archaea in coastal marine sediments account for up to half of all organic matter degradation (Jørgensen, 1982; Lovley et al., 1982) and their heightened presence can be expected in the Black Sea at this stage.

The relative abundance of archaeol to caldarchaeol (GDGT-0), otherwise referred to as ACE index, which has been proposed as a salinity proxy in marine and hypersaline environments (Turich and Freeman, 2011) is computed (Fig. 1.7a). The application of ACE index as a salinity proxy is based on the premise that archaeol are predominant in hypersaline environments with small amounts of caldarchaeol present which decreases inversely with salinity and that marine sites contained little archaeol and abundant GDGTs (Turich and Freeman, 2011). The Black Sea is marine, not hypersaline, and we can expect a dominance of GDGT-0 over archaeol in the marine phase, resulting in low ACE values (Fig. 1.7a). Although the relationship of ACE and salinity could be complex (Günther et al., 2014) as sources of GDGT-0 in various saline environments needs to be constrained before applying as a salinity proxy, estimated ACE index supports salinity trend in the Black Sea, corroborating GDGT-0/Cren (Fig. 1.7b). This highlights the coupling of redox and salinity in the Black Sea.

One of the most common applications of iso-GDGTs is in sea surface temperature (SST) reconstruction using Tetraether index of tetraethers consisting of 86 carbon atoms (TEX_{86}) (Kim et al., 2008, 2010; Schouten et al., 2002; Zhang and Liu, 2018; Zhang et al., 2016;). Estimated TEX_{86} values do not seem to correlate with the known temperature trend of the Black Sea, highlighting its limited applicability to SST reconstruction in the Black Sea (Fig. 1.7c). This can

be linked with the concern of ambiguity as to where in the water column TEX_{86} signal originates from (Zhang and Liu, 2018) with the export depth of *Thaumarchaeota,* the principal archaea group responsible for TEX_{86} signal possibly extending beyond the photic zone. Also, the Black Sea has a huge bacterial and archaeal-rich water body below a couple of hundred meters of water column, with oxygen only present in surface water. There are large amounts of photosynthetic bacteria at the photic zone of the anoxic waters, and TEX_{86} lipids are possibly made in the anoxic water column, not in the surface waters. A similar observation has been reported in the Red Sea, also with elevated salinity, where SST reconstruction from iso-GDGTs was not successful (Kim et al., 2010).

1.4.3 Effects of water column stratification on deep water microbial community.

The targeted biomarkers for the deep water used in this study are OB-GDGTs, produced by unknown anaerobic bacteria, and DAGEs produced by sulfate-reducing bacteria (Fig 1.3 d and e). Together, they provide insight into microbial activities in the deep water, extending into the sediment-water interface. While there appears to be coupling between anaerobic and sulfate-reducing bacteria in the lake phase and before basin-wide anoxia development, there is an opposite relationship with progressive anoxia development. Prior to marine incursion, increasing OB-GDGTs profile suggests decomposing organic matter from high productivity in surface water coupled with vertical mixing of the water column ensure delivery of substrate to heterotrophic bacteria in the deepwater. Alternatively, decomposing organic matter from high surface water productivity could have rapidly depleted oxygen in the water column inducing water column anoxia that supports in-situ OB-GDGTs source organism proliferation.

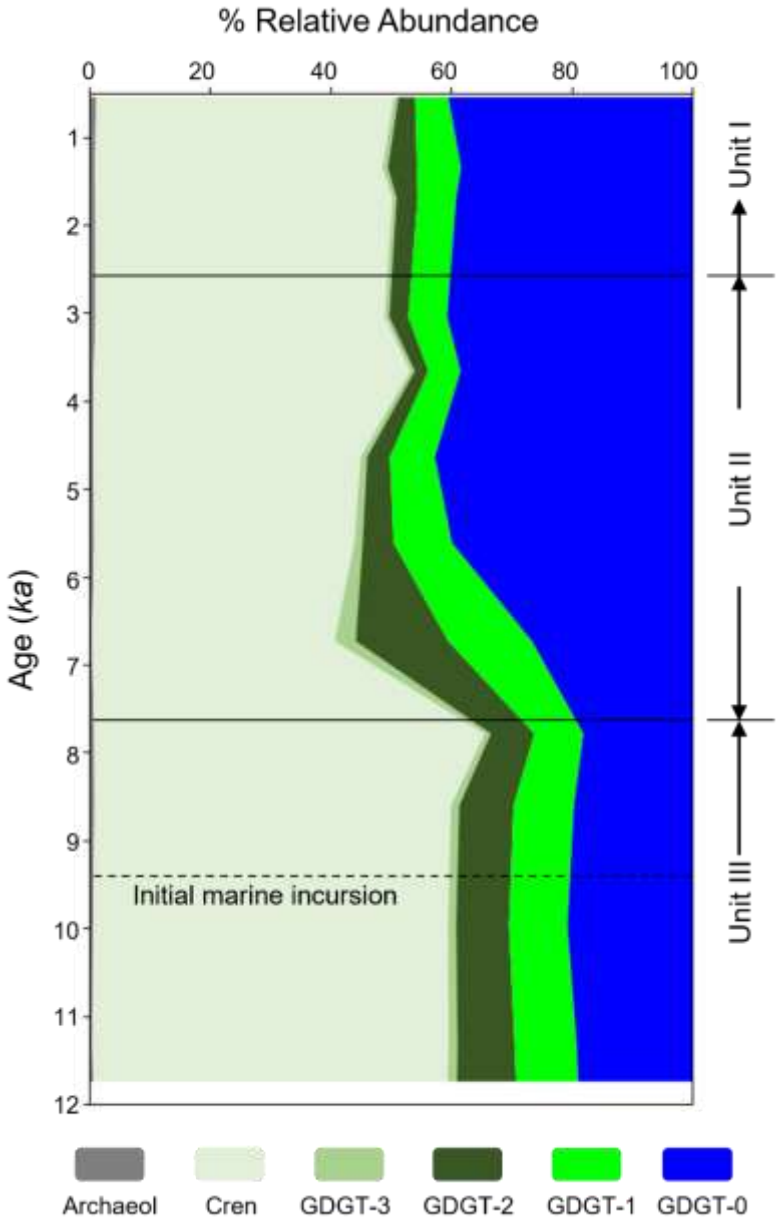


Figure 1.6: Relative abundance plot of iso-GDGTs showing their distribution in the Holocene section. GDGT-0 and Crenarchaeol (and its isomer) have the highest relative abundance with abundance decreasing with increasing number of pentane rings. The distribution also shows the higher abundance of GDGT-0 in anoxic conditions with Crenarchaeol showing a reverse trend.

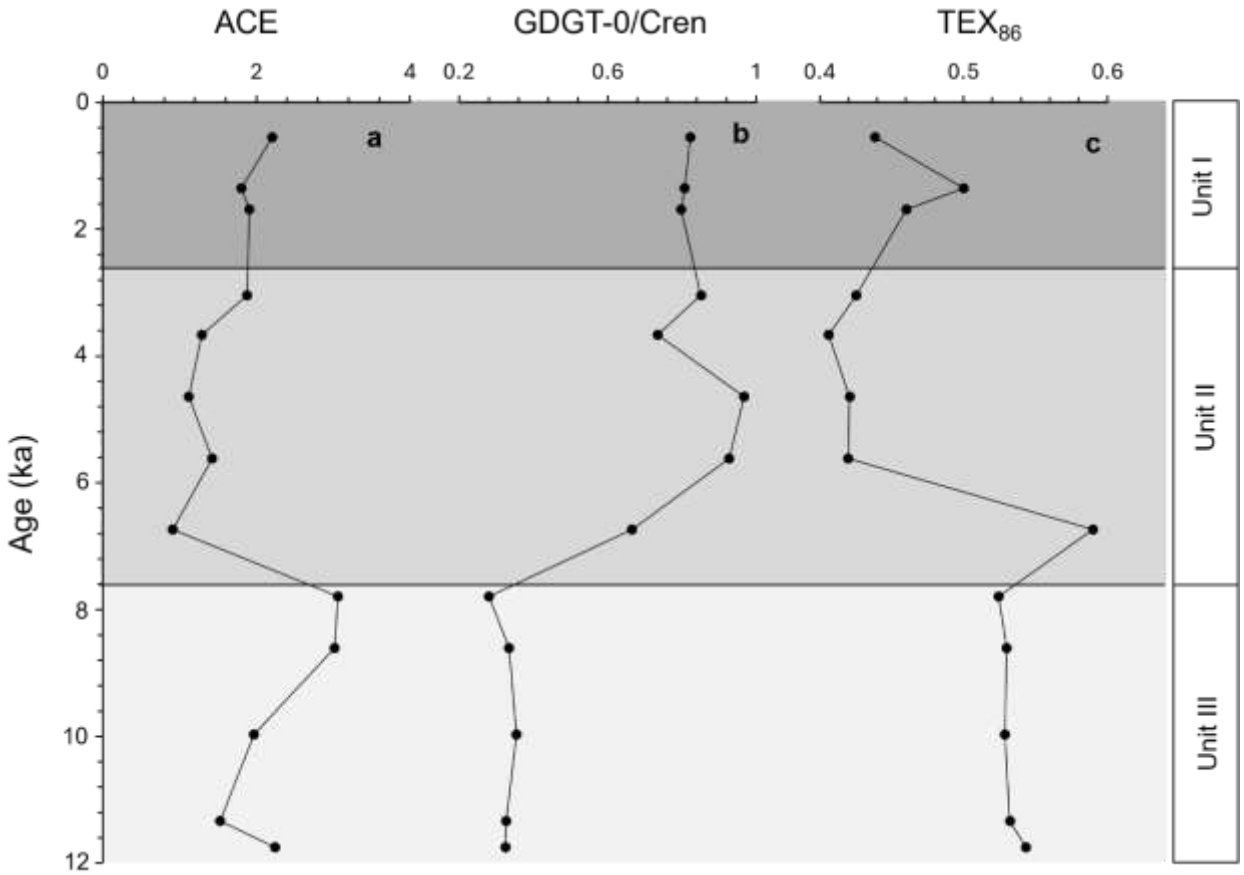


Figure 1.7: Isoprenoid GDGT proxies (a) ACE, the ratio of archaeol to GDGT-0 computed after Turich and Freeman (2011) and Li et al., (2016) shows the limitation of this proxy in tracking salinity in the Black Sea(b) GDGT-0/Cren ratio, a proxy for evaluating the contribution of GDGT-0 contributed by methanogens (Blaga et al., 2009; Bechtel et al., 2010) and (c) TEX_{86} – a sea surface temperature proxy (Schouten et al., 2002)

There are numerous methane seeps in the Black Sea that contribute large amounts of methane to the water column (Durisch-Kaiser et al., 2005). Sustained anaerobic methane oxidation by sulfate reducers (Boetius, et al., 2000; Valentine, 2002) perhaps justifies the idea of

a thriving sulfate-reducing bacteria community indicated by increasing DAGEs profile during the lake stage. Concurrently with Unit II sapropel deposition is redoxcline formation because of prevailing euxinic conditions and limited deep-water ventilation (Wegwerth et al., 2018). Progressive anoxia development supported in-situ production of OB-GDGTs (Liu et al., 2014) and suggests the source organism are well adapted to increasing salinity conditions (Fig 1.3d). Microbial dynamics at the sediment-water interface responded differently to the water column becoming euxinic.

Observed declining concentration of DAGEs during anoxia is not consistent with reported bacterial diether glycerol's (DEG) increase with deoxygenation (Naafs et al., 2024). The reason for this is not clear but plausible explanations include depletion of sulfate, the primary electron acceptor, at the sediment-water interface due to high microbial consumption rates or limited replenishment from overlying water. Sulfate limitation can consequently aid alternative microbial metabolism. For example, methanogenic archaea outperforming sulfate reducing bacteria in the absence of sufficient sulfate. Elevated sulfide concentration in the water column ultimately inhibiting sulfate reducing bacteria growth is another possibility. Stratified water column can trap decomposing organic matter due to lack of or insufficient mixing in turn affecting delivery of needed carbon to the sediment surface. In Late Holocene, OB-GDGTs and DAGEs' concentration increasing correspondingly as observed in primary producers could imply water column mixing accompanied the Late Holocene surface water freshening with increased productivity in surface and intermediate waters providing substrate for the deep microbial community.

1.5 Conclusion

This work demonstrates the successful application of a lipid biomarker inventory for better understanding the Holocene distribution of water column depth sensitive biomarker groups in the Black Sea. It reveals the dynamics of the microbial community with water chemistry and redox evolution. Differences in response of phytoplankton groups show varying adaptation of source organisms to evolving salinity and redox. Even with varying responses within a photosynthetic community, photoautotrophy increasingly dominated chemoautotrophy as the Black Sea transitioned from a brackish lake to marine. Isoprenoidal GDGTs provide insight into the rate of anoxia development and the timing of basin-wide anoxia. Inconsistency in paleotemperature reconstruction using TEX_{86} further highlighted the challenge of iso-GDGTs' export depth and the limitation of TEX_{86} as a viable SST proxy in the Black Sea. While iso-GDGTs-based proxies supported the idea of stratified water column during the Late Holocene surface freshening, OB-GDGTs and DAGEs provide a finer resolution that suggests there may be mixing in the water column and/or a return to more brackish condition at this time.

1.6 References

Abrajano, T., Aksu, A.E., Hiscott, R.N., Mudie, P.J., 2002. Aspects of carbon isotope biogeochemistry of late Quaternary sediments from the Marmara Sea and Black Sea. Mar. Geol. 190, 151–164. https://doi.org/10.1016/S0025-3227(02)00346-8

Aksu, A.E., Hiscott, R.N., Kaminski, M.A., Mudie, P.J., Gillespie, H., Abrajano, T., Yaşar, D., 2002. Last glacial–Holocene paleoceanography of the Black Sea and Marmara Sea: stable isotopic, foraminiferal and coccolith evidence. Mar. Geol. 190, 119–149. https://doi.org/10.1016/S0025-3227(02)00345-6

Arthur, M.A., Dean, W.E., 1998. Organic-matter production and preservation and evolution of anoxia in the Holocene Black Sea. Paleoceanography 13, 395–411. https://doi.org/10.1029/98PA01161

Bahr, A., Lamy, F., Arz, H.W., Major, C., Kwiecien, O., Wefer, G., 2008. Abrupt changes of temperature and water chemistry in the late Pleistocene and early Holocene Black Sea. Geochem. Geophys. Geosystems 9, 2007GC001683. https://doi.org/10.1029/2007GC001683

Bechtel, A., Smittenberg, R.H., Bernasconi, S.M., Schubert, C.J., 2010. Distribution of branched and isoprenoid tetraether lipids in an oligotrophic and a eutrophic Swiss lake: Insights into sources and GDGT-based proxies. Org. Geochem. 41, 822–832. https://doi.org/10.1016/j.orggeochem.2010.04.022

Belousov, V.V., Volvovsky, V.S., (eds) 1989. Structure and Evolution of the Earth Crust and Upper Mantle of the Black Sea. M. Nauka Publication [in Russian].Bendle, J.A.P.,

Rosell-Melé, A., Cox, N.J., Shennan, I., 2009. Alkenones, alkenoates, and organic matter in coastal environments of NW Scotland: Assessment of potential application for sea level reconstruction. Geochem. Geophys. Geosystems 10. https://doi.org/10.1029/2009GC002603

Berke, M.A., 2018. Reconstructing Terrestrial Paleoenvironments Using Sedimentary Organic Biomarkers. In: Croft, D., Su, D., Simpson, S. (eds) Methods in Paleoecology. Vertebrate Paleobiology and Paleoanthropology. Springer, Cham. https://doi.org/10.1007/978-3-319-94265-0_8

Bianchi, T.S., Mitra, S., McKee, B.A., 2002. Sources of terrestrially-derived organic carbon in lower Mississippi River and Louisiana shelf sediments: implications for differential sedimentation and transport at the coastal margin. Mar. Chem. 77, 211–223. https://doi.org/10.1016/s0304-4203(01)00088-3

Bianchi, T.S., Wysocki, L.A., Stewart, M., Filley, T.R., McKee, B.A., 2007. Temporal variability in terrestrially-derived sources of particulate organic carbon in the lower Mississippi River and its upper tributaries. Geochim. Cosmochim. Acta 71, 4425–4437. https://doi.org/10.1016/j.gca.2007.07.011

Blaga, C.I., Reichart, G.-J., Heiri, O., Sinninghe Damsté, J.S., 2009. Tetraether membrane lipid distributions in water-column particulate matter and sediments: a study of 47 European lakes along a north–south transect. J. Paleolimnol. 41, 523–540. https://doi.org/10.1007/s10933-008-9242-2

Boetius, A., K. Ravenschlag, C. J. Schubert, D. Rickert, F. Widdel, A. Giesecke, R. Amann, B. B. Jørgensen, U. Witte, and O. Pfannkuche. 2000. A marine microbial consortium apparently mediating anaerobic oxidation of methane. Nature 407:623–626.

Brumsack, H.-J., 2006. The trace metal content of recent organic carbon-rich sediments: implications for Cretaceous black shale formation. Palaeogeogr. Palaeoclimatol. Palaeoecol. 232, 344-361. http://dx.doi.org/10.1016/j.palaeo.2005.05.011.Buesseler,

Buesseler, K.O., Livingston, H.D., Casso, S.A., 1991. Mixing between oxic and anoxic waters of the Black Sea as traced by Chernobyl cesium isotopes. Deep Sea Res. Part Oceanogr. Res. Pap. 38, S725–S745. https://doi.org/10.1016/S0198-0149(10)80006-8

Codispoti, L.A., Friederich, G.E., Murray, J.W., Sakamoto, S., 1991. Chemical variability in the Black Sea: implications of data obtained with a continuous vertical proÆling system that penetrated the oxic/anoxic interface. Deep-Sea Research 38, S691±S710.

Connock, G.T., Liu, X.-L., 2023. Tocopherols and associated derivatives track the phytoplanktonic response to evolving pelagic redox conditions spanning Oceanic Anoxic Event 2. Geobiology. https://doi.org/DOI: 10.1111/gbi.12570

Connock, G.T., Owens, J.D., Liu, X.-L., 2022. Biotic induction and microbial ecological dynamics of Oceanic Anoxic Event 2. Commun. Earth Environ. 3, 136. https://doi.org/10.1038/s43247-022-00466-x

Coolen, M.J.L., Orsi, W.D., Balkema, C., Quince, C., Harris, K., Sylva, S.P., Filipova-Marinova, M., Giosan, L., 2013. Evolution of the plankton paleome in the Black Sea from the Deglacial to Anthropocene. Proc. Natl. Acad. Sci. 110, 8609–8614. https://doi.org/10.1073/pnas.1219283110

Coolen, M.J.L., Saenz, J.P., Giosan, L., Trowbridge, N.Y., Dimitrov, P., Dimitrov, D., Eglinton, T.I., 2009. DNA and lipid molecular stratigraphic records of haptophyte succession in the Black Sea during the Holocene. Earth Planet. Sci. Lett. 284, 610–621. https://doi.org/10.1016/j.epsl.2009.05.029

De Jonge, C., Stadnitskaia, A., Hopmans, E.C., Cherkashov, G., Fedotov, A., Sinninghe Damsté, J.S., 2014. In situ produced branched glycerol dialkyl glycerol tetraethers in suspended particulate matter from the Yenisei River, Eastern Siberia. Geochim. Cosmochim. Acta 125, 476–491. https://doi.org/10.1016/j.gca.2013.10.031

de la Torre, J.R., Walker, C.B., Ingalls, A.E., Könneke, M., Stahl, D.A., 2008. Cultivation of a thermophilic ammonia oxidizing archaeon synthesizing crenarchaeol. Environ. Microbiol. 10, 810–818. https://doi.org/10.1111/j.1462-2920.2007.01506.x

Durisch-Kaiser, E., Klauser, L., Wehrli, B., Schubert, C., 2005. Evidence of Intense Archaeal and Bacterial Methanotrophic Activity in the Black Sea Water Column. Appl. Environ. Microbiol. 71, 8099–8106. https://doi.org/10.1128/AEM.71.12.8099-8106.2005

Eckert, S., Brumsack, H.-J., Severmann, S., Schnetger, B., Marz, C., Frollje, H., 2013. Establishment of euxinic conditions in the Holocene Black Sea. Geology 41, 431-434. http://dx.doi.org/10.1130/G338226.1

Eglinton, T.I., Eglinton, G., 2008. Molecular proxies for paleoclimatology. Earth Planet. Sci. Lett. 275, 1–16. https://doi.org/10.1016/j.epsl.2008.07.012

Filipova-Marinova, M., Pavlov, D., Coolen, M., Giosan, L., 2013. First high-resolution marinopalynological stratigraphy of Late Quaternary sediments from the central part of the Bulgarian Black Sea area. Quat. Int. 293, 170–183. https://doi.org/10.1016/j.quaint.2012.05.002

Finetti, I., Bricchi, G., Del Ben, A, Pipan, M. and Xuan, Z. (1988) Geophysical study of the Black Sea area *Bo//. Geofis. Tear. Appl.* 30, 197-324

Giosan, L., Filip, F., Constatinescu, S., 2009. Was the Black Sea catastrophically flooded in the early Holocene? Quat. Sci. Rev. 28, 1–6. https://doi.org/10.1016/j.quascirev.2008.10.012
Giosan, L., Coolen, M.J.L., Kaplan, J.O., Constantinescu, S., Filip, F., Filipova-Marinova, M., Kettner, A.J., Thom, N., 2012. Early Anthropogenic Transformation of the Danube-Black Sea System. Sci. Rep. 2, 582. https://doi.org/10.1038/srep00582
Görür, N., 1988. Timing of opening of the Black Sea basin. Tectonophysics 147, 247–262. https://doi.org/10.1016/0040-1951(88)90189-8
Grimm, B. (Ed.), 2006. Chlorophylls and bacteriochlorophylls: biochemistry, biophysics, functions and applications, Advances in photosynthesis and respiration. Springer, Dordrecht.
Grossi, V., Mollex, D., Vinçon-Laugier, A., Hakil, F., Pacton, M., Cravo-Laureau, C., 2015. Mono- and Dialkyl Glycerol Ether Lipids in Anaerobic Bacteria: Biosynthetic Insights from the Mesophilic Sulfate Reducer Desulfatibacillum alkenivorans PF2803 ^{T}. Appl. Environ. Microbiol. 81, 3157–3168. https://doi.org/10.1128/AEM.03794-14
Günther, F., Thiele, A., Gleixner, G., Xu, B., Yao, T., Schouten, S., 2014. Distribution of bacterial and archaeal ether lipids in soils and surface sediments of Tibetan lakes: Implications for GDGT-based proxies in saline high mountain lakes. Org. Geochem. 67, 19–30. https://doi.org/10.1016/j.orggeochem.2013.11.014
Hay, B.J., Arthur, M.A., Dean, W.E., Neff, E.D., Honjo, S., 1991. Sediment deposition in the Late Holocene abyssal Black Sea with climatic and chronological implications. Deep Sea Res. Part Oceanogr. Res. Pap. 38, S1211–S1235. https://doi.org/10.1016/S0198-0149(10)80031-7
Hiscott, R.N., Aksu, A.E., Mudie, P.J., Marret, F., Abrajano, T., Kaminski, M.A., Evans, J., Çakiroğlu, A.İ., Yaşar, D., 2007. A gradual drowning of the southwestern Black Sea shelf: Evidence for a progressive rather than abrupt Holocene reconnection with the eastern Mediterranean Sea through the Marmara Sea Gateway. Quat. Int. 167–168, 19–34. https://doi.org/10.1016/j.quaint.2006.11.007
Hooper, A.B., Vannelli, T., Bergmann, D.J., Arciero, D.M., 1997. Enzymology of the oxidation of ammonia to nitrite by bacteria. Antonie Van Leeuwenhoek 71, 59–67.
Hsü, K.J., Kelts, K., 1978. Late Neogene Sedimentation in the Black Sea, in: Matter, A., Tucker, M.E. (Eds.), Modern and Ancient Lake Sediments. Wiley, pp. 129–145. https://doi.org/10.1002/9781444303698.ch7
Huang, Y., Freeman, K.H., Wilkin, R.T., Arthur, M.A., Jones, A.D., 2000. Black Sea chemocline oscillations during the Holocene: molecular and isotopic studies of marginal sediments. Org. Geochem. 31, 1525–1531. https://doi.org/10.1016/S0146-6380(00)00090-5
Huang, Y., Zheng, Y., Heng, P., Giosan, L., Coolen, M.J.L., 2021. Black Sea paleosalinity evolution since the last deglaciation reconstructed from alkenone-inferred Isochrysidales diversity. Earth Planet. Sci. Lett. 564, 116881. https://doi.org/10.1016/j.epsl.2021.116881
Jørgensen, B.B. 1982. Mineralisation of organic matter in the sea-bed—the roleof sulfate reduction. Nature 296:643–645.
Jørgensen, B.B., Fossing, H., Wirsen, C.O., Jannasch, H.W., 1991. Sulfide oxidation in the anoxic Black Sea chemocline. Deep-Sea Res. 38, 1083–1103.
Kaiser, J., Wang, K.J., Rott, D., Li, G., Zheng, Y., Amaral-Zettler, L., Arz, H.W., Huang, Y., 2019. Changes in long chain alkenone distributions and Isochrysidales groups along the Baltic Sea salinity gradient. Org. Geochem. 127, 92–103. https://doi.org/10.1016/j.orggeochem.2018.11.012

Kim, J.-H., Schouten, S., Hopmans, E.C., Donner, B., Sinninghe Damsté, J.S., 2008. Global sediment core-top calibration of the TEX86 paleothermometer in the ocean. Geochim. Cosmochim. Acta 72, 1154–1173. https://doi.org/10.1016/j.gca.2007.12.010

Kim, J.-H., Van Der Meer, J., Schouten, S., Helmke, P., Willmott, V., Sangiorgi, F., Koç, N., Hopmans, E.C., Damsté, J.S.S., 2010. New indices and calibrations derived from the distribution of crenarchaeal isoprenoid tetraether lipids: Implications for past sea surface temperature reconstructions. Geochim. Cosmochim. Acta 74, 4639–4654. https://doi.org/10.1016/j.gca.2010.05.027

Kim, B., Zhang, Y.G., 2023. Methane Index: Towards a quantitative archaeal lipid biomarker proxy for reconstructing marine sedimentary methane fluxes. Geochim. Cosmochim. Acta. https://doi.org/10.1016/j.gca.2023.06.008

Könneke, M., Bernhard, A.E., De La Torre, J.R., Walker, C.B., Waterbury, J.B., Stahl, D.A., 2005. Isolation of an autotrophic ammonia-oxidizing marine archaeon. Nature 437, 543–546. https://doi.org/10.1038/nature03911

Koga, Y., Morii, H., 2005. Recent advances in structural research on ether lipids from archaea including comparative and physiological aspects. Biosci. Biotechnol. Biochem. 69, 2019–2034.

Koga, Y., Morii, H., 2007. Biosynthesis of ether-type polar lipids in archaea and evolutionary considerations. Microbiol. Mol. Biol. Rev. 71, 97–120.

Lamy, F., Arz, H.W., Bond, G.C., Bahr, A., Patzold, J., 2006. Multicentennial-scale hydrological changes in the Black Sea and norther Red Sea during the Holocene and the Arctic/North Atlantic Oscillation. Paleoceanography 21 (1), PA1008. http://dx.doi.org/10.1029/2005PA001184.

Lattaud, J., De Jonge, C., Pearson, A., Elling, F.J., Eglinton, T.I., 2021. Microbial lipid signatures in Arctic deltaic sediments – Insights into methane cycling and climate variability. Org. Geochem. https://doi.org/10.1016/j.orggeochem.2021.104242

Layer, G., Jahn, D., Deery, E., Lawrence, A.D., Warren, M.J., 2010. 7.13 Biosynthesis of Heme and Vitamin B12. Elsevier 55.

Leininger, S., Urich, T., Schloter, M., Schwark, L., Qi, J., Nicol, G.W., Prosser, J.I., Schuster, S.C., Schleper, C., 2006. Archaea predominate among ammonia-oxidizing prokaryotes in soils. Nature 442, 806–809. https://doi.org/10.1038/nature04983

Lipsewers, Y.A., Hopmans, E.C., Sinninghe Damste, J.S., Villanueva, L., 2018. Potential recycling of thaumarchaeotal lipids by DPANN Archaea in seasonally hypoxic surface marine sediments. Org. Geochem. https://doi.org/10.1016/j.orggeochem.2017.12.007

Li, H., Lü, X., Tao, C., Han, T., Hu, P., Zhang, G., Yu, Z., Dong, C., Shao, Z., 2018. Distribution of tetraether lipids in sulfide chimneys at the Deyin hydrothermal field, southern Mid-Atlantic Ridge: Implication to chimney growing stage. Sci. Rep. 8, 8060. https://doi.org/10.1038/s41598-018-26166-1

Li, J., Pancost, R.D., Naafs, B.D.A., Yang, H., Zhao, C., Xie, S., 2016. Distribution of glycerol dialkyl glycerol tetraether (GDGT) lipids in a hypersaline lake system. Org. Geochem. 99, 113–124. https://doi.org/10.1016/j.orggeochem.2016.06.007

Lister, C.J., Hiscott, R.N., Aksu, A.E., Mudie, P.J., 2015. Compositional trends through the Holocene mud succession of the southwestern Black Sea shelf: Implications for sedimentary provenance and water-level history. Sediment. Geol. 316, 13–25. https://doi.org/10.1016/j.sedgeo.2014.11.004

Liu, H., Probert, I., Uitz, J., Claustre, H., Aris-Brosou, S., Frada, M., Not, F., de Vargas, C., 2009. Extreme diversity in noncalcifying haptophytes explains a major pigment paradox in open oceans. Proc. Natl. Acad. Sci. 106, 12803–12808. https://doi.org/10.1073/pnas.0905841106

Liu, X.-L., Summons, R.E., Hinrichs, K.-U., 2012a. Extending the known range of glycerol ether lipids in the environment: structural assignments based on tandem mass spectral fragmentation patterns. Rapid Commun. Mass Spectrom. 26, 2295–2302. https://doi.org/10.1002/rcm.6355

Liu, X.-L., Lipp, J.S., Simpson, J.H., Lin, Y.-S., Summons, R.E., Hinrichs, K.-U., 2012b. Mono- and dihydroxyl glycerol dibiphytanyl glycerol tetraethers in marine sediments: Identification of both core and intact polar lipid forms. Geochim. Cosmochim. Acta 89, 102–115. https://doi.org/10.1016/j.gca.2012.04.053

Liu, X.-L., Zhu, C., Wakeham, S.G., Hinrichs, K.-U., 2014. In situ production of branched glycerol dialkyl glycerol tetraethers in anoxic marine water columns. Mar. Chem. 166, 1–8. https://doi.org/10.1016/j.marchem.2014.08.008

Lovley DR, Dawyer DF, Klug MJ. 1982. Kinetic analysis of competition betweensulfate reducers and methanogens for hydrogen in sediments. Appl EnvironMicrobiol 43:1373–1379.

Major, C., Ryan, W., Lericolais, G., Hajdas, I., 2002. Constraints on Black Sea outflow to the Sea of Marmara during the last glacial^interglacial transition. Mar. Geol. 16.

Major, C.O., Goldstein, S.L., Ryan, W.B.F., Lericolais, G., Piotrowski, A.M., Hajdas, I., 2006. The co-evolution of Black Sea level and composition through the last deglaciation and its paleoclimatic significance. Quat. Sci. Rev. 25, 2031–2047. https://doi.org/10.1016/j.quascirev.2006.01.032

Mee, L.D., 1992. The Black Sea in crisis: a need for concerted international action. Ambio 21, 278±286.

Mitra, S., Bianchi, T.S., 2003. A preliminary assessment of polycyclic aromatic hydrocarbon distributions in the lower Mississippi River and Gulf of Mexico. Mar. Chem. 82, 273–288. https://doi.org/10.1016/s0304-4203(03)00074-4

Moss, G.P., 1986. Nomenclature of Tetrapyrroles. Pure Appl Chem 59, No. 6, 779–832.

Murray, J.W., 1991. The 1988 Black Sea Oceanographic Expedition: introduction and summary. Deep Sea Res. Part Oceanogr. Res. Pap. 38, S655–S661. https://doi.org/10.1016/S0198-0149(10)80002-0

Naafs, B.D.A., Blewett, J., Pancost, R.D., 2024. Bacterial diether lipids as a novel proxy to reconstruct past changes in sedimentary oxygenation. Geochim. Cosmochim. Acta S0016703724003922. https://doi.org/10.1016/j.gca.2024.07.036

Naeher, S., Cui, X., Summons, R. E., 2022. Biomarkers: Molecular Tools to Study Life, Environment, and Climate. *Elements*; 18 (2): 79–85. doi: https://doi.org/10.2138/gselements.18.2.79

Natalicchio, M., Birgel, D., Peckmann, J., Lozar, F., Carnevale, G., Liu, X., Hinrichs, K.-U., Pierre, F.D., 2017. An archaeal biomarker record of paleoenvironmental change across the onset of the Messinian salinity crisis in the absence of evaporites (Piedmont Basin, Italy). Org. Geochem. 113. https://doi.org/10.1016/j.orggeochem.2017.08.014

Nikishin, A.M., Cloetingh, S., Brunet, M.-F., Stephenson, R., Bolotov, S.N., Ershov, A.V., 1998. Scythian Platform and Black Sea region: Mesozoic – Cenozoic tectonic and dynamics.

In: Crasquin-Soleau, S., Barrier, E. (Eds.), Peri-Tethys Memoir 3: Stratigraphy and Evolution of Peri-Tethyan Platforms. Me´moires du Muse´um national d'Histoire naturelle, Paris, vol. 177, pp. 163 – 176.
Nikishin, A.M., Korotaev, M.V., Ershov, A.V., Brunet, M.-F., 2003. The Black Sea basin: tectonic history and Neogene–Quaternary rapid subsidence modelling. Sediment. Geol. 156, 149–168. https://doi.org/10.1016/S0037-0738(02)00286-5
Nikishin, A.M., Okay, A.I., Tüysüz, O., Demirer, A., Amelin, N., Petrov, E., 2015. The Black Sea basins structure and history: New model based on new deep penetration regional seismic data. Part 1: Basins structure and fill. Mar. Pet. Geol. 59, 638–655. https://doi.org/10.1016/j.marpetgeo.2014.08.017
Okay, A.I., Celal Şengör, A.M., Görür, N., 1994. Kinematic history of the opening of the Black Sea and its effect on the surrounding regions. Geology 22, 267. https://doi.org/10.1130/0091-7613(1994)022<0267:KHOTOO>2.3.CO;2
Özsoy, E., Rank, D., Salihoglu, I., 2002. Pycnocline and Deep Mixing in the Black Sea: Stable Isotope and Transient Tracer Measurements. Estuar. Coast. Shelf Sci. 54, 621–629. https://doi.org/10.1006/ecss.2000.0669
Panin, N., Jipa, D., 2002. Danube River Sediment Input and its Interaction with the North-western Black Sea. Estuar. Coast. Shelf Sci. 54, 551–562. https://doi.org/10.1006/ecss.2000.0664
Pareek, S., Sagar, N.A., Sharma, S., Kumar, V., Agarwal, T., González-Aguilar, G.A., Yahia, E.M., 2017. Chlorophylls: Chemistry and Biological Functions, in: Yahia, E.M. (Ed.), Fruit and Vegetable Phytochemicals. John Wiley & Sons, Ltd, Chichester, UK, pp. 269–284. https://doi.org/10.1002/9781119158042.ch14
Pearson, E.J., Juggins, S., Farrimond, P., 2008. Distribution and significance of long-chain alkenones as salinity and temperature indicators in Spanish saline lake sediments. Geochim. Cosmochim. Acta 72, 4035–4046. https://doi.org/10.1016/j.gca.2008.05.052
Pearson, A., Ingalls, A.E., 2013. Assessing the Use of Archaeal Lipids as Marine Environmental Proxies. Annu. Rev. Earth Planet. Sci. 41, 359–384. https://doi.org/10.1146/annurev-earth-050212-123947
Reimer, P.J., Bard, E., Bayliss, A., Beck, J.W., Blackwell, P.G., Ramsey, C.B., Buck, C.E., Cheng, H., Edwards, R.L., Friedrich, M., Grootes, P.M., Guilderson, T.P., Haflidason, H., Hajdas, I., Hatté, C., Heaton, T.J., Hoffmann, D.L., Hogg, A.G., Hughen, K.A., Kaiser, K.F., Kromer, B., Manning, S.W., Niu, M., Reimer, R.W., Richards, D.A., Scott, E.M., Southon, J.R., Staff, R.A., Turney, C.S.M., Van Der Plicht, J., 2013. IntCal13 and Marine13 Radiocarbon Age Calibration Curves 0–50,000 Years cal BP. Radiocarbon 55, 1869–1887. https://doi.org/10.2458/azu_js_rc.55.16947
Pitcher, A., Rychlik, N., Hopmans, E.C., Spieck, E., Rijpstra, W.I.C., Ossebaar, J., Schouten, S., Wagner, M., Sinninghe Damsté, J.S., 2010. Crenarchaeol dominates the membrane lipids of Candidatus Nitrososphaera gargensis, a thermophilic Group I.1b Archaeon. ISME J. 4, 542–552. https://doi.org/10.1038/ismej.2009.138
Prahl, F.G., Muehlhausen, L.A., Zahnle, D.L., 1988. Further evaluation of long-chain alkenones as indicators of paleoceanographic conditions. Geochim. Cosmochim. Acta 52, 2303–2310. https://doi.org/10.1016/0016-7037(88)90132-9
Rank, D., Özsoy, E., Salihoğlu, İ., 1999. Oxygen-18, deuterium and tritium in the Black Sea and the Sea of Marmara. J. Environ. Radioact. 43, 231–245. https://doi.org/10.1016/S0265-931X(98)00094-0

Repeta, D.J., 1993. A high resolution historical record of Holocene anoxygenic primary production in the Black Sea. Geochim. Cosmochim. Acta 57, 4337–4342. https://doi.org/10.1016/0016-7037(93)90334-S

Repeta, D.J., Simpson, D.J., Jorgensen, B.B., 1989. photosynthesis from the distribution of bacterio- chlorophylls in the Black Sea 342, 4.

Robinson, A.G., Rudat, J.H., Banks, C.J., Wiles, R.L.F., 1996. Petroleum geology of the Black Sea. Mar. Pet. Geol. 13, 195–223. https://doi.org/10.1016/0264-8172(95)00042-9

Robinson, A.G. (Ed.), 1997. Regional and Petroleum Geology of the Black Sea and Surrounding Region. American Association of Petroleum Geologists Memoir, vol. 68, pp. 1 – 385.

Roca, M., Chen, K., Pérez-Gálvez, A., 2016. Chlorophylls, in: Handbook on Natural Pigments in Food and Beverages. Elsevier, pp. 125–158. https://doi.org/10.1016/B978-0-08-100371-8.00006-3

Ryan, W.B.F., Pitman, W.C., Major, C.O., Shimkus, K., Moskalenko, V., Jones, G.A., Dimitrov, P., Gorür, N., Sakinç, M., Yüce, H., 1997. An abrupt drowning of the Black Sea shelf. Mar. Geol. 138, 119–126. https://doi.org/10.1016/S0025-3227(97)00007-8

Ryan, W.B.F., Major, C.O., Lericolais, G., Goldstein, S.L., 2003. Catastrophic Flooding of the Black Sea. Annu. Rev. Earth Planet. Sci. 31, 525–554. https://doi.org/10.1146/annurev.earth.31.100901.141249

Schouten, S., Hopmans, E.C., Schefuß, E., Sinninghe Damsté, J.S., 2002. Distributional variations in marine crenarchaeotal membrane lipids: a new tool for reconstructing ancient sea water temperatures? Earth Planet. Sci. Lett. 204, 265–274. https://doi.org/10.1016/S0012-821X(02)00979-2

Schouten, S., Rijpstra, W.I.C., Durisch-Kaiser, E., Schubert, C.J., Sinninghe Damsté, J.S., 2012. Distribution of glycerol dialkyl glycerol tetraether lipids in the water column of Lake Tanganyika. Org. Geochem. 53, 34–37. https://doi.org/10.1016/j.orggeochem.2012.01.009

Schouten, S., Hopmans, E.C., Sinninghe Damsté, J.S., 2013. The organic geochemistry of glycerol dialkyl glycerol tetraether lipids: A review. Org. Geochem. 54, 19–61. https://doi.org/10.1016/j.orggeochem.2012.09.006

Schubert, C.J., Coolen, M.J.L., Neretin, L.N., Schippers, A., Abbas, B., Durisch-Kaiser, E., Wehrli, B., Hopmans, E.C., Damsté, J.S.S., Wakeham, S., Kuypers, M.M.M., 2006. Aerobic and anaerobic methanotrophs in the Black Sea water column. Environ. Microbiol. 8, 1844–1856. https://doi.org/10.1111/j.1462-2920.2006.01079.x

Sinninghe Damsté , J.S., Wakeham, S.G., Kohnen, M.E.L., Hayes, J.M., de Leeuw, J.W., 1993. A 6000 year sedimentary molecular record of chemocline excursions in the Black Sea. Nature 362, 827±829

Sinninghe Damsté, J.S., Hopmans, E.C., Pancost, R.D., Schouten, S., Geenevasen, J.A.J., 2000. Newly discovered non-isoprenoid glycerol dialkyl glycerol tetraether lipids in sediments. Chem. Commun. 1683–1684. https://doi.org/10.1039/B004517I

Sinninghe Damsté, J.S., Schouten, S., Hopmans, E.C., van Duin, A.C.T., Geenevasen, J.A.J., 2002. Crenarchaeol: the characteristic core glycerol dibiphytanyl glycerol tetraether membrane lipid of cosmopolitan pelagic crenarchaeota. J. Lipid Res. 43, i. https://doi.org/10.1016/S0022-2275(20)32776-0

Sinninghe Damsté, J.S., Rijpstra, W.I.C., Hopmans, E.C., den Uijl, M.J., Weijers, J.W.H., Schouten, S., 2018. The enigmatic structure of the crenarchaeol isomer. Org. Geochem. 124, 22–28. https://doi.org/10.1016/j.orggeochem.2018.06.005

Sorokin, Y.I., 2002. The Black Sea: Ecology and Oceanography. Amsterdam, The Netherlands: Backhuys Publishers

Starostenko, V., Buryanov, V., Makarenko, I., Rusakov, O., Stephenson, R., Nikishin, A., Georgiev, G., Gerasimov, M., Dimitriu, R., Legostaeva, O., Pchelarov, V., Sava, C., 2004. Topography of the crust–mantle boundary beneath the Black Sea Basin. Tectonophysics 381, 211–233. https://doi.org/10.1016/j.tecto.2002.08.001

Tierney, J.E., Russell, J.M., 2009. Distributions of branched GDGTs in a tropical lake system: Implications for lacustrine application of the MBT/CBT paleoproxy. Org. Geochem. 40, 1032–1036. https://doi.org/10.1016/j.orggeochem.2009.04.014

Tourna, M., Stieglmeier, M., Spang, A., Könneke, M., Schintlmeister, A., Urich, T., Engel, M., Schloter, M., Wagner, M., Richter, A., Schleper, C., 2011. Nitrososphaera viennensis, an ammonia oxidizing archaeon from soil. Proc. Natl. Acad. Sci. 108, 8420–8425. https://doi.org/10.1073/pnas.1013488108

Tugolesov, D.A., Gorshkov, A.S., Meysner, L.B., Solov'yev, V.V., and Khakhalev, Y.M., 1985, The tectonics of the Black Sea trough: Geotectonics, v. 19, p. 435-445.

Turich, C., Freeman, K.H., 2011. Archaeal lipids record paleosalinity in hypersaline systems. Org. Geochem. S0146638011001598. https://doi.org/10.1016/j.orggeochem.2011.06.002

Valentine, D. L. 2002. Biogeochemistry and microbial ecology of methane in anoxic environments: a review. Antonie Leeuwenhoek 81:271–282.

Walker, M., Johnsen, S., Rasmussen, S.O., Popp, T., Steffensen, J.-P., Gibbard, P., Hoek, W., Lowe, J., Andrews, J., Björck, S., Cwynar, L.C., Hughen, K., Kershaw, P., Kromer, B., Litt, T., Lowe, D.J., Nakagawa, T., Newnham, R., Schwander, J., 2009. Formal definition and dating of the GSSP (Global Stratotype Section and Point) for the base of the Holocene using the Greenland NGRIP ice core, and selected auxiliary records. J. Quat. Sci. 24, 3–17. http://dx.doi.org/10.1002/jqs.1227.

Wegwerth, A., Eckert, S., Dellwig, O., Schnetger, B., Severmann, S., Weyer, S., Brüske, A., Kaiser, J., Köster, J., Arz, H.W., Brumsack, H.-J., 2018. Redox evolution during Eemian and Holocene sapropel formation in the Black Sea. Palaeogeogr. Palaeoclimatol. Palaeoecol. 489, 249–260. https://doi.org/10.1016/j.palaeo.2017.10.014

Weijers, J.W.H., Schouten, S., Spaargaren, O.C., Sinninghe Damsté, J.S., 2006. Occurrence and distribution of tetraether membrane lipids in soils: Implications for the use of the TEX86 proxy and the BIT index. Org. Geochem. 37, 1680–1693. https://doi.org/10.1016/j.orggeochem.2006.07.018

Weijers, J.W.H., Schouten, S., van den Donker, J.C., Hopmans, E.C., Sinninghe Damsté, J.S., 2007. Environmental controls on bacterial tetraether membrane lipid distribution in soils. Geochim. Cosmochim. Acta 71, 703–713. https://doi.org/10.1016/j.gca.2006.10.003

Woese, C.R., Kandler, O., Wheelis, M.L., 1990. Towards a natural system of organisms: Proposal for the domains Archaea, Bacteria, and Eucarya. Proc Natl Acad Sci 87, 4576–4579.

Yanchilina, A.G., Ryan, W.B.F., McManus, J.F., Dimitrov, P., Dimitrov, D., Slavova, K., Filipova-Marinova, M., 2017. Compilation of geophysical, geochronological, and geochemical evidence indicates a rapid Mediterranean-derived submergence of the Black Sea's shelf and subsequent substantial salinification in the early Holocene. Mar. Geol. 383, 14–34. https://doi.org/10.1016/j.margeo.2016.11.001

Zehr, J.P., Ward, B.B., 2002. Nitrogen Cycling in the Ocean: New Perspectives on Processes and Paradigms. Appl. Environ. Microbiol. 68, 1015–1024. https://doi.org/10.1128/AEM.68.3.1015-1024.2002

Zhang, Y.G., Pagani, M., Wang, Z., 2016. Ring Index: A new strategy to evaluate the integrity of TEX_{86} paleothermometry. Paleoceanography 31, 220–232. https://doi.org/10.1002/2015PA002848

Zhang, Y.G., Liu, X., 2018. Export Depth of the TEX86 Signal. Paleoceanogr. Paleoclimatology 33, 666–671. https://doi.org/10.1029/2018PA003337

Zonenshain, L.P., Pichon, X., 1986. Deep basins of the Black Sea and Caspian Sea as remnants of Mesozoic back-arc basins. Tectonophysics 123, 181–211. https://doi.org/10.1016/0040-1951(86)90197-6

Appendix

Table S1.1: Summary of estimated concentration of targeted lipid biomarkers. (All concentrations are reported in μg gOC^{-1})

Age (*ka*)	Chl-a-DDs	LCAs	Crenarchaeol	OB-GDGTs	DAGEs
547.4	1375.59	702.28	189.08	7.96	20.25
1351.4	1375.38	988.03	186.83	9.66	19.86
1690.1	1844.92	2294.54	205.38	13.47	26.86
3044.7	1534.22	170.59	280.26	8.61	11.64
3662.1	1474.16	156.63	218.09	9.45	8.81
4639.8	884.89	90.34	195.17	18.20	12.13
5617.5	844.01	133.68	104.37	19.45	14.72
6734.9	798.23	84.80	148.85	23.68	27.67
7788.3	176.27	112.74	141.62	10.17	41.68
8607.0	317.71	327.21	138.05	16.30	59.58
9971.5	258.15	391.03	279.03	9.61	46.49
11336.0	310.61	368.84	218.23	8.26	37.35
11745.3	344.47	255.41	170.76	6.93	38.65

Table S1.2 Estimated concentration of Sterol Chlorin Esters, an important group of Chl-*a*-DDs compounds. (All concentrations in µg gOC^{-1})

	Sterol Chlorin Esters (SCE)										
Age *(ka)*	m/z 887.5834	m/z 901.599	m/z 903.6147	m/z 915.6147	m/z 917.6303	m/z 919.646	m/z 929.6303	m/z 931.646	m/z 933.6616	m/z 945.6616	m/z 947.6773
547.4	30.47	54.48	46.69	73.57	17.26	2.30	20.67	33.97	5.76	7.46	2.10
1351.4	23.83	55.78	35.60	51.68	9.26	2.28	20.96	27.11	5.47	5.93	3.04
1690.1	33.72	81.93	57.34	85.12	13.30	3.38	29.65	38.23	8.29	10.44	4.19
3044.7	17.70	31.90	36.69	41.77	21.68	1.20	13.11	20.66	2.54	3.95	1.12
3662.1	46.06	88.94	107.55	105.53	34.47	2.73	39.52	76.94	9.31	9.95	3.44
4639.8	6.68	15.67	17.28	23.72	18.68	0.84	9.84	11.70	1.90	2.57	0.89
5617.5	7.25	13.22	17.23	22.99	4.52	2.07	11.13	12.56	7.38	10.83	5.28
6734.9	19.20	46.12	39.58	34.35	4.63	1.92	26.14	22.23	4.11	12.62	4.58
7788.3	1.70	13.13	25.70	15.87	8.42	1.91	9.81	16.49	4.06	4.89	3.50
8607.0	2.66	21.52	43.01	31.56	13.88	2.26	16.43	27.68	5.59	7.57	4.42
9971.5	1.85	16.57	32.98	33.43	8.39	1.25	12.46	20.92	4.00	6.38	2.46
11336.0	2.20	18.38	38.90	35.05	9.33	1.17	12.57	23.63	4.57	7.27	2.41
11745.3	2.03	20.72	41.13	37.32	11.70	1.41	14.02	25.85	5.11	8.81	2.86

Table S1.3: Estimated concentration of oxidative degradation derivatives, an important group of Chl-*a*-DDs compounds. (All concentrations in μg gOC^{-1}).

	Oxidative degradation derivatives								
Age *(ka)*	m/z 563.2653	m/z 827.5470	m/z 847.5732	m/z 887.5681	m/z 901.5838	m/z 903.563	m/z 917.5787	m/z 939.5481	m/z 889.5838
547.4	328.55	28.44	4.51	84.09	2.45	47.39	28.25	6.98	42.78
1351.4	324.97	20.99	4.10	85.23	2.55	41.99	15.47	3.90	29.66
1690.1	397.37	17.59	5.80	94.95	4.39	44.80	16.32	5.78	27.08
3044.7	417.49	64.83	5.82	108.36	0.66	66.71	25.22	4.84	18.93
3662.1	210.37	27.24	6.81	38.47	1.23	20.41	7.97	4.23	12.37
4639.8	243.28	21.32	6.42	71.19	0.34	25.67	15.00	4.01	14.11
5617.5	244.32	7.41	3.17	66.62	0.19	42.64	23.10	3.24	6.97
6734.9	99.33	12.23	2.70	39.58	2.64	13.62	5.01	2.66	4.28
7788.3	1.83	2.34	0.34	2.25	3.82	2.18	1.06	0.20	0.00
8607.0	4.50	5.09	0.62	4.25	7.55	2.86	1.96	0.30	0.25
9971.5	5.05	4.67	0.47	4.38	5.15	3.43	2.33	0.26	0.15
11336	14.62	5.65	0.56	6.56	4.84	6.21	3.38	0.29	0.22
11745.3	5.54	7.49	0.87	7.94	9.57	6.33	3.43	0.23	0.21

Table S1.4: Estimated concentration of direct hydrolysis products, an important group of Chl-*a*-DDs compounds. (All concentrations in μg gOC^{-1})

	Direct hydrolysis Products					
Age *(ka)*	**m/z 813.5677**	**m/z 815.5834**	**m/z 835.5371**	**m/z 871.5732**	**Hydroxychlorophyllones-a**	**Methoxylchlorophyllones-a**
547.4	166.55	7.93	4.64	1.06	259.28	67.99
1351.4	150.85	3.28	2.14	25.05	330.34	93.90
1690.1	217.04	4.03	3.31	9.59	436.02	195.26
3044.7	224.73	14.60	3.23	15.76	349.53	21.20
3662.1	277.11	32.59	6.12	63.22	215.66	25.94
4639.8	145.96	14.10	1.95	21.67	177.91	12.16
5617.5	127.83	2.25	4.90	0.25	164.39	32.27
6734.9	146.42	0.94	5.17	56.71	131.23	60.25
7788.3	27.86	0.46	0.11	0.00	2.08	26.26
8607.0	52.20	0.62	0.05	0.31	7.31	53.24
9971.5	46.29	0.40	0.17	1.27	4.92	38.54
11336.0	55.64	0.40	0.11	1.21	8.59	46.85
11745.3	64.70	0.62	0.04	2.71	6.58	57.26

Table S1.5: Estimated concentration of Archaeol and isoprenoid GDGT compounds. (All concentrations are in μg gOC^{-1})

Age	archaeol	Cren. isomer	Cren	GDGT-3	GDGT-2	GDGT-1	GDGT-0
547.4	3.17	2.80	167.97	2.61	9.48	19.07	140.45
1351.4	3.24	7.57	210.65	3.98	22.02	33.56	176.05
1690.1	4.34	7.11	271.92	4.05	19.75	36.23	222.66
3044.7	2.25	2.48	135.57	2.19	9.06	18.55	117.45
3662.1	1.36	1.87	139.75	1.98	6.05	14.46	104.01
4639.8	1.63	2.08	146.77	3.51	12.65	25.10	143.85
5617.5	1.40	1.29	103.08	3.26	12.40	23.42	96.69
6734.9	1.19	5.84	189.34	16.92	74.27	67.46	129.78
7788.3	1.94	2.36	215.72	3.47	24.30	27.33	61.37
8607.0	2.92	4.34	275.92	6.51	42.66	47.46	93.82
9971.5	1.46	2.81	202.58	4.70	30.53	33.90	72.81
11336.0	0.95	2.50	184.33	4.66	29.92	32.60	61.10
11745.3	1.41	2.99	186.09	5.03	31.44	33.17	61.42

Table S1.6: Estimated concentration of overly branched GDGT compounds. (All concentrations are in μg gOC^{-1})

Age *(ka)*	OB-GDGT-1064	OB-GDGT-1078	OB-GDGT-1092	OB-GDGT-1106	OB-GDGT-1120	OB-GDGT-1134
547.4	1.78	1.38	1.16	1.79	1.01	0.85
1351.4	2.28	1.67	1.33	1.99	1.29	1.09
1690.1	3.09	2.28	1.61	2.79	1.90	1.80
3044.7	2.14	1.47	1.13	1.83	1.09	0.95
3662.1	2.19	1.67	0.99	2.24	1.30	1.05
4639.8	4.87	3.43	2.20	4.10	2.34	1.26
5617.5	5.56	4.13	2.25	3.26	2.47	1.78
6734.9	6.81	5.30	2.54	7.22	1.30	0.51
7788.3	2.02	1.13	0.98	2.70	2.17	1.17
8607.0	3.50	1.81	1.65	5.77	2.49	1.08
9971.5	2.26	1.14	1.11	3.28	1.23	0.61
11336.0	2.43	1.25	0.79	2.71	0.75	0.32
11745.3	2.28	1.16	0.65	2.02	0.56	0.26

Table S1.7: Estimated concentration of dialkyl glycerol ether compounds. (All concentrations are in µg gOC^{-1})

Age *(ka)*	**DAGE 514**	**DAGE 528**	**DAGE 542**	**DAGE 556**	**DAGE 570**	**DAGE 584**
547.4	5.52	4.07	4.17	2.84	1.81	1.54
1351.4	5.70	4.09	4.86	1.55	1.41	1.78
1690.1	8.07	5.16	5.88	3.32	1.52	2.36
3044.7	3.38	2.63	2.56	1.12	0.65	1.00
3662.1	3.39	2.25	1.32	0.31	0.39	0.90
4639.8	3.04	2.26	2.23	1.58	1.54	1.18
5617.5	3.66	3.28	2.49	2.34	1.46	1.13
6734.9	6.12	6.04	5.13	4.47	2.29	2.96
7788.3	10.64	9.93	6.77	3.80	2.05	6.29
8606.9	16.03	13.37	10.13	5.82	1.89	9.21
9971.5	11.09	10.38	8.80	4.61	3.46	6.09
11335.9	9.28	9.17	6.10	4.06	1.82	5.54
11745.3	9.42	9.88	7.62	4.72	0.94	4.68

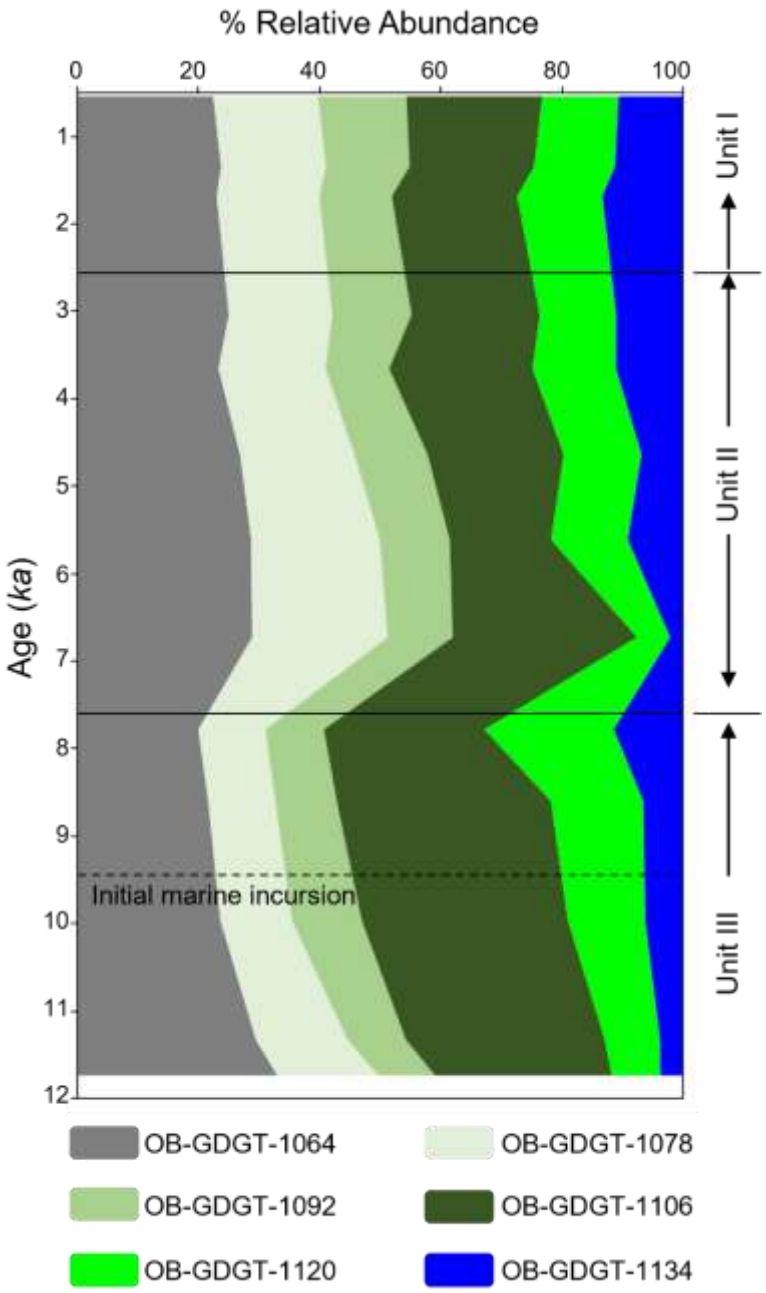


Figure S1.1: Relative abundance plot of overly branched GDGT compounds showing their distribution across Holocene. A marked change in all compounds is noticeable at the start of Unit II sapropel deposition, with all distribution otherwise showing little variation across other sedimentological and salinity boundaries.

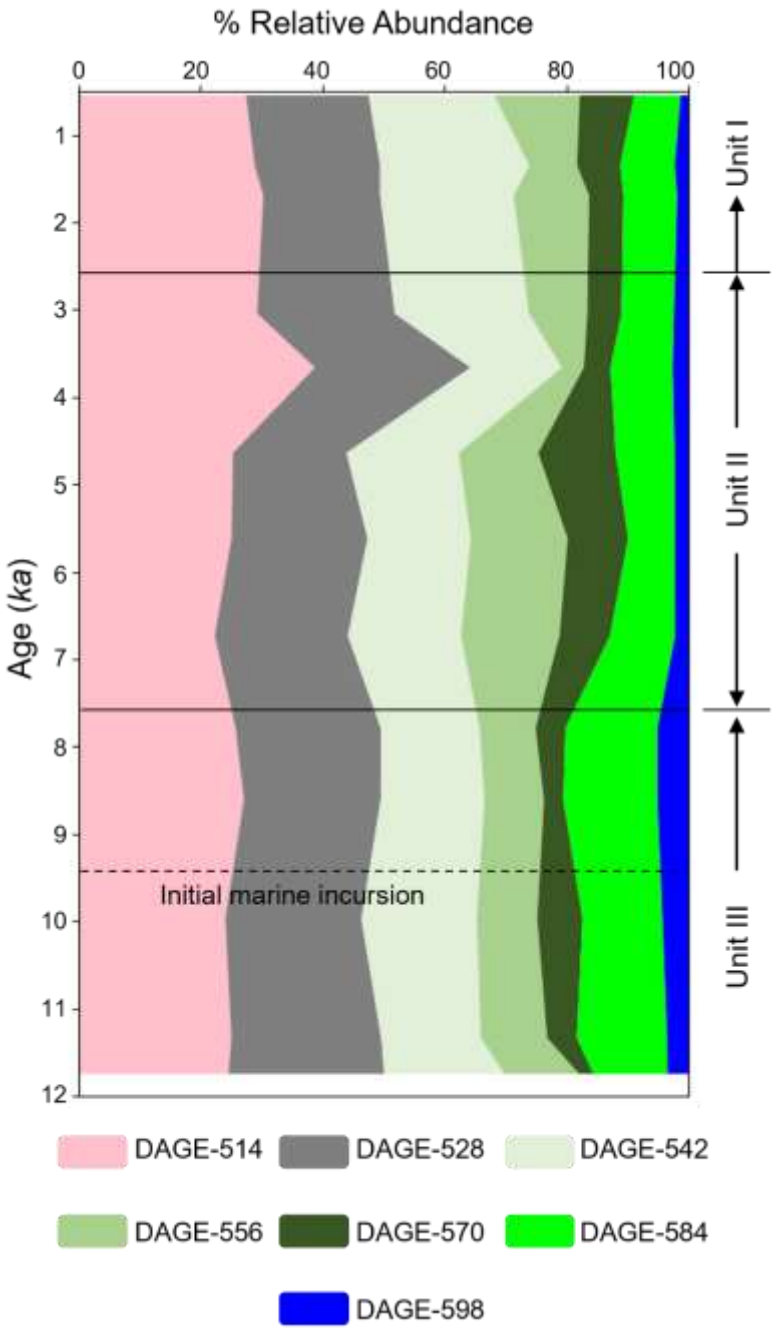


Figure S1.2: Relative abundance plot of DAGE compounds. These compounds show the least amount of variation across salinity and redox boundary providing further validation of less impact due to changes in water column redox condition and water chemistry changes.

Chapter 2: Simultaneous analysis of long-chain alkenones and chlorophyll derivatives offers new insights into the ecology of *Isochrysis* algae in the Holocene Black Sea

Authors: Olawale O. Alo[1], Junpeng Fu[1], Wenshuo Zhao[1], Yi Ge Zhang[2], Yongsong Huang[3], Xiao-Lei Liu[1]

Affiliations:[1]School of Geosciences, University of Oklahoma, Norman, OK 73019, USA.

[2]State Key Laboratory of Isotope Geochemistry, Guangzhou Institute of Geochemistry, Chinese Academy of Sciences, Guangzhou, China
[3]Department of Earth, Environmental and Planetary Science, Brown University, Providence, RI 02912, USA

Abstract

New lipid biomarker analytical protocols provide the advantage of integrating an extensive compound inventory rather than a single class of biomarkers to study the progressive evolution of phytoplankton in the Black Sea associated with water chemistry shifts in the Holocene, especially the development of photic zone euxinia (PZE). Long-chain alkenones (LCAs) and chlorophyll-*a* degradation derivatives (Chl-*a*-DDs) are two distinct groups of biomarkers for phytoplankton. While Chl-*a*-DDs are ubiquitous in eukaryotic phytoplankton and cyanobacteria, LCAs are primarily produced by certain species of haptophyte algae, particularly from the family *Isochrysidaceae*. We therefore use the distributions of LCAs and Chl-*a*-DDs to reconstruct activities of algae and other phytoplankton in the Black Sea during the development of euxinic conditions in the Holocene. Twenty-five Chl-*a*-DDs compounds (without counting their isomers) and nineteen LCAs (C_{37} to C_{40} with varying degrees of unsaturation) were identified and quantified, highlighting the effectiveness of the analytical protocol for comprehensive analysis of phytoplanktonic lipid biomarkers in sediments. Following the initial incursion of Mediterranean Sea water around 9.4 ka, the Black Sea water column began equilibrating to higher salinity, leading to stratification and PZE starting around 7.6 ka. The development of PZE led to a quick decline in *Isochrysis* productivity due to high salinity in surface waters. The dramatic increase of organic matter content in sediment at the same time can be attributed to both the sustained proliferation of other phytoplankton species (high productivity), such as nitrogen-fixing cyanobacteria, and a stratified water column (enhanced preservation). A quick recovery in *Isochrysis* productivity around 2.6 ka coincides with the Late Holocene surface water freshening in the western Black Sea, implying reduced surface water salinity and extra nutrient delivery favored *Isochrysis* growth. This work highlights the potential of using LCAs and Chl-*a*-DD distributions in sediments to separately reconstruct the past activities of *Isochrysis* algae versus other phytoplankton species in ancient marine environments.

2.1 Introduction

Phytoplankton are a diverse group of microscopic photosynthetic organisms found in aquatic environments. They are an integral part of the aquatic food web, making up about half of global net primary productivity (Field et al., 1998).There are several methods for studying phytoplankton changes in sedimentary records including microfossil analysis (e.g Gersonde and Schrader, 1984; Koç et al., 1999), biogeochemical proxies (e.g. Coolen et al., 2013; Pearson et al., 2008; Tani et al., 2009; Winder and Sommer, 2012), sedimentary DNA (Armbrecht et al., 2019; Coolen et al., 2004, 2013; Yan et al., 2023; Zhang et al., 2021), and bulk sediment characteristics (e.g. Contreras et al., 2018; Henderson et al., 2024; Meyers, 2003; Silliman et al., 1996). Whilst microfossil analysis is suitable for studying diatoms, coccolithophores, and dinoflagellates, for example, because of the silica, calcareous and dinocysts respectively preserved in the sedimentary records of these phytoplankton groups, many algae do not leave microscopically visible fossil. A chemical method that can simultaneously analyze important classes of biomarkers in the same run can enable efficient reconstruction of past water chemistry changes.

Late Pleistocene – Holocene history of the Black Sea has been a major focus of scientific study (Bahr et al., 2008; Nikishin et al., 2015, 2003; Piper, 2016; Reimer et al., 2013; Rohling et al., 2015; Tolun et al., 2002; Wilkin et al., 1997), particularly due to its continuous sediment archive, which records recent climate changes and the transition of the Black Sea from a brackish lake to a marine system. The incursion of denser, saline Mediterranean water following the last deglaciation (Aksu et al., 2002; Bahr et al., 2008; Lister et al., 2015; Ryan et al., 1997) created a density barrier which restricted surface and deep water mixing, and ultimately led to development of anoxia in the water column, making the Black Sea the world's largest anoxic

basin (Abrajano et al., 2002; Coolen et al., 2013; Hay et al., 1991; Huang et al., 2000; Sinninghe Damsté et al., 1993). A continuously anoxic water column and sustained productivity soon led to shoaling of the chemocline (Gross, 1974) with the present-day chemocline estimated to be at 80 – 100 m (Jørgensen et al., 1991; Murray et al., 1989; Repeta et al., 1989; Tugrul et al., 1992). A steep chemical gradient demarcates the transition from surface oxic water to intermediate anoxic water in the Black Sea, where both intense microbial remineralization of organic matter and anoxygenic primary production by photoautotrophic bacteria (e.g. *Chlorobium sp.*) coexist (Repeta et al., 1989). Since environmental perturbation often leads to changes of biotic communities, the Black Sea evolution has been studied using various paleobiological and organic geochemical approaches, such as using pollen, spores and dinoflagellate cysts to define a high resolution Late Quaternary stratigraphy of the Black Sea deposition (Filipova-Marinova et al., 2013) and using records of the first and final invasion periods of *Emiliana huxleyi* to study the changes of past salinity and climate (Hay et al., 1991). Coolen et al., (2009) described combined lipid biomarker and fossil DNA analyses to investigate the evolution of Black Sea haptophyte. They reported *Isochrysis* in the Black Sea was gradually replaced by *E. huxleyi* as alkenone producers beyond 7.27 ka.

Changes in redox state and salinity during the Holocene, driven by marine incursions, likely triggered dynamic and continuous shifts in all microbial communities, including surface water phytoplankton. *Isochrysis* algae with distinct physiological traits, as compared to other phytoplankton groups, would have responded differently to changes in water chemistry in the Black Sea. In this study, we conducted a comprehensive analysis of long-chain alkenones (LCAs) and chlorophyll-a degradation derivatives (Chl-*a*-DDs) using a newly developed

reversed-phase LC-ESI-qTOF-MS protocol (Connock et al., 2022; Liu, 2023) to investigate the distinct ecological responses of *Isochrysis* algae during Holocene transitions in the Black Sea.

2.2. Materials and methods

2.2.1 Sample preparation and lipid analysis

The samples used for this study are from the Giant Gravity Core (GGC18) collected from the western portion of the Black Sea (42°46.569''N; 28°40.647''E) in 2006, from a water depth of 971 m during cruise AK06 on the R/V *Akademik* (Coolen et al., 2009; Filipova-Marinova et al., 2013; Huang et al., 2021).Sample preparation and analytical procedure is modified after Connock et al., (2022). Approximately 0.5 g from each of the freeze-dried samples was transferred to 4ml vials, and 500 ng of internal standard – C_{46} glycerol trialkyl glycerol tetraether (C_{46}-GTGT), was added for semi- quantitative analysis of targeted compounds. To recover the total lipid extract (TLE) of each sample, 1.5 mL of Dichloromethane (DCM) : Methanol (MeOH) (1:1) solution was added, vortexed to achieve homogenization, followed by ultrasonication in water bath for twenty minutes. The extraction of TLE through sonication was followed by centrifugation for five minutes at 3000 rpm after which the supernatant was carefully transferred to a 2 ml vial and gently blown down under a stream of N_2. This procedure (adding 1.5 mL 1:1 DCM:MeOH, ultrasonication, centrifugation, transferring and drying under N_2 stream) was repeated two more times and then 1.5 mL of pure DCM was used for the fourth extraction. The combined TLE of each sample was redissolved in 1 ml pure MeOH, ultrasonicated for 10 minutes, centrifuged at 3000 rpm for five minutes and 500 µL (of the TLE redissolved in MeOH) was transferred into a 2 ml injection vial for lipid analysis. The LC-qToF-MS analysis was performed with an Agilent 1290 series UPLC system coupled to Agilent 6530 qTOF mass spectrometer through an Agilent jet stream dual electrospray ionization (AJS-ESI) interface. The

ESI drying gas (N_2) temperature was set at 300°C, the N_2 flow rate was 8 L min^{-1} and the nebulizer gas (N_2) pressure was 35 psi. The qTOF parameters were set to: capillary voltage 3.5 kV, fragmentor voltage 175 V; skimmer voltage 65 V and octupole voltage 750 V in auto MS/MS scanning mode with MS range of m/z 50-2000 and MS/MS range of m/z 20-2000. Separation of compounds was achieved by injecting 10 µl samples onto an ACE UltraCore Super C_{18} column (5 µm, 2.1 × 250 mm, ACE, Aberdeen, UK) maintained at 45°C. The LC program was set at a flow rate of 0.2 mL min^{-1}, first hold 100% A for 5 min, and to 70% A and 30% B in 25 min, followed by a gradient to 50% B at 50 min and hold for 5 min, and finally re-equilibrated with 100% A at a flow rate of 0.4 mL min^{-1} for 5 min, where eluent A was 95: 5: 0.04 :0.10 of methanol/H_2O/formic acid/14.8 M NH_3(aq.) and B was 50: 50: 0.04: 0.10 of hexane/2-propanol/formic acid/14.8 M NH_3(aq.).

2.2.2 Bulk measurements

Approximately 200 mg of freeze-dried samples prepared in 2 ml vials were sent to the Stable Isotope Geoscience facility at Texas A&M University, College Station. Bulk organic geochemical measurements of total organic carbon (TOC) and organic carbon and nitrogen isotope analyses were done following methods described in Brankovits et al., (2021) and McDermott et al., (2019). Samples were progressively acidified with 1M hydrochloric acid for 24 hours or until effervescence ceased, then desiccated at 50°C and homogenized into powder. Analysis was done using an Erba NA 1500 Elemental Analyzer that is attached to a Thermo Scientific Conflo IV and a Thermo Scientific Delta V Advantage isotope ratio mass spectrometer (irms). Decarbonated sample was combusted at a temperature of 1020°C with pure oxygen by passing samples through a chromium and cobalt reactor bed which oxidizes any gas produced by combustion. To reduce nitrogen oxides to nitrogen gas amenable for irms analysis, the gases

produced by combustion were passed through a secondary reduction, filled with copper wire kept at a temperature of 650°C. In-line bed anhydrous magnesium perchlorate was used to trap water produced through sample combustion. Using an intra-run calibration conducted with a methionine standard prepared in 5 different masses, peak areas of the mass-to-charge ratios of the combusted samples were converted to total mass of carbon and nitrogen. Organic carbon and nitrogen isotopic ratios ($\delta^{13}C_{org}$ and $\delta^{15}N_{org}$) are reported relative to the standard Vienna Pee Dee Belemnite (VPDB) and Air respectively, in per mil (‰) using an analytical precision for two international standards, USGS 40 and USGS 41.

2.2.3 Targeted lipid biomarkers

In this study, Chl-*a*-DDs and LCAs were analyzed to study the dynamics of phytoplankton as water chemistry changed in the Black Sea during its last transition (Fig. 2.1). The LCAs, a series of C_{37}-C_{40} containing two to four unsaturated methyl and ethyl ketones (Liu et al., 2009; Pearson et al., 2008; Prahl et al., 1988), are an important class of biomarkers for haptophytes in marine environments. They are ubiquitous and often well preserved in marine sediments (Pearson et al., 2008). Haptophytes are unicellular phytoplankton and together with cyanobacteria, diatoms, dinoflagellates and prasinophytes make up the bulk of primary producers in the ocean (Kaiser et al., 2019). This therefore makes LCAs an important biomarker for tracking the contribution of haptophytes to primary productivity. The Chl-*a*-DDs, including chlorophyllone-*a* (Harris et al., 1995), pyropheophytin-a (Nguyen et al., 2022), pheophytin-a, 13^2-OH-Pheophytin-a, 15^1-OH-lactone-Pheophytin-a (Bale et al., 2011; Stuart Walker and Keely, 2004), and steryl chlorin esters (SCEs) (Prowse and Maxwell, 1991; King and Repeta, 1991; Talbot et al., 1999) are degradation derivatives of chlorophyll-*a* commonly found in sediments.

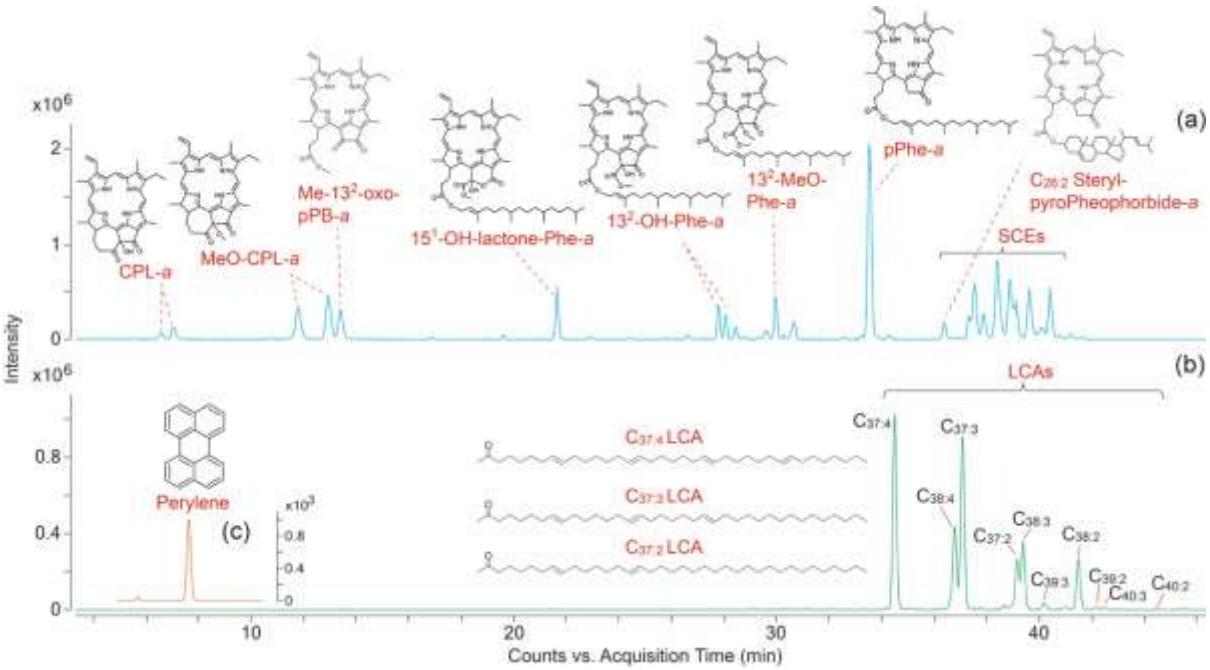


Figure 2.1. Extracted ion chromatograms (EICs) of LC-ESI-qTOF-MS illustrating the distributions of targeted biomarker groups in a Black Sea sediment extract. (a) Tentatively identified Chl-*a*-DDs, with molecular structures of key representative compounds. Twenty-five compounds were identified as Chl-*a*-DDs based on their characteristic fragmentation patterns of cyclic tetrapyrroles observed during collision-induced dissociation (CID) at 20 and 200 eV. Details of Chl-*a*-DD identification have been presented in Liu (2023). (b) C_{37} to C_{40} LCAs with varying degrees of unsaturation (see Liao et al., 2023, for details on LC-MS-based LCA analysis). (c) Detection of perylene. Identification of perylene is based on its identical mass and retention time to the commercial standard (Sigma-Aldrich, St. Louis, MO, USA). Note: Due to its relatively low abundance, the perylene peak is displayed on a separate signal intensity scale on its right side.

Twenty-five identified Chl-a-DDs compounds are integrated for their concentration. The Chl-*a*-DDs are used in combination with LCAs as biomarkers to reconstruct the primary productivity changes that accompanied the transition of Black Sea water chemistry as well as the impact of photic zone euxinia (PZE) in the Holocene.

Additionally, perylene is analyzed as an indicator of terrestrial input. This polycyclic aromatic hydrocarbon (PAH), composed of five fused benzene rings, has been detected in both marine and freshwater sediments (Aizenshtat, 1973; Silliman et al., 1998). Although its origin remains debated (Aizenshtat, 1973; Grice et al., 2007; Silliman et al., 1998; Suzuki et al., 2010; Zhang et al., 2014), numerous studies suggest a primary source from forest fungi (Hanke et al., 2019; Marynowski et al., 2013; Suzuki et al., 2010; Zhang et al., 2014).

2.3 Results and discussions

The concentrations of Chl-*a*-DDs (Fig. 2.2a) and LCAs (Fig. 2.2b) in Holocene Black Sea sediments vary across salinity/redox boundaries, sedimentological transitions, and climatic shifts. While both groups have comparable concentration ranges (176.3–1,844.9 μg/g OC for Chl-*a*-DDs and 50.2–2,294.5 μg/g OC for LCAs), their distributions differ significantly across depositional stages. The ratio of Chl-*a*-DDs to LCAs (Fig. 2c), serves as a proxy for the relative contribution of *Isochrysis* algae versus other phytoplankton groups to primary productivity. Bulk organic geochemical parameters (Fig. 2.2d–f) further characterize the climate-driven water chemistry changes and dynamic evolutions of the Holocene Black Sea phytoplankton community. The three sapropel units of Holocene Black Sea deposit are characterized by distinct primary productivity patterns, water chemistry, and climatic influences. Results and ratios of detected LCAs are reported and discussed in chapter 3.

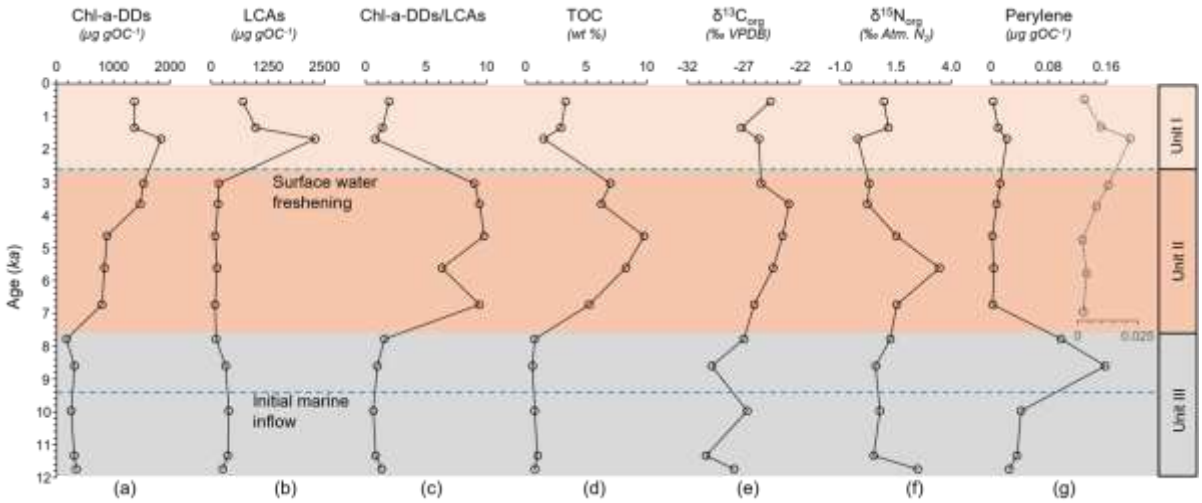


Figure 2.2. Absolute concentrations of targeted lipids and bulk organic geochemistry. The concentrations of Chl-*a*-DDs (a) and LCAs (b) illustrate their changes across sedimentological and salinity boundaries. The Chl-*a*-DDs/LCAs ratio (c) indicates reduced *Isochrysis* algal contribution to primary production during the PZE development stage (Unit II), followed by recovery during surface water freshening (Unit I). Total organic carbon (TOC) (d) and isotope ratios of carbon (e) and nitrogen (f) provide insights into primary productivity dynamics throughout the studied interval. Perylene concentration changes (g) suggest an increased forest vegetation coverage during the climatic optimum around ~9 ka and enhanced river discharge during the Late Holocene (Unit I), and another slight increase (see the expanded view in dashed line) occurred right after the surface water freshening event. Blue dashed lines mark the estimated timing of initial marine inflow and surface water freshening. Raw data of these plots is summarized in Table. 2.1

2.3.1 Stable *Isochrysis* algae contribution to a low primary productivity before the onset of PZE (11.7 to 7.6 ka, Unit III)

Sapropel Unit III, as classified by Hay et al. (1991), encompasses the later lake phase (11.7–9.4 ka) and the initial period of Mediterranean (marine) inflow (9.4–7.6 ka). This section exhibits the lowest Chl-*a*-DD concentrations, ranging from 176.3 to 344.5 µg/g OC, with an average of 281.4 µg/g OC (Fig. 2a). The LCAs follow a similar trend, with concentrations

between 112.7 and 391 µg/g OC, averaging 291 µg/g OC. A slight decline in LCA concentration occurs following the onset of marine inflow. Although this period marks the beginning of increasing salinity and the emergence of marine phytoplankton species—such as *Emiliania huxleyi*, which appeared around 9.3 ka (Coolen et al., 2013), the relative abundance of haptophytes remains stable. This stability is indicated by Chl-*a*-DDs/LCAs values ranging from 0.7 to 1.6, suggesting that prior to the onset of euxinic conditions, the overall phytoplankton composition remained largely unchanged.

The low abundance of sedimentary organic matter, with TOC averaging less than 1 wt% (Fig. 2.2d), and the consistently low Chl-*a*-DDs concentration (TOC-normalized; Fig. 2a) in Unit III suggest that primary productivity was relatively low. This challenges previous interpretations that attribute the low organic matter content to poor preservation in an oxygenated water column during the lake phase (Bahr et al., 2008; Filipova-Marinova et al., 2013; Major et al., 2002; Ryan et al., 1997). We argue that if poor organic matter preservation were the primary limiting factor, Chl-*a*-DDs concentrations would not remain uniformly low compared to the much higher concentration preserved under euxinic condition in Unit II, unless chlorophylls were selectively degraded over other lipids which is hard to test.

Perylene concentrations reach their highest levels in the entire Holocene record during this stage (Fig. 2g), progressively increasing and peaking around ~9 ka, coinciding with the Holocene climate optimum (Coolen et al., 2013; Wanner et al., 2008). The expansion of dense forest cover in the surrounding region may have contributed to elevated perylene levels in Black Sea sediments. During this same period, $\delta^{13}C_{org}$ and $\delta^{15}N_{org}$ values exhibit strong oscillations, ranging from -27.8 to -30.3‰ and 0.5 to 2.5‰, respectively. This isotopic variability likely

reflects the mixing of terrestrial with aquatic organic matter, driven by significant terrestrial input.

2.3.2 Suppressed Isochrysis algae growth due to PZE development (7.6 to 2.6 ka, Unit II)

The timing of the initial Mediterranean inflow into the Black Sea remains debated, but many studies suggest it occurred approximately 2,000 years before the 7.6 ka Unit II–Unit III sedimentological boundary (e.g., Degens and Ross, 1972; Glenn and Arthur, 1985; Hiscott et al., 2007; Major et al., 2006; Soulet et al., 2011). After this incursion, water column stratification likely took time to fully develop. The onset of stratification and the establishment of PZE in the Black Sea is estimated to have occurred around 7.6 ka (Arthur and Dean, 1998; Arthur and Sageman, 2012). This transition was driven by a strong salinity gradient, increased nutrient input (Arthur and Dean, 1998; Soulet et al., 2011), sulfide production by sulfate-reducing bacteria in anoxic conditions (Bahr et al., 2005; Giosan et al., 2009), and oxygen depletion due to organic matter decomposition.

During this stage, consistent with the findings of Coolen et al. (2013), our data show a progressive increase in TOC, peaking at approximately 10 wt% around 4.6 ka (Fig. 2d). While TOC values as high as 20 wt% have been reported for this interval at other sites (Arthur and Sageman, 2012), the relatively lower organic richness in our study is likely due to its shelf location and higher sedimentation rates compared to the more organic-rich sapropels found in the basin center. The dramatic increase in TOC in Unit II has been attributed to enhanced organic matter preservation under fully developed euxinic conditions in the Black Sea (Hollander and McKenzie, 1991; Hollander et al., 1992; Hodell and Schelske, 1998; Brenner et al., 1999).

Our data also indicate a stepwise increase in Chl-*a*-DDs concentrations (Fig. 2a), averaging 1,107.1 µg/g OC—a significant rise from the Unit III average of 281.4 µg/g OC. This

suggests that, in addition to improved preservation, enhanced primary productivity contributed to the high TOC levels in Unit II. However, primary productivity typically declines in a stratified water column due to restricted vertical nutrient flux from deep water to the photic zone. Arthur and Dean (1998) proposed that the rapid spillover of Mediterranean water could have temporarily enhanced vertical mixing and nutrient cycling, leading to a short-term (2–3 ka) burst in surface-water productivity during the early stages of Unit II deposition. However, this mechanism cannot explain the long-term (~7 kyr) continuous increase in Chl-*a*-DDs concentrations. Instead, external nutrient inputs, such as riverine influx, may have mitigated nutrient limitations, supporting sustained phytoplankton growth in the stratified Black Sea.

In contrast to the elevated Chl-*a*-DDs concentrations in Unit II, LCAs concentrations (Fig. 2b) declined at the onset of PZE and remained consistently low throughout Unit II, averaging just 127.2 μg/g OC. Consequently, the Chl-*a*-DDs/LCAs ratio (Fig. 2c) increased significantly, suggesting suppressed growth of *Isochrysis* algae within the sustained phytoplankton community. Perylene concentrations remained relatively low during this period, indicating reduced forest coverage associated with the dry and cooler subboreal climate (Wanner et al., 2008). This climatic shift led to peak marine conditions in the Black Sea and a sharp increase in surface water salinity (Coolen et al., 2013), likely suppressing *Isochrysis* algae growth.

This phase also exhibits a positive carbon isotope excursion (+CIE, ~4 ‰ increase) (Fig. 2e), associated with the gradual establishment of PZE. The +CIE can be attributed to enhanced organic carbon burial (reflected in increasing TOC), which leads to ^{12}C depletion in the dissolved inorganic carbon (DIC) reservoir, enriching the newly produced organic matter in ^{13}C and increasing $\delta^{13}C_{org}$ values (Meyers, 2003). Additionally, as the chemocline rose with intensified

PZE, phytoplankton communities became restricted to shallower surface waters with higher irradiation. This shift in organic matter production from deeper to the shallow euphotic zone likely contributed to the observed +CIE. Studies show that particulate organic matter produced by phytoplankton residing in shallow mix layer with high-light and low-nutrient conditions is enriched in ^{13}C compared to deeper photic zone sources (Close and Henderson, 2020; Henderson et al., 2024). Thus, dominant organic carbon export from the shallow euphotic zone under euxinic conditions likely contributed to the ~4 ‰ +CIE observed in Unit II.

As the Black Sea transitioned to marine conditions following the initial Mediterranean inflow, a progressive increase in $\delta^{15}N_{org}$ values (Fig. 2f) occurred cross the upper Unit III and the lower part of Unit II. Enhanced denitrification (Kirkpatrick et al., 2012) and anaerobic ammonium oxidation (anammox) (Jensen et al., 2008) in the developing anoxic to euxinic conditions likely drove this positive $\delta^{15}N_{org}$ excursion. Both processes lead to nitrogen loss and significantly enrich the nitrogen isotopic signature of the remaining nitrogen pool, which influences phytoplankton and organic matter. Following this ^{15}N enrichment, when the Black Sea became fully euxinic at ~5.6 ka, the $\delta^{15}N_{org}$ values declined to between -0.2‰ and 1.5‰. This shift is likely due to increased nitrogen fixation by cyanobacteria, which preferentially fix atmospheric N_2, producing organic matter with lower $\delta^{15}N_{org}$ values (Fogel and Cifuentes, 1993; Brenner et al., 1999; Talbot and Laerdal, 2000). The proliferation of nitrogen-fixing cyanobacteria likely resulted from long-term nitrogen loss due to denitrification and anammox. These shifts in the phytoplankton community, including the restriction to the shallow euphotic zone and competition for limited nitrogen sources, likely contributed to the observed decline of *Isochrysis* algae in the Black Sea during this period.

2.3.3 Resurgence of *Isochrysis* algae associated with the late Holocene surface water freshening (2.6 ka to present, Unit I)

The Black Sea Sapropel Unit I is primarily composed of coccolith marl. The TOC exhibits a steep decline from Unit II to this stage (Fig. 2d), primarily due to dilution by high coccolith-carbonate fluxes (Arthur and Dean, 1998). Changes in precipitation patterns and increased glacial meltwater inflow following the onset of the subatlantic climate (Wanner et al., 2008) likely contributed to enhanced freshwater discharge from major rivers such as the Danube, Dnieper, and Don into the Black Sea during the Late Holocene (Giosan et al., 2009).

Our data indicates that perylene concentrations (Fig. 2.2g) increased from the upper part of Unit II into Unit I. While they did not return to pre-anoxia levels, they remained higher than those observed during peak anoxic conditions, supporting the notion of increased surface runoff from land into the Black Sea during this period. This intensified river discharge not only enhanced nutrient delivery (Arthur and Sageman, 2012) and increased sedimentation rates (Esin et al., 2010) but also contributed to a reduction in surface water salinity around 2.6 ka (Giosan et al., 2012; Van Der Meer et al., 2008).

These hydrological and nutrient shifts strongly influenced phytoplankton community composition. Increased nutrient input and surface water freshening during this phase facilitated a rapid expansion of *Isochrysis* algae, as evinced by the high abundance of coccoliths and a sharp increase in LCA concentrations (Fig. 2.2b) in Unit I. As a result, Chl-*a*-DDs concentrations remained high (Fig. 2.2a), while the Chl-*a*-DDs/LCAs ratio declined sharply (Fig. 2.2c). The increased nutrient availability and chemocline fluctuations, driven by substantial freshwater input, likely extended the habitable depth range for phytoplankton, contributing to a slight negative shift in carbon isotope values (Fig. 2.2e).

2.4 Conclusion

This work underscores the significance of LC-ESI-qTOF-MS application in analyzing a lipid inventory of phytoplankton. Coupled with bulk organic geochemical data, the distributions of Chl-*a*-DDs and LCAs in the sediment record reveal distinct responses of *Isochrysis* algae compared to other phytoplankton groups to changes in Black Sea water chemistry during the Holocene transitions. Before the onset of euxinia (11.7–7.6 ka), *Isochrysis* algae maintained stable abundance within the phytoplankton community, as shown by the consistent Chl-*a*-DDs/LCAs ratio, while overall primary productivity remained low. During this period, marked by relatively stable salinity and nutrient conditions, *Isochrysis* algae competed with other groups and exhibited stable growth. The establishment of euxinic conditions around 7.6 ka, characterized by water column stratification, reduced *Isochrysis* growth, primarily due to increased salinity, and probably due to limited vertical mixing and nutrient availability as well. This resulted in a sharp decline in *Isochrysis* abundance, as reflected in the decreased Chl-*a*-DDs/LCAs ratio, while other groups, such as nitrogen-fixing cyanobacteria, adapted to the anoxic environment and proliferated. Increased organic carbon burial and isotope excursions of carbon and nitrogen further supported a shift in phytoplankton community dynamics. In contrast, during the Late Holocene (2.6 ka to present), heightened river discharge and surface water freshening triggered a resurgence of *Isochrysis* algae. This phase, marked by higher nutrient input and reduced salinity, created favorable conditions for *Isochrysis*, leading to a rapid increase in their abundance and a corresponding decline in the Chl-*a*-DDs/LCAs ratio. Overall, *Isochrysis* algae demonstrated a clear and distinct response to salinity, redox, and nutrient changes in the Black Sea, providing a constant contribution to primary productivity before the initial marine

inflow, suppression under fully developed euxinia, and resurgence with freshwater input, while other phytoplankton groups exhibited varying adaptive responses.

2.5 References

Abrajano, T., Aksu, A.E., Hiscott, R.N., Mudie, P.J., 2002. Aspects of carbon isotope biogeochemistry of late Quaternary sediments from the Marmara Sea and Black Sea. Mar. Geol. 190, 151–164. https://doi.org/10.1016/S0025-3227(02)00346-8

Aizenshtat, Z., 1973. Perylene and its geochemicalsignificance. Geochlmica Cosmochlmica Acta Vol. 37, 559 to 587.

Aksu, A.E., Hiscott, R.N., Kaminski, M.A., Mudie, P.J., Gillespie, H., Abrajano, T., Yaşar, D., 2002. Last glacial–Holocene paleoceanography of the Black Sea and Marmara Sea: stable isotopic, foraminiferal and coccolith evidence. Mar. Geol. 190, 119–149. https://doi.org/10.1016/S0025-3227(02)00345-6

Armbrecht, L.H., Coolen, M.J.L., Lejzerowicz, F., George, S.C., Negandhi, K., Suzuki, Y., Young, J., Foster, N.R., Armand, L.K., Cooper, A., Ostrowski, M., Focardi, A., Stat, M., Moreau, J.W., Weyrich, L.S., 2019. Ancient DNA from marine sediments: Precautions and considerations for seafloor coring, sample handling and data generation. Earth-Sci. Rev. 196, 102887. https://doi.org/10.1016/j.earscirev.2019.102887

Arthur, M.A., Dean, W.E., 1998. Organic-matter production and preservation and evolution of anoxia in the Holocene Black Sea. Paleoceanography 13, 395–411. https://doi.org/10.1029/98PA01161

Arthur, M.A., Sageman, B.B., 2012. Sea-level control on Source-rock Development: Perspectives from the Holocene Black Sea, the Mid-Cretaceous western interior Basin of North America, and the Late Devonian Appalachian Basin. SEPM (Society for Sedimentary Geology). https://doi.org/10.2110/pec.05.82

Bahr, A., Lamy, F., Arz, H., Kuhlmann, H., Wefer, G., 2005. Late glacial to Holocene climate and sedimentation history in the NW Black Sea. Mar. Geol. 214, 309–322. https://doi.org/10.1016/j.margeo.2004.11.013

Bahr, A., Lamy, F., Arz, H.W., Major, C., Kwiecien, O., Wefer, G., 2008. Abrupt changes of temperature and water chemistry in the late Pleistocene and early Holocene Black Sea. Geochem. Geophys. Geosystems 9, 2007GC001683. https://doi.org/10.1029/2007GC001683

Bale, N.J., Airs, R.L., Llewellyn, C.A., 2011. Type I and Type II chlorophyll-a transformation products associated with algal senescence. Org. Geochem. 42, 451–464. https://doi.org/10.1016/j.orggeochem.2011.03.016

Brankovits, D., Little, S.N., Winkler, T.S., Tamalavage, A.E., Mejía-Ortíz, L.M., Maupin, C.R., Yáñez-Mendoza, G., Van Hengstum, P.J., 2021. Changes in Organic Matter Deposition Can Impact Benthic Marine Meiofauna in Karst Subterranean Estuaries. Front. Environ. Sci. 9, 670914. https://doi.org/10.3389/fenvs.2021.670914

Brenner, M., Whitmore, T.J., Curtis, J.H., Hodell, D.A., Schelske, C.L., 1999. Stable isotope (δ13C and δ15N) signatures of sedimented organic matter as indicators of historic lake trophic state. J. Paleolimnol. 22, 205–221. https://doi.org/10.1023/A:1008078222806

Close, H.G., Henderson, L.C., 2020. Open-Ocean Minima in δ13C Values of Particulate Organic Carbon in the Lower Euphotic Zone. Front. Mar. Sci. 7, 540165. https://doi.org/10.3389/fmars.2020.540165

Connock, G.T., Owens, J.D., Liu, X.-L., 2022. Biotic induction and microbial ecological dynamics of Oceanic Anoxic Event 2. Commun. Earth Environ. 3, 136. https://doi.org/10.1038/s43247-022-00466-x

Contreras, S., Werne, J.P., Araneda, A., Urrutia, R., Conejero, C.A., 2018. Organic matter geochemical signatures (TOC, TN, C/N ratio, δ13C and δ15N) of surface sediment from lakes distributed along a climatological gradient on the western side of the southern Andes. Sci. Total Environ. 630, 878–888. https://doi.org/10.1016/j.scitotenv.2018.02.225

Coolen, M., Muyzer, G., Rijpstra, W.I., Schouten, S., Volkman, J.K., Sinninghe Damsté, J.S., 2004. Combined DNA and lipid analyses of sediments reveal changes in Holocene haptophyte and diatom populations in an Antarctic lake. Earth Planet. Sci. Lett. 223, 225–239. https://doi.org/10.1016/j.epsl.2004.04.014

Coolen, M.J.L., Orsi, W.D., Balkema, C., Quince, C., Harris, K., Sylva, S.P., Filipova-Marinova, M., Giosan, L., 2013. Evolution of the plankton paleome in the Black Sea from the Deglacial to Anthropocene. Proc. Natl. Acad. Sci. 110, 8609–8614. https://doi.org/10.1073/pnas.1219283110

Coolen, M.J.L., Saenz, J.P., Giosan, L., Trowbridge, N.Y., Dimitrov, P., Dimitrov, D., Eglinton, T.I., 2009. DNA and lipid molecular stratigraphic records of haptophyte succession in the Black Sea during the Holocene. Earth Planet. Sci. Lett. 284, 610–621. https://doi.org/10.1016/j.epsl.2009.05.029

Degens, E.T., Ross, D.A., 1972. Chronology of the Black Sea over the last 25,000 years. Chem. Geol. 10, 1–16. https://doi.org/10.1016/0009-2541(72)90073-3

Esin, N.V., Yanko-Hombach, V., Kukleva, O.N., 2010. Mathematical model of the Late Pleistocene and Holocene transgressions of the Black Sea. Quat. Int. 225, 180–190. https://doi.org/10.1016/j.quaint.2009.11.014

Field, C.B., Behrenfeld, M.J., Randerson, J.T., Falkowski, P., 1998. Primary Production of the Biosphere: Integrating Terrestrial and Oceanic Components. Science 281, 237–240. https://doi.org/10.1126/science.281.5374.237

Filipova-Marinova, M., Pavlov, D., Coolen, M., Giosan, L., 2013. First high-resolution marinopalynological stratigraphy of Late Quaternary sediments from the central part of the Bulgarian Black Sea area. Quat. Int. 293, 170–183. https://doi.org/10.1016/j.quaint.2012.05.002

Fogel, M.L., Cifuentes, L.A., 1993. Isotope Fractionation during Primary Production, in: Engel, M.H., Macko, S.A. (Eds.), Organic Geochemistry: Principles and Applications, Topics in Geobiology. Springer US, Boston, MA, pp. 73–98. https://doi.org/10.1007/978-1-4615-2890-6_3

Gersonde, R., Schrader, H., 1984. Marine planktic diatom correlation of lower Messinian deposits in the western Mediterranean. Mar. Micropaleontol. 9, 93–110. https://doi.org/10.1016/0377-8398(84)90006-9

Giosan, L., Filip, F., Constatinescu, S., 2009. Was the Black Sea catastrophically flooded in the early Holocene? Quat. Sci. Rev. 28, 1–6. https://doi.org/10.1016/j.quascirev.2008.10.012

Giosan, L., Coolen, M.J.L., Kaplan, J.O., Constantinescu, S., Filip, F., Filipova-Marinova, M., Kettner, A.J., Thom, N., 2012. Early Anthropogenic Transformation of the Danube-Black Sea System. Sci. Rep. 2, 582. https://doi.org/10.1038/srep00582

Glenn, C.R., Arthur, M.A., 1985. Sedimentary and geochemical indicators of productivity and oxygen contents in modern and ancient basins: The Holocene Black Sea as the “type” anoxic basin. Chem. Geol. 48, 325–354. https://doi.org/10.1016/0009-2541(85)90057-9

Grice, K., Nabbefeld, B., Maslen, E., 2007. Source and significance of selected polycyclic aromatic hydrocarbons in sediments (Hovea-3 well, Perth Basin, Western Australia)

spanning the Permian–Triassic boundary. Org. Geochem. 38, 1795–1803. https://doi.org/10.1016/j.orggeochem.2007.07.001
Gross, M.G., 1974. DEGENS, E. T., AND D. A. ROSS [EDS.]. 1974. The Black Sea—Geology, chemistry, and biology. American Association of Petroleum Geologists, Tulsa, Oklahoma, ix + 633 p. $33.00. Limnol. Oceanogr. 19, 1016–1017. https://doi.org/10.4319/lo.1974.19.6.1016
Hanke, U.M., Lima-Braun, A.L., Eglinton, T.I., Donnelly, J.P., Galy, V., Poussart, P., Hughen, K., McNichol, A.P., Xu, L., Reddy, C.M., 2019. Significance of Perylene for Source Allocation of Terrigenous Organic Matter in Aquatic Sediments. Environ. Sci. Technol. 53, 8244–8251. https://doi.org/10.1021/acs.est.9b02344
Harris, P.G., Pearce, G.E.S., Peakman, T.M., Maxwell, J.R., 1995. A widespread and abundant chlorophyll transformation product in aquatic environments. Org. Geochem. 23, 183–187. https://doi.org/10.1016/0146-6380(95)00006-Z
Hay, B.J., Arthur, M.A., Dean, W.E., Neff, E.D., Honjo, S., 1991. Sediment deposition in the Late Holocene abyssal Black Sea with climatic and chronological implications. Deep Sea Res. Part Oceanogr. Res. Pap. 38, S1211–S1235. https://doi.org/10.1016/S0198-0149(10)80031-7
Henderson, L.C., Wittmers, F., Carlson, C.A., Worden, A.Z., Close, H.G., 2024. Variable carbon isotope fractionation of photosynthetic communities over depth in an open-ocean euphotic zone. Proc. Natl. Acad. Sci. 121, e2304613121. https://doi.org/10.1073/pnas.2304613121
Hiscott, R.N., Aksu, A.E., Mudie, P.J., Marret, F., Abrajano, T., Kaminski, M.A., Evans, J., Çakiroğlu, A.İ., Yaşar, D., 2007. A gradual drowning of the southwestern Black Sea shelf: Evidence for a progressive rather than abrupt Holocene reconnection with the eastern Mediterranean Sea through the Marmara Sea Gateway. Quat. Int. 167–168, 19–34. https://doi.org/10.1016/j.quaint.2006.11.007
Hodell, D.A., Schelske, C.L., 1998. Production, sedimentation, and isotopic composition of organic matter in Lake Ontario. Limnol. Oceanogr. 43, 200–214. https://doi.org/10.4319/lo.1998.43.2.0200
Hollander, D.J., McKenzie, J.A., 1991. CO2 control on carbon-isotope fractionation during aqueous photosynthesis: A paleo-pCO2 barometer. Geology 19, 929–932. https://doi.org/10.1130/0091-7613(1991)019<0929:CCOCIF>2.3.CO;2
Hollander, D.J., McKenzie, J.A., Haven, H.L. ten, 1992. A 200 year sedimentary record of progressive eutrophication in lake Greifen (Switzerland): Implications for the origin of organic-carbon-rich sediments. Geology 20, 825–828. https://doi.org/10.1130/0091-7613(1992)020<0825:AYSROP>2.3.CO;2
Huang, Y., Freeman, K.H., Wilkin, R.T., Arthur, M.A., Jones, A.D., 2000. Black Sea chemocline oscillations during the Holocene: molecular and isotopic studies of marginal sediments. Org. Geochem. 31, 1525–1531. https://doi.org/10.1016/S0146-6380(00)00090-5
Jensen, M.M., Kuypers, M.M.M., Gaute, L., Thamdrup, B., 2008. Rates and regulation of anaerobic ammonium oxidation and denitrification in the Black Sea. Limnol. Oceanogr. 53, 23–36. https://doi.org/10.4319/lo.2008.53.1.0023
Jørgensen, B.B., Fossing, H., Wirsen, C.O., Jannasch, H.W., 1991. Sulfide oxidation in the anoxic Black Sea chemocline. Deep-Sea Res. 38, 1083–1103.
Kaiser, J., Wang, K.J., Rott, D., Li, G., Zheng, Y., Amaral-Zettler, L., Arz, H.W., Huang, Y., 2019. Changes in long chain alkenone distributions and Isochrysidales groups along the

Baltic Sea salinity gradient. Org. Geochem. 127, 92–103. https://doi.org/10.1016/j.orggeochem.2018.11.012
King, L.L., Repeta, D.J., 1991. Novel pyropheophorbide steryl esters in Black Sea sediments. Geochim. Cosmochim. Acta 55, 2067–2074. https://doi.org/10.1016/0016-7037(91)90044-6
Kirkpatrick, J.B., Fuchsman, C.A., Yakushev, E., Staley, J.T., Murray, J.W., 2012. Concurrent activity of anammox and denitrifying bacteria in the Black Sea. Front. Microbiol. 3. https://doi.org/10.3389/fmicb.2012.00256
Koç, N., Hodell, D. A., Kleiven, H., Labeyrie, L., 1999. High-resolution Pleistocene diatom biostratigraphy of Site 983 and correlations with isotope stratigraphy. Proceedings of the Ocean Drilling Program, 162 Scientific Results, 162, Ocean Drilling Program, 1999, Proceedings of the Ocean Drilling Program, 10.2973/odp.proc.sr.162.035.1999. hal-02958678
Liao, S., Liu, X.-L., Manz, K.E., Pennell, K.D., Novak, J., Santos, E., Huang, Y., 2023. Comprehensive analysis of alkenones by reversed-phase HPLC-MS with unprecedented selectivity, linearity and sensitivity. Talanta 260, 124653. https://doi.org/10.1016/j.talanta.2023.124653
Lister, C.J., Hiscott, R.N., Aksu, A.E., Mudie, P.J., 2015. Compositional trends through the Holocene mud succession of the southwestern Black Sea shelf: Implications for sedimentary provenance and water-level history. Sediment. Geol. 316, 13–25. https://doi.org/10.1016/j.sedgeo.2014.11.004
Liu, H., Probert, I., Uitz, J., Claustre, H., Aris-Brosou, S., Frada, M., Not, F., de Vargas, C., 2009. Extreme diversity in noncalcifying haptophytes explains a major pigment paradox in open oceans. Proc. Natl. Acad. Sci. 106, 12803–12808. https://doi.org/10.1073/pnas.0905841106
Liu, X., 2023. Collision-induced dissociation as “mass spectrometric filter” for rapid screening of tetrapyrrole derivatives and their chelated metal species in complex biological and environmental samples. Rapid Commun. Mass Spectrom. 37, e9413. https://doi.org/10.1002/rcm.9413
Major, C., Ryan, W., Lericolais, G., Hajdas, I., 2002. Constraints on Black Sea outflow to the Sea of Marmara during the last glacial^interglacial transition. Mar. Geol. 16.
Major, C.O., Goldstein, S.L., Ryan, W.B.F., Lericolais, G., Piotrowski, A.M., Hajdas, I., 2006. The co-evolution of Black Sea level and composition through the last deglaciation and its paleoclimatic significance. Quat. Sci. Rev. 25, 2031–2047. https://doi.org/10.1016/j.quascirev.2006.01.032
Marynowski, L., Smolarek, J., Bechtel, A., Philippe, M., Kurkiewicz, S., Simoneit, B.R.T., 2013. Perylene as an indicator of conifer fossil wood degradation by wood-degrading fungi. Org. Geochem. 59, 143–151. https://doi.org/10.1016/j.orggeochem.2013.04.006
McDermott, E.G., Mullens, B.A., Mayo, C.E., Roark, E.B., Maupin, C.R., Gerry, A.C., Hamer, G.L., 2019. Laboratory evaluation of stable isotope labeling of Culicoides (Diptera: Ceratopogonidae) for adult dispersal studies. Parasit. Vectors 12, 411. https://doi.org/10.1186/s13071-019-3671-9
Meyers, P.A., 2003. Applications of organic geochemistry to paleolimnological reconstructions: a summary of examples from the Laurentian Great Lakes. Org. Geochem. 34, 261–289. https://doi.org/10.1016/S0146-6380(02)00168-7

Murray, J.W., Jannasch, H.W., Honjo, S., Anderson, R.F., Reeburgh, W.S., Top, Z., Friederich, G.E., Codispoti, L.A., Izdar, E., 1989. Unexpected changes in the oxic/anoxic interface in the Black Sea. Nature 338, 411–413. https://doi.org/10.1038/338411a0

Nguyen, D.D., Sauer, J.S., Camarda, L.P., Sherman, S.L., Prather, K.A., Golden, S.S., Pomeroy, R., Dorrestein, P.C., Simkovsky, R., 2022. Grazer-induced changes in molecular signatures of cyanobacteria. Algal Res. 61, 102575. https://doi.org/10.1016/j.algal.2021.102575

Nikishin, A.M., Korotaev, M.V., Ershov, A.V., Brunet, M.-F., 2003. The Black Sea basin: tectonic history and Neogene–Quaternary rapid subsidence modelling. Sediment. Geol. 156, 149–168. https://doi.org/10.1016/S0037-0738(02)00286-5

Nikishin, A.M., Okay, A.I., Tüysüz, O., Demirer, A., Amelin, N., Petrov, E., 2015. The Black Sea basins structure and history: New model based on new deep penetration regional seismic data. Part 1: Basins structure and fill. Mar. Pet. Geol. 59, 638–655. https://doi.org/10.1016/j.marpetgeo.2014.08.017

Pearson, E.J., Juggins, S., Farrimond, P., 2008. Distribution and significance of long-chain alkenones as salinity and temperature indicators in Spanish saline lake sediments. Geochim. Cosmochim. Acta 72, 4035–4046. https://doi.org/10.1016/j.gca.2008.05.052

Piper, D.Z., 2016. Geochemistry of the Black Sea during the last 15 kyr: A protracted evolution of its hydrography and ecology. Paleoceanography 31, 1117–1137. https://doi.org/10.1002/2016PA002949

Prahl, F.G., Muehlhausen, L.A., Zahnle, D.L., 1988. Further evaluation of long-chain alkenones as indicators of paleoceanographic conditions. Geochim. Cosmochim. Acta 52, 2303–2310. https://doi.org/10.1016/0016-7037(88)90132-9

Prowse, W.G., Maxwell, J.R., 1991. High molecular weight chlorins in a lacustrine shale. Org. Geochem. 17, 877–886. https://doi.org/10.1016/0146-6380(91)90029-J

Reimer, P.J., Bard, E., Bayliss, A., Beck, J.W., Blackwell, P.G., Ramsey, C.B., Buck, C.E., Cheng, H., Edwards, R.L., Friedrich, M., Grootes, P.M., Guilderson, T.P., Haflidason, H., Hajdas, I., Hatté, C., Heaton, T.J., Hoffmann, D.L., Hogg, A.G., Hughen, K.A., Kaiser, K.F., Kromer, B., Manning, S.W., Niu, M., Reimer, R.W., Richards, D.A., Scott, E.M., Southon, J.R., Staff, R.A., Turney, C.S.M., van der Plicht, J., 2013. IntCal13 and Marine13 Radiocarbon Age Calibration Curves 0–50,000 Years cal BP. Radiocarbon 55, 1869–1887. https://doi.org/10.2458/azu_js_rc.55.16947

Repeta, D.J., Simpson, D.J., Jorgensen, B.B., 1989. photosynthesis from the distribution of bacterio- chlorophylls in the Black Sea 342, 4.

Rohling, E.J., Marino, G., Grant, K.M., 2015. Mediterranean climate and oceanography, and the periodic development of anoxic events (sapropels). Earth-Sci. Rev. 143, 62–97. https://doi.org/10.1016/j.earscirev.2015.01.008

Ryan, W.B.F., Pitman, W.C., Major, C.O., Shimkus, K., Moskalenko, V., Jones, G.A., Dimitrov, P., Gorür, N., Sakinç, M., Yüce, H., 1997. An abrupt drowning of the Black Sea shelf. Mar. Geol. 138, 119–126. https://doi.org/10.1016/S0025-3227(97)00007-8

Silliman, J.E., Meyers, P.A., Bourbonniere, R.A., 1996. Record of postglacial organic matter delivery and burial in sediments of Lake Ontario. Org. Geochem. 24, 463–472. https://doi.org/10.1016/0146-6380(96)00041-1

Silliman, J.E., Meyers, P.A., Eadie, B.J., 1998. Perylene: an indicator of alteration processes or precursor materials? Org. Geochem. 29, 1737–1744. https://doi.org/10.1016/S0146-6380(98)00056-4

Sinninghe Damsté, J.S., Wakeham, S.G., Kohnen, M.E.L., Hayes, J.M., de Leeuw, J.W., 1993. A 6,000–year sedimentary molecular record of chemocline excursions in the Black Sea. Nature 362, 827–829. https://doi.org/10.1038/362827a0

Soulet, G., Ménot, G., Lericolais, G., Bard, E., 2011. A revised calendar age for the last reconnection of the Black Sea to the global ocean. Quat. Sci. Rev. 30, 1019–1026. https://doi.org/10.1016/j.quascirev.2011.03.001

Stuart Walker, J., Keely, B.J., 2004. Distribution and significance of chlorophyll derivatives and oxidation products during the spring phytoplankton bloom in the Celtic Sea April 2002. Org. Geochem. 35, 1289–1298. https://doi.org/10.1016/j.orggeochem.2004.06.017

Suzuki, N., Yessalina, S., Kikuchi, T., 2010. Probable fungal origin of perylene in Late Cretaceous to Paleogene terrestrial sedimentary rocks of northeastern Japan as indicated from stable carbon isotopes. Org. Geochem. 41, 234–241. https://doi.org/10.1016/j.orggeochem.2009.11.010

Talbot, H.M., Head, R.N., Harris, R.P., Maxwell, J.R., 1999. Distribution and stability of steryl chlorin esters in copepod faecal pellets from diatom grazing. Org. Geochem. 30, 1163–1174. https://doi.org/10.1016/S0146-6380(99)00095-9

Talbot, M.R., Lærdal, T., 2000. The Late Pleistocene - Holocene palaeolimnology of Lake Victoria, East Africa, based upon elemental and isotopic analyses of sedimentary organic matter. J. Paleolimnol. 23, 141–164. https://doi.org/10.1023/A:1008029400463

Tani, Y., Matsumoto, G.I., Soma, M., Soma, Y., Hashimoto, S., Kawai, T., 2009. Photosynthetic pigments in sediment core HDP-04 from Lake Hovsgol, Mongolia, and their implication for changes in algal productivity and lake environment for the last 1Ma. Quat. Int. 205, 74–83. https://doi.org/10.1016/j.quaint.2009.02.007

Tolun, L., Çağatay, M.N., Carrigan, W.J., 2002. Organic geochemistry and origin of Late Glacial–Holocene sapropelic layers and associated sediments in Marmara Sea. Mar. Geol. 190, 47–60. https://doi.org/10.1016/S0025-3227(02)00342-0

Tugrul, S., Basturk, O., Saydam, C., Yilmaz, A., 1992. Changes in the hydrochemistry of the Black Sea inferred from water density profiles. Nature 359, 137–139. https://doi.org/10.1038/359137a0

Van Der Meer, M.T.J., Sangiorgi, F., Baas, M., Brinkhuis, H., Sinninghe Damsté, J.S., Schouten, S., 2008. Molecular isotopic and dinoflagellate evidence for Late Holocene freshening of the Black Sea. Earth Planet. Sci. Lett. 267, 426–434. https://doi.org/10.1016/j.epsl.2007.12.001

Wanner, H., Beer, J., Bütikofer, J., Crowley, T.J., Cubasch, U., Flückiger, J., Goosse, H., Grosjean, M., Joos, F., Kaplan, J.O., Küttel, M., Müller, S.A., Prentice, I.C., Solomina, O., Stocker, T.F., Tarasov, P., Wagner, M., Widmann, M., 2008. Mid- to Late Holocene climate change: an overview. Quat. Sci. Rev. 27, 1791–1828. https://doi.org/10.1016/j.quascirev.2008.06.013

Wilkin, R., Arthur, M., Dean, W., 1997. History of water-column anoxia in the Black Sea indicated by pyrite framboid size distributions. Earth Planet. Sci. Lett. 148, 517–525. https://doi.org/10.1016/S0012-821X(97)00053-8

Winder, M., Sommer, U., 2012. Phytoplankton response to a changing climate. Hydrobiologia 698, 5–16. https://doi.org/10.1007/s10750-012-1149-2

Yan, D., Tiamiyu, B.B., Liu, J., Lan, J., Xu, H., Hou, W., Wen, H., Gu, M., Yan, H., Tan, Z., An, Z., Han, Y., 2023. Lake sediment DNA reveals the response of phytoplankton to warming. Quat. Sci. Rev. 317, 108293. https://doi.org/10.1016/j.quascirev.2023.108293

Zhang, X., Xu, Y., Ruan, J., Ding, S., Huang, X., 2014. Origin, distribution and environmental significance of perylene in Okinawa Trough since last glaciation maximum. Org. Geochem. 76, 288–294. https://doi.org/10.1016/j.orggeochem.2014.09.008

Zhang, H., Huo, S., Yeager, K.M., Wu, F., 2021. Sedimentary DNA record of eukaryotic algal and cyanobacterial communities in a shallow Lake driven by human activities and climate change. Sci. Total Environ. 753, 141985. https://doi.org/10.1016/j.scitotenv.2020.141985

Appendix

Table 2.1: Estimated concentrations of targeted biomarkers and bulk geochemistry data

Age *(ka)*	Chl-*a*-DDs *(µg/gOC)*	LCAs *(µg/gOC)*	Chl-*a*-DDs /LCAs	TOC *(wt %)*	$\delta^{13}C_{org}$ *(‰ VPDB)*	$\delta^{15}N_{org}$ *(‰ Atm.N_2)*	Perylene *(µg/gOC)*
547.4	1375.59	702.28	1.95	3.32	-24.64	0.97	0.0028
1351.5	1375.38	988.03	1.39	2.93	-27.21	1.16	0.0097
1690.1	1844.92	2294.54	0.80	1.50	-25.67	-0.21	0.0219
3044.7	1534.22	170.59	8.99	7.01	-25.48	0.30	0.0128
3662.2	1474.16	156.63	9.41	6.25	-23.00	0.22	0.0079
4639.8	884.88	90.34	9.79	9.78	-23.57	1.53	0.0020
5617.5	844.00	133.68	6.31	8.28	-24.40	3.47	0.0038
6734.9	798.23	84.80	9.41	5.25	-26.08	1.54	0.0024
7788.3	176.27	112.74	1.56	0.76	-26.99	1.25	0.0971
8607.0	317.71	327.21	0.97	0.58	-29.83	0.60	0.1581
9971.5	258.15	391.03	0.66	0.75	-26.70	0.78	0.0416
11336.0	310.61	368.84	0.84	0.99	-30.33	0.50	0.0361
11745.3	344.47	255.41	1.35	0.80	-27.86	2.48	0.0253

Chapter 3: Long chain alkenone distribution provides insight into haptophytes' ecological dynamics and response to climate variation in the Black Sea during the Holocene

Authors: Olawale O. Alo[1*], Yi Ge Zhang[2], Yongsong Huang[3], Xiao-Lei Liu[1]

Affiliations:[1]School of Geosciences, University of Oklahoma, Norman, OK 73019, USA
[2]State Key Laboratory of Isotope Geochemistry, Guangzhou Institute of Geochemistry, Chinese Academy of Sciences, Guangzhou, China
[3]Department of Earth, Environmental and Planetary Sciences, Brown University, Providence, RI 02912, USA

Abstract

In its recent history, the Black Sea has had changes in temperature and water chemistry because of climate-induced sea-level changes that characterized the Late Pleistocene and the Holocene. It therefore represents an exceptional sediment archive for studying biological responses to the most recent environmental and climatic perturbations of its geological history. The distribution of long chain alkenones (LCAs) in sediments is closely linked to the ecological evolution of haptophytes, a key group of phytoplankton. In this study, we report the diversity and distribution of LCAs analyzed with reversed-phase liquid chromatography electrospray ionization quadrupole time-of-flight mass spectrometry (RPLC-ESI-qTOF-MS), across the salinity and sedimentological boundaries in the Holocene. The LCAs with carbon chain lengths ranging from 37- 40 (C_{37} - C_{40}) and two to four double bonds were detected.
This method effectively achieved baseline resolution between alkenones with different numbers of double bonds. Additionally, baseline resolution was attained for C37 alkenone double bond positional isomers (C37:3a and C37:3b), as well as clear separation of C38Me and C38Et alkenone peaks. The C_{37} and C_{38} alkenones dominate the sedimentary sequence, while C_{39} and C_{40} alkenones are present in relatively low abundance. The dramatic changes in water chemistry in the Black Sea during the studied interval appear to have little impact on the relative abundance of C_{37} and C_{38}-dominated alkenone distribution, though some variation in the relative abundance of C_{40} alkenones is observed. The C_{38} alkenones are the most diverse group with methyl- and ethyl- tetra, tri- and di-unsaturated compounds, followed by C_{37} alkenones with C_{39} and C_{40} alkenones being the least diverse. The abundance of tetra-unsaturated compounds decreases with increasing carbon chain length and is undetected in C_{40} alkenones. This study established a viable method that improves on detection of a wider range and diversity of alkenones which can be invaluable for paleoenvironmental reconstruction.

3.1 Introduction

Haptophytes are unicellular phytoplankton and together with cyanobacteria, diatoms, dinoflagellates and prasinophytes make up the bulk of primary producers in the ocean (Kaiser et al., 2019). Long chain alkenones (LCAs), a series of C_{35}-C_{42} methyl (Me) and ethyl (Et) ketones containing two to four double bonds (Brassell et al., 1986; Liu et al., 2009; Longo et al., 2018, 2016; Pearson et al., 2008; Prahl et al., 1988; Zhao et al., 2014), make up an important class of lipid biomarkers for haptophytes in marine environments. They have been reported in geological deposits extending back to the Cretaceous (Brassell and Dumitrescu, 2004; Farrimond et al., 1986) and those with chain length > C_{40} are reported exclusively in surface sediments of hypersaline lakes (Zhao et al., 2014). The C_{37}Me and C_{38}Et are usually the most abundant LCAs in marine and lake environments (Yao et al., 2022). The LCAs distributions are known to be sensitive to temperature and salinity and have been used as paleotemperature and salinity proxies in different environments (Chivall et al., 2014; Freeman and Wakeham, 1992; Huang et al., 2021; Kaiser et al., 2019, 2017; Pearson et al., 2008; Prahl et al., 1988). The $U_{37}^{K'}$ is the most applied LCA paleothermometer, which is based on the ratio of di-unsaturated and tri-unsaturated C_{37}Me ketone (Prahl and Wakeham, 1987). Although nutrient levels (Epstein et al., 1998), and lateral advection (Ausín et al., 2022) have been reported to have only little effects on the application of $U_{37}^{K'}$ as a paleothermometer, limitations of the $U_{37}^{K'}$ proxy, for example, degradation effects, are still debated (Freeman and Wakeham, 1992; Harvey, 2000; Hoefs et al., 1998; Prahl et al., 1989; Rontani et al., 2008, 2013; Sikes et al., 1991). The application of $U_{37}^{K'}$ is also restricted to open-ocean depositional environments due to the non-widespread occurrence of coastal haptophytes (Bendle et al., 2009; Kaiser et al., 2019; Mercer et al., 2005). Non-linearity of $U_{37}^{K'}$ computed sea surface temperature (SST) at low and high temperature levels as well as

seasonality bias at high latitudes have been reported (Novak et al., 2022; Tierney and Tingley, 2018). Contributions of LCAs by multiple species, also referred to as species mixing, is another limitation (Coolen, 2004; Longo et al., 2016; Theroux et al., 2010).

The Black Sea is a back-arc basin, that opened from Cretaceous to Paleocene (Dinu et al., 2005; Görür, 1988; Nikishin et al., 2003; Okay et al., 1994; Robinson et al., 1996; Zonenshain and Pichon, 1986), located between the Arabian, Anatolian, and Eurasian plates (Dogan, 2017) and surrounded by alpine mountains (Hippolyte et al., 2018; Meredith and Egan, 2002). Huang et al., (2021) reported the paleosalinity changes of the Black Sea since the last deglaciation by investigating the evolution of *Isochrysidales* diversity. They reported the distributions of alkenones in a sediment core of the Black Sea and applied RIK $_{37}$ and C_{38}Me/C_{38}Et indices to quantify the salinity evolution over the last 16.6 ka. Their data show that the Black Sea has evolved from a near freshwater lake at 16.6 ka to oligohaline by 9.4 ka and a subsequent emergence of Group II *Iscochrysidales* as the dominant alkenone source because of later increase in surface water salinity beyond Group I haptophytes' tolerance. One of the implications of Black Sea's paleosalinity and ecological dynamics is that using $U_{37}^{K'}$ to reconstruct Black Sea's Sea surface temperature (SST) would encounter species mixing problems. This is because there are periods in the Holocene when *E. huxleyi* (Group III) is the dominant species, when $U_{37}^{K'}$ can probably be applied to calculate SST. However, there are also periods of strong salinity variations/decreases in the Holocene when Group II species become dominant. Group II species have a more complex ecology and easily cause bias to SST reconstruction (Yao et al., 2022). Using $U_{38ME}^{K'}$, instead of $U_{37}^{K'}$, for reconstructing SST during the Holocene has been proposed (Novak et al., 2022) as Group II *Isochrysidales* generally do not make (or make only trace amounts of) C_{38}Me ketones. The Black Sea was a low salinity lake during the deglacial event to

early Holocene and the species of haptophytes contributing alkenones are Group I and II (Huang et al., 2021). In this study, we investigate the impact of climatic events in the Holocene on the ecology of long-chain alkenone (LCA)-producing haptophytes in the Black Sea.

3.2. Materials and analytical procedure

3.2.1 Samples and sampling resolution

Samples, covering ~11.7 ka of deposit, from the Giant Gravity Core (GGC18) recovered from the Black Sea during cruise AK06 on the R/V *Akademik* in 2006 (Coolen et al., 2009; Filipova-Marinova et al., 2013; Huang et al., 2021) were used for this study. Fresh sediments collected from the core were freeze dried and grounded into fine powder for lipid extraction. Based on Hay et al., (1991)'s classification of Black Sea sediments into 3 sapropel units, the sample distribution in units I, II and III, were 3, 5 and 5 samples respectively.

3.2.2 Alkenone Analysis with RPLC-ESI-qTOF-MS

Sample preparation and analytical procedure are modified after Connock et al., (2022). From ~ 0.5 g of sediment taken from each sample to which 500 ng of internal standards – C_{46} glycerol trialkyl glycerol tetraether (C_{46}-GTGT) and Ni tetraphenylporphyrin (Ni-TPP), were added for quantitative analysis of targeted compounds, total lipid extracts (TLEs) were collected using a three times extraction with 1.5 mL DCM:MeOH (1:1) and a fourth time with pure DCM. This was achieved through the sediment being suspended with 2mL of solvent solution in a 4mL glass vial, vortexed and ultrasonicated in water bath for 20 minutes before centrifuging for 5 minutes at 3000 rpm. The supernatant was then carefully transferred after each cycle and dried under gentle N_2 stream and repeated. The combined TLE of each sample was redissolved in 1 mL MeOH, ultrasonicated for 10 minutes, centrifuged at 3000 rpm for 5 minutes and 500 μL (of

the TLE redissolved in MeOH) was transferred into a 2 mL injection vial for lipid analysis. RPLC-qTOF-MS was performed with an Agilent 1290 series UPLC system coupled to Agilent 6530 qTOF mass spectrometer through an Agilent jet stream dual electrospray ionization (AJS-ESI) interface. N_2 is both the nebulizer gas and ESI drying gas, with the temperature of the drying gas set to 300°C at a flow rate of 8 L min^{-1} and the nebulizer gas pressure being 35 psi. We set the qTOF parameters as follows: capillary voltage 3.5 kV, fragmentor voltage 175 V; skimmer voltage 65 V and octupole voltage 750 V in auto MS/MS scanning mode with MS range of m/z 50-2000 and MS/MS range of m/z 20-2000. For compounds separation, 10 µL sample was injected onto an ACE UltraCore Super C_{18} column (5 µm, 2.1 × 250 mm, ACE, Aberdeen, UK) maintained at 45°C. LC program was set at a flow rate of 0.2 mL min^{-1}, first hold 100% A for 5 min, and to 70% A and 30% B in 25 min, followed by a gradient to 50% B at 50 min and hold for 5 min, and finally re-equilibrated with 100% A at a flow rate of 0.4 mL min^{-1} for 5 min, where eluent A was 95: 5: 0.04 :0.10 of methanol/H_2O/formic acid/14.8 M NH_3(aq.) and B was 50: 50: 0.04: 0.10 of hexane/2-propanol/formic acid/14.8 M NH_3(aq.). Compound identification follows the protocol described in Liao et al., (2023a). Unlike the normal-phase HPLC-APCI-MS method (Becker et al., 2015), which exhibits poor chromatographic separation between alkenones of varying chain lengths and degrees of unsaturation, this method achieved baseline resolution between alkenones with different numbers of double bonds. Additionally, baseline resolution was attained for C_{37} alkenone double bond positional isomers ($C_{37:3a}$ and $C_{37:3b}$), as well as clear separation of C_{38Me} and C_{38Et} alkenone peaks.

3.2.3 Alkenone-based proxies discussed in this study

The ratio of C_{37} isomeric ketone, RIK_{37}, is computed after Longo et al., (2016) and it represents the ratio of C37:3a isomer to the sum of C37:3 ‘a’ and ‘b’ isomers (equation 1),

respectively representing double bond positions at $\Delta^{7,14,21}$ and $\Delta^{14,21,28}$ (Longo et al., 2016; Huang et al., 2021). Percentage abundances of the tetra unsaturated C_{37} alkenone, $\%C_{37:4}$, was computed as the amount of $C_{37:4}$ expressed as a percentage of all C_{37} alkenones (equation 2) (Huang et al., 2021). The $U_{37}^{K'}$ is arguably the most applied LCA proxy for paleotemperature reconstruction. Estimation of $U_{37}^{K'}$ is based on equation (3) after (Prahl and Wakeham, 1987). The $C_{38}Me/C_{38}Et$ was computed by dividing the sum of $C_{38}Me$ ketones by the sum of $C_{38}Et$ ketones (equation 4) (Huang et al., 2021).

$$RIK_{37} = (C_{37:3a}) / (C_{37:3a} + C_{37:3b}) \quad (1)$$

$$\%C_{37:4} = (C_{37:4}) * 100 / (C_{37:2} + C_{37:3} + C_{37:4}) \quad (2)$$

$$U_{37}^{K'} = C_{37:2} / (C_{37:2} + C_{37:3}) \quad (3)$$

$$C_{38}Me/C_{38}Et = (C_{38:2}Me + C_{38:3}Me + C_{38:4}Me)/(C_{38:2}Et + C_{38:3}Et + C_{38:4}Et) \quad (4)$$

3. 3 Results

3.3.1 Diversity of LCAs in the Black Sea sediment

Applying the recently developed RPLC-ESI-qTOF-MS method (Liao et al., 2023a), we identified C_{37}, C_{38} and C_{39} LCAs with two to four double bonds and C_{40} LCAs with two and three double bonds (Fig. 3.1) in the analyzed Black Sea sediments. The C_{40} LCAs are present only as ethyl ketones, whereas C_{37} LCAs occur exclusively as methyl ketones. Both methyl and ethyl ketone derivatives are found in C_{38} and C_{39} LCAs (Fig. 3.1). Isomers with varying double bond configurations (Longo et al., 2013) are observed for tri-unsaturated C_{37} and C_{38} LCAs, specifically the ‘a’ and ‘b’ isomers of $C_{37:3}Me$, $C_{38:3}Me$, and $C_{38:3}Et$ (Fig. 3.1).

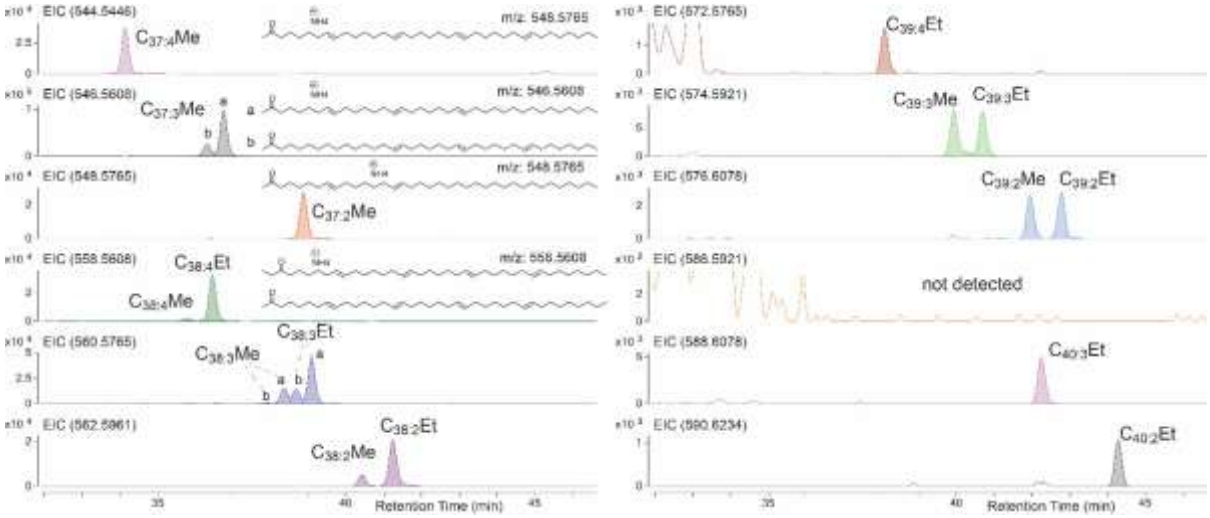


Figure 3.1: Extracted ion chromatograms (EICs) of RPLC-ESI-qTOF-MS showing the detection of LCAs in a representative sample.

3.3.2 LCAs distribution in the Black Sea sediments

In sediments of the GGC18 core, C_{37} LCAs have concentrations ranging from 8.1 to 868.2 µg/g OC, while C_{38}, C_{39} and C_{40} LCAs range from 12.2 to 1147.1 µg/g OC, 2.7 to 272.4 µg/g OC and 0.2 to 16.3 µg/g OC, respectively. The total estimated concentration of LCAs spans a broad range, from 84.8 to 2294.5 µg/g OC. Overall, LCAs of different carbon chain lengths display similar depth profiles in the Black Sea GGC18 core (Fig. 3.2). With respect to overall trend, concentrations were lowest in Unit II as anoxia developed in the basin, except for a slight interval observed in C40 around ~5.6 ka. The later part of the lake stage and early start of Mediterranean incursion (~11.7 – 7.6 ka) display a slightly higher concentration, highlighting adaptability to brackish water conditions. Concentrations are highest in Unit I, with a pronounced shift at the Unit II – Unit I boundary.

Among C_{37} ketones, $C_{37:3a}$ has the highest concentration, ranging from 0.8 to 625.3 µg/g OC, followed by $C_{37:2}$, which ranges from 5.3 to 183.3 µg/g OC. The $C_{37:3b}$ and $C_{37:4}$ exhibit concentration ranges of 0.1 to 33.4 µg/g OC and 0 to 55. µg/g OC, respectively (Fig. 3.3). $C_{37:3b}$

shows a high sensitivity to salinity with an increasing trend before which reverses almost immediately at the initial marine incursion at ~9.4 ka (Fig. 3.3b). Although there is a slight increase in estimated concentration, the magnitude of the concentration does not get to pre-connection levels. From approximately 4.6 ka to the present, $C_{37:2}$ concentration becomes elevated, possibly due to shifts in algal communities from marine to brackish conditions and increased sea surface temperature in the western Black Sea (Huang et al., 2021; Novak et al., 2022).

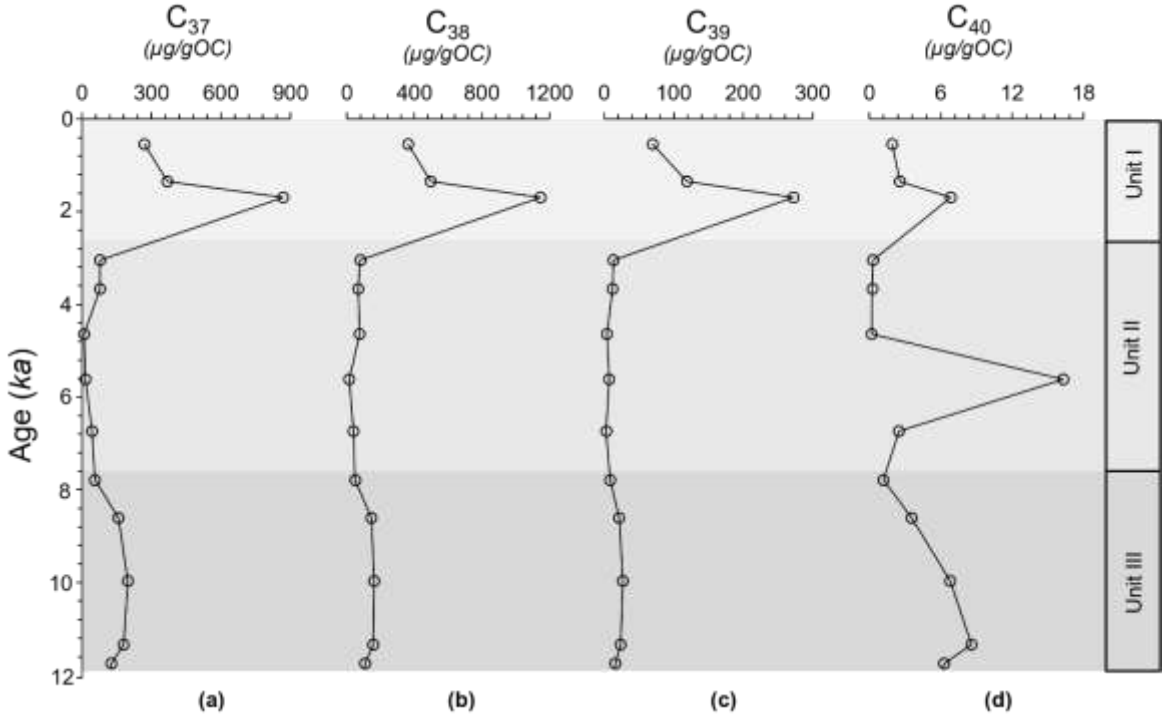


Figure 3.2: Estimated concentration of detected alkenones classes. C_{37} and C_{38} have the highest concentrations and similar profile. C_{39} and C_{40} have lower concentrations, with C_{40} having a slightly different profile. All concentrations are in µg gOC^{-1}

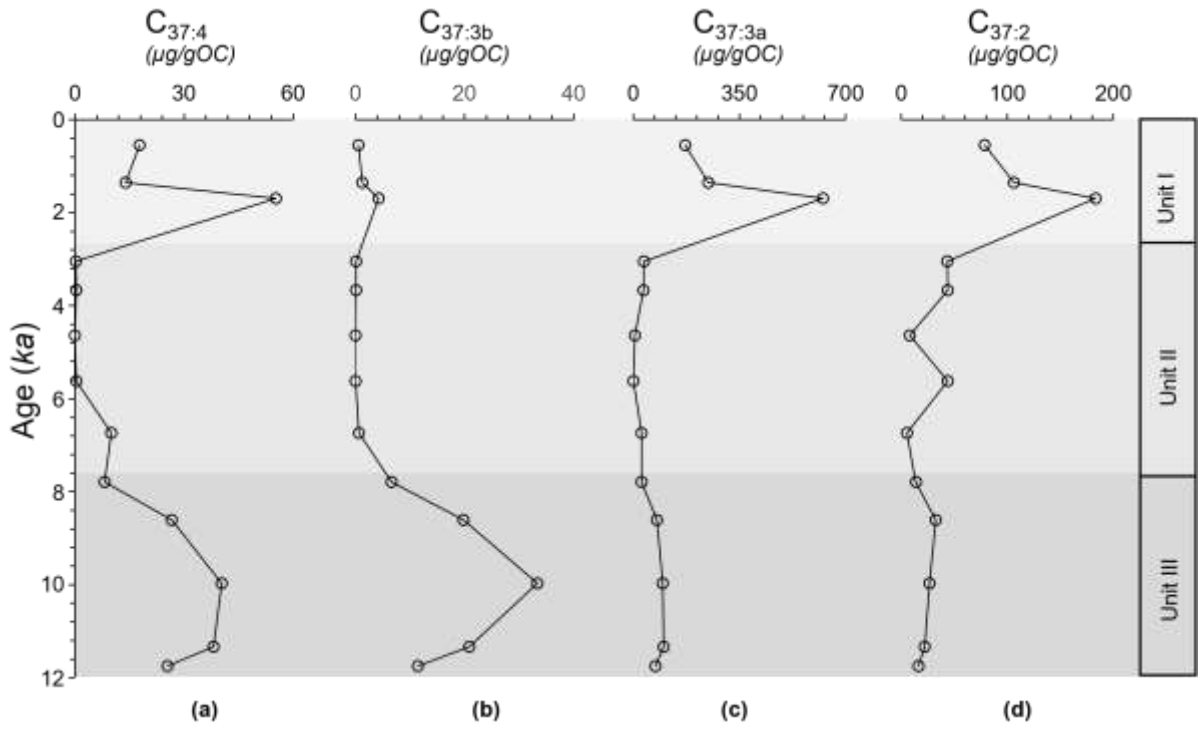


Figure 3.3: Estimated concentrations of C_{37} alkenones with different unsaturation degrees and configurations (the a, and b isomers). Concentrations are expressed in µg gOC^{-1}.

3.3.3 C_{37} and C_{38} based proxies

The RIK_{37} is not temperature sensitive and has been proposed as a salinity proxy for fresh to oligohaline waters (Longo et al., 2016). Between 11.7 to 9.4 ka, RIK_{37} values decreased showing brackish conditions of the Black Sea. From ~9.4 ka, there is a shift towards increasing values which further increased with the start of anoxia and water column stratification at around 7.6 ka signifying increasing salinity. The RIK_{37} ratio values from the past ~ 6ka is approximately 1, which is indicative of Black Sea salinity levels exceeding Group I haptophytes' tolerance (Longo et al., 2016, Zheng et al., 2019).

The $\%C_{37:4}$ has been reported to be sensitive to both temperature and salinity and can be used to infer the relative contributions of different Isochrysidales groups (Rosell-Melé,1998).

However, it appears to be better for estimating Isochrysidales contributions estimation rather than temperature reconstruction, based on estimated data from this study. The $\%C_{37:4}$ values diagnostic of Isochrysidales source are approximately >50 to 60%, ~5 to 50% and <5% for Group I, Group II and Group III, respectively (Huang et al., 2021). The Holocene section of the Black Sea is dominated by Group II and Group III. The interval prior to the start of rapid salinity increase and anoxia development with $\%C_{37:4}$ values between 14.9 to 21.2 % clearly falling in the range for Group II. With continuous inflow of the Mediterranean water to the Black Sea, values dropped to as low as 0.3 %, signifying dominance of Group III Isochrysidales (Fig. 3.4b).

Four isomers were detected in tri-unsaturated C_{38} ketone (Fig. 1), with $C_{38:3}$Me and $C_{38:3}$Et each showing two isomers with different double bond configurations (Dillon et al., 2016). Assignment of molecular structures was based on the eluting order and relative abundance of identified structures in GC-FID, as described in Liao et al. (2023a). The C_{38}Me/C_{38}Et data provide insights into haptophyte ecological dynamics related to salinity variations (Novak et al., 2022). The C_{38}Me/C_{38}Et profile (Fig. 3.4d) does not align so much with previously reported values and pattern for the Black Sea (e.g. Liao et al., 2023b; Novak et al., 2022; Hunag et al., 2021).

3.4 Discussion

3.4.1 Factors controlling the distribution of LCAs in the Black Sea

In addition to the decreasing concentrations of LCAs with increasing carbon chain length, our data show a notable trend where each LCA class maintains nearly consistent relative levels across the Holocene sequence. While the factors controlling carbon chain length in LCAs are not fully understood, growth temperature (Brassell et al., 1986; Prahl and Wakeham, 1987), nutrient

availability, and cell growth rate (Prahl and Wakeham, 1987) are recognized as key influences on the degree of unsaturation degree.

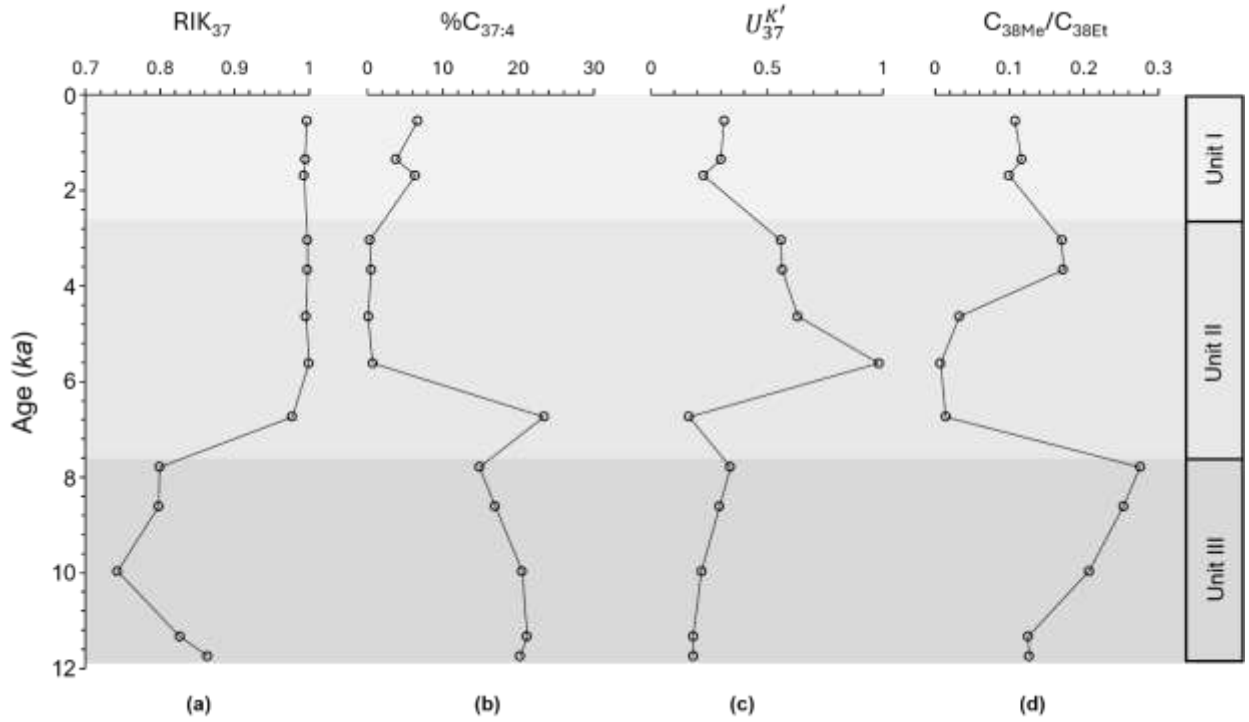


Fig. 3.4: C_{37} and C_{38} alkenone proxies. (a) RIK_{37}, a salinity indicator shows the salinity evolution in the Holocene. (b) $\%C_{37:4}$ another salinity indicator gives a good correlation with RIK_{37}. (C) $U_{37}^{K'}$ data does not show a good temperature profile for the Holocene Black Sea. (d) $C_{38}Me/C_{38}Et$ a potential salinity indicator

The timing and nature of the Black Sea's reconnection with the Mediterranean remain debated (Filipova-Marinova et al., 2013; Major et al., 2002, 2006; Ryan et al., 1997; Vidal et al., 2010). However, it is widely accepted that the Black Sea has experienced salinity fluctuations linked to temperature variations since the last deglaciation (Aksu et al., 2002; Bahr et al., 2008; Hiscott et al., 2007; Major et al., 2002; Ryan et al., 1997). However, there are variations in

degrees of unsaturation within each LCA class (Figs 3.3, S3.1, S3.2). Lower temperature favors the synthesis of more double bonds in LCAs (Brassell et al., 1986), but there appears to be other factors that control this.

Our data depict a decreasing trend in the amount of tetra-unsaturated LCAs with increasing carbon chain length which is supported by culture experiments (Yao et al., 2019). The exact control for this observation is, however, not well understood. Tri-unsaturated alkenone appears to perhaps be the physiologically "more stable" alkenone with di- and tetra unsaturation being compounds formed in response to physiological, chemical or ecological changes. Another observation in the relationship between unsaturation and carbon chain length is the near absence of tetra-unsaturated alkenones with increasing salinity and redox evolution. In C_{37} - C_{39} alkenones where tetra-unsaturated compounds are detected, their concentration along salinity trends reveal a possible control on their abundance. In Unit III which represents the late stage of the lake phase and earliest part of the reconnection where the water column has not equilibrated, the relative abundance of the tetra-unsaturated compounds was more pronounced. However, as Mediterranean inflow persisted and water stratification developed, tetra-unsaturated compounds were either only slightly detected or not detected. Late Holocene surface water freshening has been suggested in the Black Sea (Novak et al., 2022). A detection of these tetra-unsaturated compounds correlating with the period of reported surface water freshening further supports possible salinity control on the distribution of alkenone unsaturation.

The decline in estimated concentrations of all detected alkenone classes at the Unit III – Unit II boundary, supports a dramatic shift in water chemistry during this transition when the Black Sea turned into a stratified water column. Reduced nutrient availability in the surface waters, possibly due to restricted terrestrial nutrient inflow and/or water column stratification

limiting vertical circulation, could be a factor. Alternatively, as proposed by Prahl and Wakeham (1987), this decline in concentration might result from poor LCA preservation rather than a production decline. Also, the development of euxinic conditions in the water column may have created an environment suitable for heterotrophic bacteria decomposing phytoplanktonic lipids.

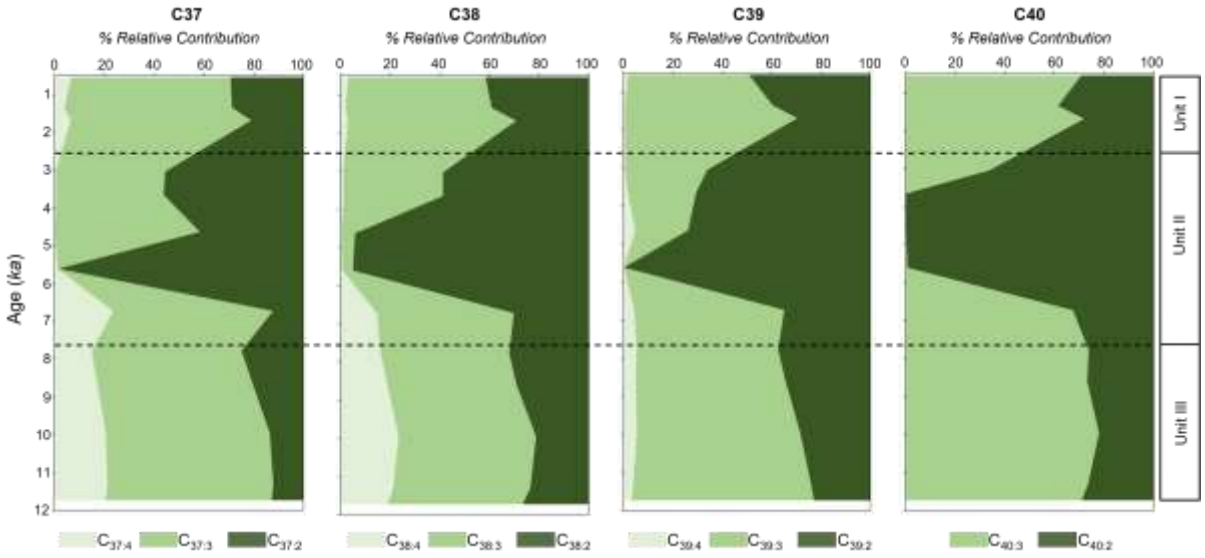


Figure 3.5: Percent relative abundance plot of detected alkenones clearly characterizes the climate-induced salinity and redox changes of the Holocene. Di-unsaturated alkenones dominate with anoxia development. Tetra-unsaturated compounds progressively decreased with increasing carbon chain length. (Where isomers and methyl-, ethyl- compounds were detected they were summed into the respective unsaturation class).

3.4.2 Re-evaluating Black Sea's salinity evolution and limitation of $U_{37}^{K'}$ in paleotemperature reconstruction

The RIK_{37} and $C_{38}Me/C_{38}Et$ ratios have been reported as salinity indicators (Huang et al., 2021; Novak et al., 2022), offering salinity proxies beyond a single alkenone carbon chain length. Group II *Isochrysidales* have a wide range of salinity tolerance and temperature sensitivities (Theroux et al., 2013; Toney et al., 2012) and therefore have an ecology ranging from freshwater to marine. Both Group I and Group III *Isochrysidales* make C_{38} methyl ketones, but Group II do not (Huang et al., 2021), implying that $C_{38}Me/C_{38}Et$ can be used to estimate the relative change of Group II *Isochrysidales*. While $C_{38}Me/C_{38}Et$ data offers some insight into the salinity trend in the early Holocene, it does not offer an accurate salinity trend in the Mid Holocene (Fig. 3.4c). The RIK_{37} offers a more accurate and consistent salinity proxy, with more freshening between the start of Holocene to the time of first Mediterranean water delivery. Although equilibration of the water column to marine was not immediate, there is an immediate response in the source organism to the marine water delivery evinced by the increasing trend of RIK_{37} values between 9.4 and 7.6 ka. Although the data set used for this study does not provide the highest level of resolution, RIK_{37} attaining a value of approximately 1 as soon as ~6.7 ka, provides some insight as to the nature of the reconnection. Equilibration of the water column to fully marine in about ~ 3kyr suggests a more gradual rather than catastrophic nature of Mediterranean inflow. The return to warm temperatures in the Holocene that triggered the reconnection of the Black Sea to the global ocean is characterized by a reduction in the contribution of LCA-producing haptophytes to the organic matter pool, as the absolute concentration of all detected LCAs classes decreased, a likely indication of the salinity and/or temperature intolerance of the microbial community.

The increase in salinity of the Black Sea in the Holocene interval is supported by the decreasing trend, albeit with a slight variation, of $\%C_{37:4}$. The haptophyte community must have shifted predominantly to Group III haptophytes by Mid Holocene where $\%C_{37:4}$ values were less than 1%.

Species mixing, lower temperature limits and restriction to open-ocean depositional environments (Muller et al., 1998; Tierney and Tingley, 2018; Mercer et al., 2005; Bendle et al., 2009; Kaiser et al., 2019) are some of the main challenges to the use of $U_{37}^{K'}$ to reconstruct sea surface temperature. Although the absolute sea surface temperature was not estimated, $U_{37}^{K'}$ data does not give a good correlation with temperature evolution across the Black Sea in the Holocene. This observation further validates the limitation of $U_{37}^{K'}$ in sea surface temperature reconstruction in the Black Sea.

3.5 Conclusion

Through the application of RPLC-ESI-qTOF-MS we showed the diversity and distribution of LCAs in the Black Sea. Although the focus of this work is not to compute past SST, we use LCA data and supporting data to describe the impact of temperature and water chemistry variation in the Black Sea over the last ~ 11.7 ka, an interval covering the Holocene. Separation of many otherwise co-eluting alkenones was achieved and proved that this method provides an advantage over the normal-phase HPLC method. We reported the correlation of salinity increase to the disappearance or reduction of tetra-unsaturated alkenones. Potentially, salinity and temperature coupling in the Black Sea is expected, but there is no single reported proxy for this postulation yet. The major temperature and water chemistry shifts that occurred at the start of Holocene are reflected in the alkenone-producing community of the Black Sea, further helping to provide insight into timing and nature of the reconnection of the Black Sea to

the global ocean. There might be an internal regulatory mechanism for haptophytes' synthesis of carbon chain length that limits the effects of temperature and salinity control,but clearly salinity and temperature affect the degree of unsaturation.

3.6 References

Aksu, A.E., Hiscott, R.N., Yas, D., 2002. Seismic stratigraphy of Late Quaternary deposits from the southwestern Black Sea shelf: evidence for non-catastrophic variations in sea-level during the last V10 000 yr. Mar. Geol. 34.

Ausín, B., Haghipour, N., Bruni, E., Eglinton, T., 2022. The influence of lateral transport on sedimentary alkenone paleoproxy signals. Biogeosciences 19, 613–627. https://doi.org/10.5194/bg-19-613-2022

Bahr, A., Lamy, F., Arz, H.W., Major, C., Kwiecien, O., Wefer, G., 2008. Abrupt changes of temperature and water chemistry in the late Pleistocene and early Holocene Black Sea. Geochem. Geophys. Geosystems 9, 2007GC001683. https://doi.org/10.1029/2007GC001683

Becker, K.W., Lipp, J.S., Versteegh, G.J.M., Wörmer, L., Hinrichs, K.-U., 2015. Rapid and simultaneous analysis of three molecular sea surface temperature proxies and application to sediments from the Sea of Marmara. Org. Geochem. 85, 42–53. https://doi.org/10.1016/j.orggeochem.2015.04.008

Bendle, J.A.P., Rosell-Melé, A., Cox, N.J., Shennan, I., 2009. Alkenones, alkenoates, and organic matter in coastal environments of NW Scotland: Assessment of potential application for sea level reconstruction. Geochem. Geophys. Geosystems 10. https://doi.org/10.1029/2009GC002603

Brassell, S.C., Dumitrescu, M., 2004. Recognition of alkenones in a lower Aptian porcellanite from the west-central Pacific. Org. Geochem. 35, 181–188. https://doi.org/10.1016/j.orggeochem.2003.09.003

Brassell, S.C., Eglinton, G., Marlowe, I.T., Pflaumann, U., Sarnthein, M., 1986. Molecular stratigraphy: a new tool for climatic assessment. Nature 320, 129–133. https://doi.org/10.1038/320129a0

Chivall, D., M'Boule, D., Sinke-Schoen, D., Sinninghe Damsté, J.S., Schouten, S., Van Der Meer, M.T.J., 2014. Impact of salinity and growth phase on alkenone distributions in coastal haptophytes. Org. Geochem. 67, 31–34. https://doi.org/10.1016/j.orggeochem.2013.12.002

Connock, G.T., Owens, J.D., Liu, X.-L., 2022. Biotic induction and microbial ecological dynamics of Oceanic Anoxic Event 2. Commun. Earth Environ. 3, 136. https://doi.org/10.1038/s43247-022-00466-x

Coolen, M., 2004. Combined DNA and lipid analyses of sediments reveal changes in Holocene haptophyte and diatom populations in an Antarctic Lake. Earth Planet. Sci. Lett. 223, 225–239. https://doi.org/10.1016/j.epsl.2004.04.014

Coolen, M.J.L., Saenz, J.P., Giosan, L., Trowbridge, N.Y., Dimitrov, P., Dimitrov, D., Eglinton, T.I., 2009. DNA and lipid molecular stratigraphic records of haptophyte succession in the Black Sea during the Holocene. Earth Planet. Sci. Lett. 284, 610–621. https://doi.org/10.1016/j.epsl.2009.05.029

Dillon, J.T., Longo, W.M., Zhang, Y., Torozo, R., Huang, Y., 2016. Identification of double-bond positions in isomeric alkenones from a lacustrine haptophyte: Alkenone double-bond positional isomers in a lacustrine haptophyte. Rapid Commun. Mass Spectrom. 30, 112–118. https://doi.org/10.1002/rcm.7414

Dinu, C., Wong, H.K., Tambrea, D., Matenco, L., 2005. Stratigraphic and structural characteristics of the Romanian Black Sea shelf. Tectonophysics 410, 417–435. https://doi.org/10.1016/j.tecto.2005.04.012
Dogan, K., 2017. Seismicity and Tectonics of the Black Sea. Int. J. Earth Sci. Geophys. 3. https://doi.org/10.35840/2631-5033/1811
Epstein, B.L., D'Hondt, S., Quinn, J.G., Zhang, J., Hargraves, P.E., 1998. An effect of dissolved nutrient concentrations on alkenone-based temperature estimates. Paleoceanography 13, 122–126. https://doi.org/10.1029/97PA03358
Farrimond, P., Eglinton, G., Brassell, S.C., 1986. Alkenones in Cretaceous black shales, Blake-Bahama Basin, western North Atlantic. Org. Geochem. 10, 897–903. https://doi.org/10.1016/S0146-6380(86)80027-4
Filipova-Marinova, M., Pavlov, D., Coolen, M., Giosan, L., 2013. First high-resolution marinopalynological stratigraphy of Late Quaternary sediments from the central part of the Bulgarian Black Sea area. Quat. Int. 293, 170–183. https://doi.org/10.1016/j.quaint.2012.05.002
Freeman, K., Wakeham, S., 1992. Variations in the distributions and isotopic compositions of alkenones in Black Sea particles and sediments. Adv. Org. Geochem. 19, 277–285.
Görür, N., 1988. Timing of opening of the Black Sea basin. Tectonophysics 147, 247–262. https://doi.org/10.1016/0040-1951(88)90189-8
Harvey, H.R., 2000. Alteration processes of alkenones and related lipids in water columns and sediments. Geochem. Geophys. Geosystems 1. https://doi.org/10.1029/2000GC000054
Hay, B.J., Arthur, M.A., Dean, W.E., Neff, E.D., Honjo, S., 1991. Sediment deposition in the Late Holocene abyssal Black Sea with climatic and chronological implications. Deep Sea Res. Part Oceanogr. Res. Pap. 38, S1211–S1235. https://doi.org/10.1016/S0198-0149(10)80031-7
Hippolyte, J.-C., Murovskaya, A., Volfman, Y., Yegorova, T., Gintov, O., Kaymakci, N., Sangu, E., 2018. Age and geodynamic evolution of the Black Sea Basin: Tectonic evidences of rifting in Crimea. Mar. Pet. Geol. 93, 298–314. https://doi.org/10.1016/j.marpetgeo.2018.03.009
Hiscott, R.N., Aksu, A.E., Mudie, P.J., Marret, F., Abrajano, T., Kaminski, M.A., Evans, J., Çakiroğlu, A.İ., Yaşar, D., 2007. A gradual drowning of the southwestern Black Sea shelf: Evidence for a progressive rather than abrupt Holocene reconnection with the eastern Mediterranean Sea through the Marmara Sea Gateway. Quat. Int. 167–168, 19–34. https://doi.org/10.1016/j.quaint.2006.11.007
Hoefs, M.J.L., Versteegh, G.J.M., Rijpstra, W.I.C., de Leeuw, J.W., Damsté, J.S.S., 1998. Postdepositional oxic degradation of alkenones: Implications for the measurement of palaeo sea surface temperatures. Paleoceanography 13, 42–49. https://doi.org/10.1029/97PA02893
Huang, Y., Zheng, Y., Heng, P., Giosan, L., Coolen, M.J.L., 2021. Black Sea paleosalinity evolution since the last deglaciation reconstructed from alkenone-inferred Isochrysidales diversity. Earth Planet. Sci. Lett. 564, 116881. https://doi.org/10.1016/j.epsl.2021.116881
Kaiser, J., van der Meer, M.T.J., Arz, H.W., 2017. Long-chain alkenones in Baltic Sea surface sediments: New insights. Org. Geochem. 112, 93–104. https://doi.org/10.1016/j.orggeochem.2017.07.002
Kaiser, J., Wang, K.J., Rott, D., Li, G., Zheng, Y., Amaral-Zettler, L., Arz, H.W., Huang, Y., 2019. Changes in long chain alkenone distributions and Isochrysidales groups along the

Baltic Sea salinity gradient. Org. Geochem. 127, 92–103. https://doi.org/10.1016/j.orggeochem.2018.11.012

Liao, S., Liu, X.-L., Manz, K.E., Pennell, K.D., Novak, J., Santos, E., Huang, Y., 2023. Comprehensive analysis of alkenones by reversed-phase HPLC-MS with unprecedented selectivity, linearity and sensitivity. Talanta 260, 124653. https://doi.org/10.1016/j.talanta.2023.124653

Liao, S., Novak, J., Huang, Y., 2023b. Exploring the theoretical upper temperature limit of alkenone unsaturation indices: Implications for paleotemperature reconstructions. Org. Geochem. 180, 104606. https://doi.org/10.1016/j.orggeochem.2023.104606

Liu, H., Probert, I., Uitz, J., Claustre, H., Aris-Brosou, S., Frada, M., Not, F., de Vargas, C., 2009. Extreme diversity in noncalcifying haptophytes explains a major pigment paradox in open oceans. Proc. Natl. Acad. Sci. 106, 12803–12808. https://doi.org/10.1073/pnas.0905841106

Longo, W.M., Dillon, J.T., Tarozo, R., Salacup, J.M., Huang, Y., 2013. Unprecedented separation of long chain alkenones from gas chromatography with a poly(trifluoropropylmethylsiloxane) stationary phase. Org. Geochem. 65, 94–102. https://doi.org/10.1016/j.orggeochem.2013.10.011

Longo, W.M., Huang, Y., Yao, Y., Zhao, J., Giblin, A.E., Wang, X., Zech, R., Haberzettl, T., Jardillier, L., Toney, J., Liu, Z., Krivonogov, S., Kolpakova, M., Chu, G., D'Andrea, W.J., Harada, N., Nagashima, K., Sato, M., Yonenobu, H., Yamada, K., Gotanda, K., Shinozuka, Y., 2018. Widespread occurrence of distinct alkenones from Group I haptophytes in freshwater lakes: Implications for paleotemperature and paleoenvironmental reconstructions. Earth Planet. Sci. Lett. 492, 239–250. https://doi.org/10.1016/j.epsl.2018.04.002

Longo, W.M., Theroux, S., Giblin, A.E., Zheng, Y., Dillon, J.T., Huang, Y., 2016. Temperature calibration and phylogenetically distinct distributions for freshwater alkenones: Evidence from northern Alaskan lakes. Geochim. Cosmochim. Acta 180, 177–196. https://doi.org/10.1016/j.gca.2016.02.019

Major, C., Ryan, W., Lericolais, G., Hajdas, I., 2002. Constraints on Black Sea outflow to the Sea of Marmara during the last glacial^interglacial transition. Mar. Geol. 16.

Major, C.O., Goldstein, S.L., Ryan, W.B.F., Lericolais, G., Piotrowski, A.M., Hajdas, I., 2006. The co-evolution of Black Sea level and composition through the last deglaciation and its paleoclimatic significance. Quat. Sci. Rev. 25, 2031–2047. https://doi.org/10.1016/j.quascirev.2006.01.032

Mercer, J.L., Zhao, M., Colman, S.M., 2005. Seasonal variations of alkenones and UK37 in the Chesapeake Bay water column. Estuar. Coast. Shelf Sci. 63, 675–682. https://doi.org/10.1016/j.ecss.2005.01.011

Meredith, D.J., Egan, S.S., 2002. The geological and geodynamic evolution of the eastern Black Sea basin: insights from 2-D and 3-D tectonic modelling. Tectonophysics 350, 157–179. https://doi.org/10.1016/S0040-1951(02)00121-X

Mu¨ller P. J., Kirst G. and Ruhland G., et al. (1998) Calibration of the alkenone paleotemperature index UK'37 based on core-tops from the eastern South Atlantic and the global ocean (60°N-60° S). Geochim. Cosmochim. Acta 62, 1757–1772

Nikishin, A.M., Korotaev, M.V., Ershov, A.V., Brunet, M.-F., 2003. The Black Sea basin: tectonic history and Neogene–Quaternary rapid subsidence modelling. Sediment. Geol. 156, 149–168. https://doi.org/10.1016/S0037-0738(02)00286-5

Novak, J., McGrath, S.M., Wang, K.J., Liao, S., Clemens, S.C., Kuhnt, W., Huang, Y., 2022. U 38 M E K ′ Expands the linear dynamic range of the alkenone sea surface temperature proxy. Geochim. Cosmochim. Acta 328, 207–220. https://doi.org/10.1016/j.gca.2022.04.021

Okay, A.I., Celal Şengör, A.M., Görür, N., 1994. Kinematic history of the opening of the Black Sea and its effect on the surrounding regions. Geology 22, 267. https://doi.org/10.1130/0091-7613(1994)022<0267:KHOTOO>2.3.CO;2

Pearson, E.J., Juggins, S., Farrimond, P., 2008. Distribution and significance of long-chain alkenones as salinity and temperature indicators in Spanish saline lake sediments. Geochim. Cosmochim. Acta 72, 4035–4046. https://doi.org/10.1016/j.gca.2008.05.052

Prahl, F.G., de Lange, G.J., Lyle, M., Sparrow, M.A., 1989. Post-depositional stability of long-chain alkenones under contrasting redox conditions. Nature 341, 434–437. https://doi.org/10.1038/341434a0

Prahl, F.G., Muehlhausen, L.A., Zahnle, D.L., 1988. Further evaluation of long-chain alkenones as indicators of paleoceanographic conditions. Geochim. Cosmochim. Acta 52, 2303–2310. https://doi.org/10.1016/0016-7037(88)90132-9

Prahl, F.G., Wakeham, S.G., 1987. Calibration of unsaturation patterns in long-chain ketone compositions for palaeotemperature assessment. Nature 330, 367–369. https://doi.org/10.1038/330367a0

Robinson, A.G., Rudat, J.H., Banks, C.J., Wiles, R.L.F., 1996. Petroleum geology of the Black Sea. Mar. Pet. Geol. 13, 195–223. https://doi.org/10.1016/0264-8172(95)00042-9

Rontani, J.-F., Harji, R., Guasco, S., Prahl, F.G., Volkman, J.K., Bhosle, N.B., Bonin, P., 2008. Degradation of alkenones by aerobic heterotrophic bacteria: Selective or not? Org. Geochem. 39, 34–51. https://doi.org/10.1016/j.orggeochem.2007.10.003

Rontani, J.-F., Volkman, J.K., Prahl, F.G., Wakeham, S.G., 2013. Biotic and abiotic degradation of alkenones and implications for U37K′ paleoproxy applications: A review. Org. Geochem. 59, 95–113. https://doi.org/10.1016/j.orggeochem.2013.04.005

Rosell-Melé, A., 1998. Interhemispheric appraisal of the value of alkenone indices as temperature and salinity proxies in high-latitude locations. Paleoceanography 13, 694–703. https://doi.org/10.1029/98PA02355

Ryan, W.B.F., Pitman, W.C., Major, C.O., Shimkus, K., Moskalenko, V., Jones, G.A., Dimitrov, P., Gorür, N., Sakinç, M., Yüce, H., 1997. An abrupt drowning of the Black Sea shelf. Mar. Geol. 138, 119–126. https://doi.org/10.1016/S0025-3227(97)00007-8

Sikes, E.L., Farrington, J.W., Keigwin, L.D., 1991. Use of the alkenone unsaturation ratio U37k to determine past sea surface temperatures: core-top SST calibrations and methodology considerations. Earth Planet. Sci. Lett. 104, 36–47. https://doi.org/10.1016/0012-821X(91)90235-A

Theroux, S., D'Andrea, W.J., Toney, J., Amaral-Zettler, L., Huang, Y., 2010. Phylogenetic diversity and evolutionary relatedness of alkenone-producing haptophyte algae in lakes: Implications for continental paleotemperature reconstructions. Earth Planet. Sci. Lett. 300, 311–320. https://doi.org/10.1016/j.epsl.2010.10.009

Theroux, S., Toney, J., Amaral-Zettler, L., Huang, Y., 2013. Production and temperature sensitivity of long chain alkenones in the cultured haptophyte Pseudoisochrysis paradoxa. Org. Geochem. 62, 68–73. https://doi.org/10.1016/j.orggeochem.2013.07.006

Tierney, J.E., Tingley, M.P., 2018. BAYSPLINE: A New Calibration for the Alkenone Paleothermometer. Paleoceanogr. Paleoclimatology 33, 281–301. https://doi.org/10.1002/2017PA003201

Toney, J.L., Theroux, S., Andersen, R.A., Coleman, A., Amaral-Zettler, L., Huang, Y., 2012. Culturing of the first 37:4 predominant lacustrine haptophyte: Geochemical, biochemical, and genetic implications. Geochim. Cosmochim. Acta 78, 51–64. https://doi.org/10.1016/j.gca.2011.11.024

Vidal, L., Ménot, G., Joly, C., Bruneton, H., Rostek, F., Çağatay, M.N., Major, C., Bard, E., 2010. Hydrology in the Sea of Marmara during the last 23 ka: Implications for timing of Black Sea connections and sapropel deposition: PALEOHYDROLOGY OF THE SEA OF MARMARA. Paleoceanography 25. https://doi.org/10.1029/2009PA001735

Yao, Y., Zhao, J., Longo, W.M., Li, G., Wang, X., Vachula, R.S., Wang, K.J., Huang, Y., 2019. New insights into environmental controls on the occurrence and abundance of Group I alkenones and their paleoclimate applications: Evidence from volcanic lakes of northeastern China. Earth Planet. Sci. Lett. 527, 115792. https://doi.org/10.1016/j.epsl.2019.115792

Yao, Y., Zhao, J., Vachula, R.S., Liao, S., Li, G., Pearson, E.J., Huang, Y., 2022. Phylogeny, alkenone profiles and ecology of Isochrysidales subclades in saline lakes: Implications for paleosalinity and paleotemperature reconstructions. Geochim. Cosmochim. Acta 317, 472–487. https://doi.org/10.1016/j.gca.2021.11.001

Zhao, J., An, C., Longo, W.M., Dillon, J.T., Zhao, Y., Shi, C., Chen, Y., Huang, Y., 2014. Occurrence of extended chain length C41 and C42 alkenones in hypersaline lakes. Org. Geochem. 75, 48–53. https://doi.org/10.1016/j.orggeochem.2014.06.006

Zheng, Y., Heng, P., Conte, M.H., Vachula, R.S., Huang, Y., 2019. Systematic chemotaxonomic profiling and novel paleotemperature indices based on alkenones and alkenoates: potential for disentangling mixed species input. Org. Geochem. 128, 26–41.

Zonenshain, L.P., Pichon, X., 1986. Deep basins of the Black Sea and Caspian Sea as remnants of Mesozoic back-arc basins. Tectonophysics 123, 181–211. https://doi.org/10.1016/0040-1951(86)90197-6

Appendix

Table S3.1: Estimated concentration of each class of detected long-chain alkenones. (All concentrations are in µg gOC^{-1})

Age (ka)	C37	C38	C39	C40
547.4	268.16	362.76	69.42	1.94
1351.4	369.13	497.06	119.26	2.59
1690.1	868.18	1147.14	272.35	6.86
3044.7	78.26	78.62	13.39	0.33
3662.1	77.93	66.52	11.92	0.25
4639.8	12.77	73.56	3.82	0.19
5617.5	45.01	29.55	18.01	41.11
6734.9	42.72	36.83	2.75	2.49
7788.3	55.16	47.90	8.49	1.20
8607.0	157.56	144.52	21.56	3.56
9971.5	196.96	160.32	26.94	6.80
11336.0	180.19	156.44	23.64	8.57
11745.3	125.57	107.29	16.28	6.27

Table S3.2: Estimated concentration of C_{37} alkenones of varying saturation levels. (All concentrations are in µg gOC^{-1})

Age *(ka)*	**C37:4**	**C37:3b**	**C37:3a**	**C37:2**
547.4	17.80	0.581	170.997	78.778
1351.4	14.02	1.281	247.418	106.408
1690.1	55.29	4.254	625.342	183.297
3044.7	0.25	0.075	34.374	43.565
3662.1	0.40	0.077	33.603	43.855
4639.8	0.02	0.020	4.676	8.052
5617.5	0.32	0.010	0.811	43.870
6734.9	10.00	0.619	26.841	5.261
7788.3	8.19	6.659	26.511	13.795
8607.0	26.66	19.798	78.342	32.758
9971.5	40.37	33.355	96.393	26.844
11336.0	38.12	20.829	99.281	21.958
11745.3	25.42	11.450	72.495	16.200

Table S3.3: Estimated concentration of C38 alkenones with different number of double bonds and methyl- or ethyl- compounds. (All concentrations are in µg gOC^{-1})

Age *(ka)*	**C38:4Me**	**C38:4Et**	**C38:3aMe**	**C38:3bEt**	**C38:3aEt**	**C38:2Me**	**C38:2Et**
547.4	2.82	8.05	0.56	94.18	105.75	31.88	119.52
1351.4	7.29	2.09	0.56	138.34	153.96	43.89	150.94
1690.1	28.35	4.56	2.09	377.83	397.43	73.25	263.63
3044.7	0.40	0.34	0.21	13.20	18.21	10.84	35.41
3662.1	0.32	0.45	0.23	9.68	16.69	9.22	29.94
4639.8	0.12	0.08	1.18	0.46	2.40	1.04	68.29
5617.5	0.01	0.08	0.09		0.34	0.11	28.91
6734.9		5.35	0.39	0.47	19.47	0.14	11.02
7788.3	0.65	7.04	6.50	3.63	14.67	3.19	12.21
8607.0	1.49	25.59	18.57	13.02	43.60	9.13	33.14
9971.5	1.71	35.63	19.09	17.31	52.39	6.69	27.50
11336.0	0.95	32.02	12.20	9.86	64.30	4.24	32.88
11745.3	0.79	19.40	8.07	6.30	44.00	3.20	25.51

Table S3.4: Estimated concentration of C39 alkenones with different number of double bonds and methyl- or ethyl- compounds. (All concentrations are in µg gOC^{-1})

Age *(ka)*	**C39:4**	**C39:3Me**	**C39:3Et**	**C39:2Me**	**C39:2Et**
547.4	1.12	4.21	29.81	1.49	32.79
1351.4	0.50	4.48	66.94	3.65	43.70
1690.1	1.13	14.85	175.28	4.80	76.28
3044.7	0.07	0.30	4.16	1.36	7.51
3662.1	0.19	0.40	2.89	1.51	6.93
4639.8	0.18	0.09	0.73	1.88	0.95
5617.5	0.00	0.10	0.10	15.14	2.67
6734.9	0.11	1.48	0.19	0.82	0.14
7788.3	0.44	1.60	3.25	0.87	2.32
8607.0	1.02	4.00	9.09	2.04	5.40
9971.5	1.42	8.04	9.79	3.48	4.21
11336.0	0.88	9.68	7.39	2.99	2.71
11745.3	0.52	7.16	4.85	1.85	1.90

Table S3.5: Estimated concentration of C40 alkenones with two and three double bonds. They exist as ethyl- compounds. (Concentrations are in µg gOC^{-1})

Age *(ka)*	**C40:3Et**	**C40:2Et**
547.4	1.37	0.57
1351.4	1.59	1.00
1690.1	4.93	1.93
3044.7	0.11	0.22
3662.1		0.25
4639.8		0.19
5617.5	0.21	40.90
6734.9	1.68	0.82
7788.3	0.88	0.31
8607.0	2.60	0.96
9971.5	5.29	1.51
11336.0	6.29	2.28
11745.3	4.44	1.83

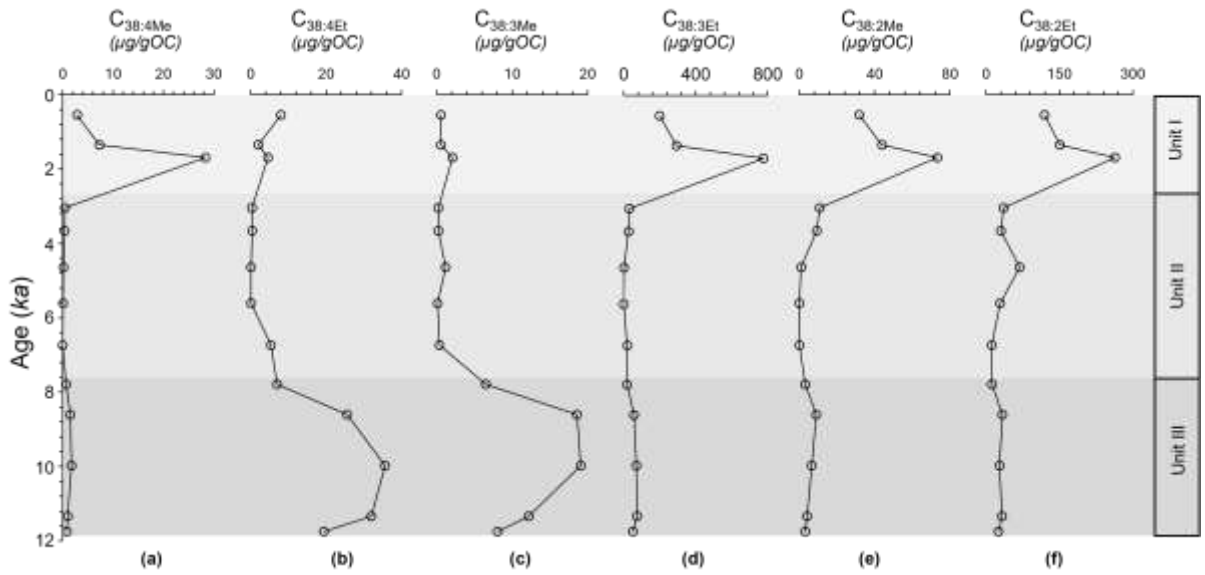


Figure S3.1: Estimated concentration of C38 alkenones showing the diversity of compounds. $C_{38:4}$Et and $C_{38:3}$Me show preference for brackish conditions due to their higher abundance during the lake stage. All other detected compounds have similar profiles – suppressed abundance with increasing salinity and water column stratification and a sign of recovery in Late Holocene. All concentrations are in µg gOC^{-1}

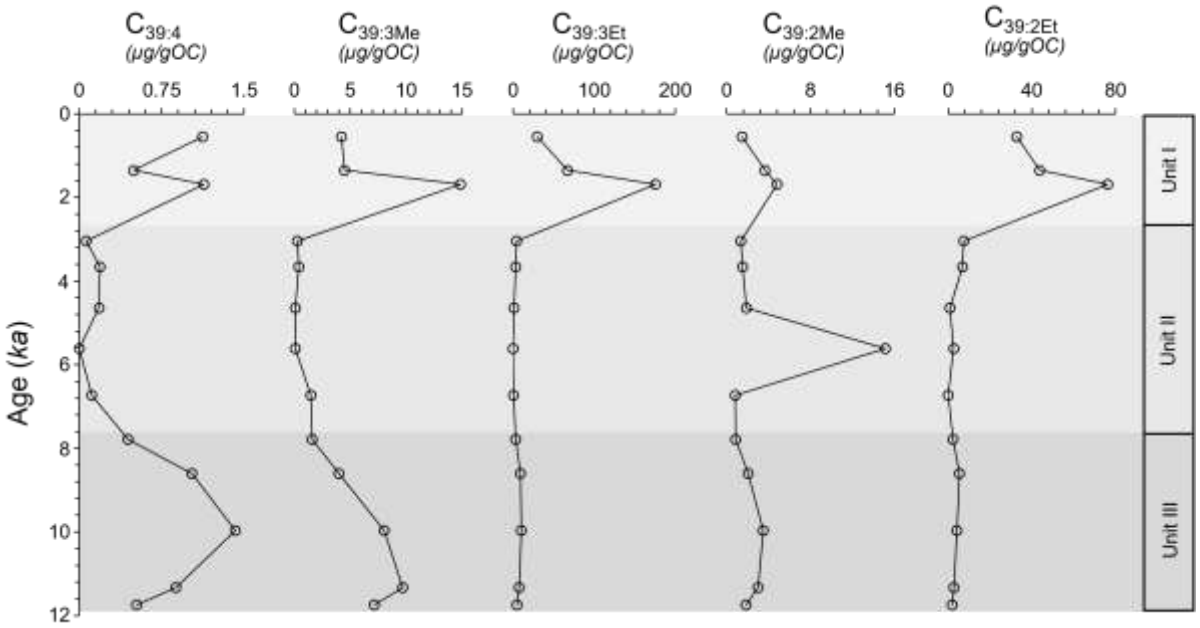


Figure S3.2: Estimated concentration of C39 alkenones. C39:4, C39:3Me and C39:2Me have pronounced higher abundance in the lake stage that gradually decreased as increasing salinity. All detected compounds have similar profiles in Late Holocene. All concentrations are in μg gOC^{-1}

Summary and Implications for future research

This research provides further validation for the use of integrated lipid biomarker inventory approach to minimizing bias in reconstructing planktonic community's response to paleoenvironmental conditions. Successful simultaneous analysis of several distinct groups of lipid biomarkers in a single run, with high baseline resolution of many otherwise co-eluting compounds, provides an analytical advantage in protocol simplicity and high(er) detection limit and accuracy. In addition, development of proxies and ratios that can be used qualitatively and quantitatively to aid interpretations and complement existing proxies can be more easily achieved as trends, relationships and associations can be established within and between different lipid biomarker groups. Chl-*a*-DDs/LCAs reported in this research as a potential indicator of relative *Isochrysis* algae contribution to other phytoplankton is an example. Also, the postulation of salinity being a major control on LCAs unsaturation degree, based on observed holistic trend underscores the edge that detection and quantification of multiple biomarker compounds simultaneously provides. Unique responses within and between photoautotrophic and chemoautotrophic organisms to changing salinity and redox conditions help with better characterizing the dynamics and interaction of the photic zone and the chemocline.

The successful application of this analytical approach to characterizing Holocene Black Sea, in addition to the initial application to a much older geologic event, Ocean Anoxic Event – 2 (Connock 2021), sets up application of the method to study more recent sediments and possibly an environment with anthropogenic imprints as a potential next step. Brownie Lake, a ferruginous and meromictic lake provides a perfect history and sediment record for the proposed next step.